STRUCTURAL AND PHOTOELECTRON EMISSION PROPERTIES OF CHEMICAL VAPOR DEPOSITION GROWN DIAMOND FILMS

DISSERTATION

Presented to the Graduate Council of the

University of North Texas in Partial

Fulfillment of the Requirements

For the Degree of

DOCTOR OF PHILOSOPHY

By

Ikerionwu Asiegbu Akwani, B.S., M.S.

Denton, Texas

August, 1998

Akwani, Ikerionwu-Asiegbu, Structural and photoelectron emission properties of chemical vapor deposition grown diamond films. Doctor of Philosophy (Physics), August, 1998, 158 pp., 4 tables, 56 illustrations, references, 140 titles.

The effects of methane (CH_4), diborone ($B_2 H_6$) and nitrogen (N_2) concentrations on the structure and photoelectron emission properties of chemical vapor deposition (CVD) polycrystalline diamond films were studied. The diamond films were grown on single-crystal Si substrates using the hot-tungsten filament CVD technique. Raman spectroscopy and x-ray photoelectron spectroscopy (XPS) were used to characterize the different forms of carbon in the films, and the fraction of sp^3 carbon to sp^3 plus sp^2 carbon at the surface of the films, respectively. Scanning electron microscopy (SEM) was used to characterize the surface morphology of the films. The photoelectron emission properties were determined by measuring the energy distributions of photoemitted electrons using ultraviolet photoelectron spectroscopy (UPS), and by measuring the photoelectric current as a function of incident photon energy.

We found that the structure and photoelectron emission properties of the polycrystalline diamond films are strongly dependent on the growth conditions. We observed for the first time, a continuous and significant decrease in the photoelectric threshold as the fraction of sp^3 carbon to sp^3 plus sp^2 carbon in the film decreases. By varying the CH_4 concentration from 0.10% to 0.70%, we observed a decrease in photoelectric threshold from 4.8 eV to 3.9 eV as the percent of sp^3 carbon at the surface

decreases from 91% to 55%.

We observed that the percent of sp^3 carbon at the surface is independent of the boron concentrations used during growth. Measurement of the photoelectric current and electron energy distributions show that the photoelectric threshold is insensitive to the boron concentration, although, the boron doping modified the surface morphology and photoemission intensity. The photoemission intensity increases with microcrystlline diamond content and the photoelectric threshold is about 4.4 eV.

By varying the partial pressure of the N_2 gas used during growth, from 15 to 25 millitorr, we observed a decrease in photoelectric threshold from approximately 4.27 eV to 4.09 eV as the percent of sp^3 carbon at the surface decreased from 76% to 50%.

Analyses of the photocurrent measurements show that the electron emission is due to valence band emission. Following these observations, we propose that the decrease in photoelectric threshold is due to a decrease in the band gap of the sp^3 - sp^2 carbon networks at the grain boundaries, in agreement with recent theoretical calculations.

STRUCTURAL AND PHOTOELECTRON EMISSION PROPERTIES OF CHEMICAL VAPOR DEPOSITION GROWN DIAMOND FILMS

DISSERTATION

Presented to the Graduate Council of the

University of North Texas in Partial

Fulfillment of the Requirements

For the Degree of

DOCTOR OF PHILOSOPHY

By

Ikerionwu Asiegbu Akwani, B.S., M.S.

Denton, Texas

August, 1998

ACKNOWLEDGMENTS

This work was supported by the Texas Advanced Research Program under Award No. 003594038 and Award No. 003594053; the National Aeronautic and Space Administration under Award No. NAG-1-1468; and by the National Science Foundation under Award No. DMR-9311724, and National Science Foundation under Award No. DMR-9705187.

I would like to thank Dr. Jose Perez and Dr. David Golden for their guidance, continued support and encouragement throughout my graduate studies, and also, for making this dissertation possible. I would like to thank Dr. Chris Littler and Dr. Sandra Ward for many useful discussions and for their advice during the course of this project.

I would like to thank Edward Sosa, Jamie Castillega and John Bernhard for helping with data acquisition and making useful comments and suggestions, and also for their friendship and great sense of humor.

Special thanks are expressed to Chidi Obi, Dr. B. Ubanwa, Ambrosio Rouse, S. Sue, Song Lim, Richard Stallcup II, Carol Bowden, Jennifer White, and many others for their support.

Finally, I would like to thank my family for their love and support.

TABLE OF CONTENTS

LIST OF TABLES

LIST OF ILLUSTRATIONS

page

CHAPTER I

INTRODUCTION

1.1 Introduction

In this dissertation, structural and electron emission properties of chemical vapor deposition (CVD) polycrystalline diamond films grown using methane, boron and nitrogen doping are presented. The present chapter is divided into two main parts: the first part deals with the motivation of these studies and a brief summary of experimental results. The second part describes the basic theory of photoemission from solids, discussing in particular the threshold energy for photoexcitation.

Man-made diamond has long been considered an important scientific and technological material since it was first reported in 1952 [1]. This consideration is based on the extraordinary properties of diamond. Diamond is a crystalline form of carbon in which each carbon atom is tetrahedrally bonded by four neighboring atoms. The atoms of crystalline diamond are densely packed and interconnected by strong sp^3 bonds. These qualities make diamond crystals unique in many of their properties, as shown in Table 1.1. For example, diamond is the hardest known nature material. One implication of the

Table 1.1 Selected applications of diamond as related to its key properties

	Tools, abrasives, structural components, bearings	Heat sinks, coatings, coated fibers, medical implants	X-ray windows, tubes, masks, IR windows, radomes, laser windows	High speed and high temperature radiation hard electronics, capacitors, vac. microelectronics	Displays, UV detectors, optical switches, waveguides
Mechanical Properties					
High hardness (~90 GPA)					
High bulk modulus (5 x 10^{11} N/m^2)					
High wear resistance	◊	◊	◊		
Very low coefficient of friction (<0 1)					
Thermal Properties					
Very high thermal conductivity (20 W/cm/K at 198 K)					
Superior thermal shock resistance					
Very low coefficient of linear expansion (0.8 x 10^{-6} at 293 K)	◊	◊	◊	◊	◊
Chemical Properties					
Chemically inert					
Subject to oxidation at temperatures in excess of ~600° C	◊	◊	◊	◊	
Optical Properties					
Transmission over a very broad spectral range from, UV to the far IR			◊		◊
Low refractive index (2.41)					
Electronic and Opto-electronic Properties					
Wide band gap (5.2 eV)					
Very high electricbreakdown field (2 x 10^7 V/cm)					
High carrier mobilities (electron-1900 V/cm^2; holes 1600 V/cm^2)		◊		◊	◊
Low dielectric constant (5.5)					
Negative electron affinity					
UV photoconductivity					

strong bonds and light atoms is the transportation of phonons through the material at high velocity with low scattering, thus making diamond the best heat conductor at room temperature. This property can be utilized as a heat sink for high power devices and lasers. Because of its wide band gap of 5.2 eV, diamond exhibits the widest spectral transmission range of any known solid [2]. This property, with hardness and chemical inertness, makes diamond a suitable material for transmissive optical components. In addition, the recent discovery of negative electron affinity (NEA) in diamond has generated considerable interest in diamond as an electron emitter in flat panel displays (FEDs) [3].

For centuries, natural diamonds were mainly used as jewelry and for grinding and lapping applications because of their brilliance and hardness, respectively. Diamond has potentially useful semiconducting and mechanical properties. However, naturally occurring diamonds are rare and prohibitively expensive and would not be good for many applications. Synthetic production of large single heteroepitaxial diamond is one of the major obstacles in realizing diamond technology. Early efforts in diamond synthesis involved high-pressure high-temperature (HTHP) processes that converted graphite into diamond. The deposition of diamond film using CVD process, pioneered by Augus and Spitsyn [4], and the theoretical progress in the understanding of electronic states in solids have led to the current interest in the use of diamond for semiconducting and optical applications. This interest has resulted in unprecedented developments in experimental techniques for diamond deposition and characterization.

1.2 Chemical Vapor Deposition

Many different techniques are now used to deposit diamond from the gas phase such as: hot filament CVD [5-8], microwave plasma CVD [9-10], DC discharge plasma [11], and various combinations of these [12]. A common feature of all these techniques is that the morphology, structure and electronic properties of the deposited film depend on the growth conditions. In spite of all the recent progress, fundamental mechanism of CVD diamond growth is not well understood and is the subject of considerable current interest. In general, diamond films produced by these techniques on non-diamond substrates are polycrystalline and contain varying amounts of non-diamond carbon such as graphite. Many of the basic properties of polycrystalline diamond films depend on the morphology and the structure of the film such as crystallinity, crystal orientations and grain size. The aforementioned problems are limiting the applications of CVD diamond.

For many applications, a large single crystal diamond film is needed. The inability to produce high quality single-crystal heteroepitaxial diamond films is due to the large lattice mismatch between diamond and other substrates. This inability is also due to the complexity of the CVD process, which involves many interdependent parameters such as gas composition, substrate temperature, filament temperature, filament position and gas pressure. Several experimental and theoretical studies have attempted to correlate surface morphology and structure of diamond films with these deposition parameters with the aim of understanding the basic growth mechanism and properties of diamond films [13-15]. It has been established that the morphology and structure of CVD diamond films are

strongly dependent on the deposition conditions.

To understand the effects of methane, boron and nitrogen doping on the electron emission properties of CVD diamond films, diamond films were grown on Si substrates by thermal dissociation of methane and hydrogen gases using hot-tungsten filament assisted CVD techniques.

The films were characterized using different characterization techniques including scanning electron microscopy (SEM), x-ray photoelectron spectroscopy (XPS) and Raman spectroscopy (RS). Electron emission characteristics of polycrystalline CVD diamond films were studied by measuring the photoelectric current as a function of incident photon energy, and by measuring the energy distribution of photo-emitted electrons using single frequency photo-excitation. These experimental techniques and experimental setup are described in details in chapter 3.

1.3 Effects of $sp^3/(sp^2+ sp^3)$ Ratio on Electron Emission

The ability of carbon to form both sp^3(diamond) and sp^2(graphite) bonds should have an effect on the electronic properties of CVD diamond. Numerous studies have shown that CVD polycrystalline diamond films contain varying amounts of non-diamond carbon that are dependent on the growth conditions. A variety of techniques, including Raman spectroscopy (RS) [16-17], x-ray photoelectron spectroscopy (XPS) [18], and nuclear magnetic resonance (NMR) [19] have been used to identify and quantify the different carbon phases present in CVD polycrystalline diamond. However, the effects of

these phases on electron emission characteristics have not been reported. An investigation of the effects of such structural changes on the electron emission properties of diamond may lead to an increased understanding of electron emission with important applications ranging from field emission flat panel displays to electron microscopes.

In chapter 4, the study of the effect of methane concentration on the photoelectric threshold of polycrystalline CVD grown diamond films are discussed. It was found that the photoelectric threshold decreases as the percent of $sp^3/(sp^2+ sp^3)$ carbon fraction on the surface of the film decreases.

1.4 Effects of Boron and Nitrogen doping on Electronic Properties.

Electronic and optical properties of a semiconductor are very dependent on the number and types of impurities and defects present. The ability to control impurity and defect concentrations is essential for the development of diamond films for device applications. Some applications of diamond films require controlled incorporation of impurities such as doping of n-type and p-type regions, while other applications are hindered by unintentional contamination by impurities or defects. CVD diamond films grown on non-diamond substrates are polycrystalline and therefore contain grain boundaries that contain defects that act as recombination centers for electron-hole pairs and scattering centers for carriers thereby increasing the lifetime and decreasing the mobility of the carriers.

The possibility of doping diamond is an important consideration in applications of CVD diamond. A number of dopants and methods of incorporation have been studied. P-

type conductivity by boron doping has been achieved in diamond by implantation [20] and gas phase reaction [21]. The ionization energy for boron in diamond is about 0.37 eV, as a result boron impurities are only partially ionized at room temperature. On the other hand, producing n-type doping has currently not been achieved. Because of the close packing and rigidity of the diamond lattice, incorporation of atoms larger than carbon is not easily achieved. Therefore, dopants which are normally used to produce n-type doping in silicon, such as P or As are not suitable for diamond. Alternative dopants such as nitrogen and lithuim have been investigated, but few studies have been reported.

Although doping by implantation is achievable in the case of boron, the damage introduced and the difficulties associated with removing the implantation damage by annealing limit the applicability of this method. Alternatively, doping by diffusion, which is a standard method used in the semiconductor industry, appears impractical because of the low diffusivity of most elements in diamond. The temperatures necessary to produce sufficiently high diffusion rates can lead to structural transformation and changes in basic properties. Doping of diamond by introducing dopant-containing gases such as diborane (H_2B_6) during the film deposition process is the most commonly used method that avoids the above problems and is capable of producing controlled amount of impurities with low defect densities. Boron and nitrogen doping of CVD diamond films using dopant gases has been reported to modify the morphology, crystallinity and structure of the resulting films [22, 23]. However, the correlation between the growth conditions and dopant concentrations and photoelectron emission characteristics has not been reported. The

problem is complicated by the ability of carbon to form both sp^3(diamond) and sp^2(graphite) bonds. Nitrogen is known to be one of the impurities in both natural and synthetic HTHP diamond and can exist either in large aggregates or dispersed in substitutional sites [24]. The substitutional incorporation of nitrogen and boron distorts the diamond lattice and modifies its structural and electronic properties, in addition, effects of boron and nitrogen impurities on electron energy levels and photoelectron emission properties is important and has not been reported.

In chapter 5, the effects of boron doping on the photoelectron emission of poly-crystalline CVD diamond films are discussed. It was found that the $sp^3/(sp^2+ sp^3)$ carbon fraction and photoelectric threshold is independent of boron doping used, but the boron doping modified the surface morphology and result in high emission intensity where the microcrystalline content is highest.

The effects of nitrogen partial pressure on photoelectron emission characteristics of polycrystalline CVD diamond films are discussed in chapter 6. Unlike the boron doped films, nitrogen was found to affect the $sp^3/(sp^2+ sp^3)$ carbon fraction and the photoelectric threshold similar to that of methane concentration.

Negative electron affinity surfaces have a conduction band above the vacuum level thus allowing electrons to easily escape from the surface. Negative electron affinity of diamond was first observed by Himpsel [25]. Field emission from diamond surfaces is observed to occur at applied fields that are very low in comparison to those required for emission from Si, GaAs, Ge and metal surfaces. The mechanism responsible for the high

electron emission from undoped or p-type diamond is not yet understood. Undoped diamond is an insulator, which should make stable electron field emission at low fields impossible. In p-type semiconducting diamond the Fermi level is about 5.00 eV below the vacuum level, which does not facilitate low voltage electron emission. Although a number of possible mechanisms for electron field emission from diamond surfaces have been proposed and studied, no consensus has been established. These mechanisms include NEA, defects, sharpness of diamond crystallites and graphitic inclusions in the diamond films [26, 27, 28, 29]. An understanding of the process of electron emission from CVD diamond is crucial in advancing diamond film technology for flat panel display applications.

1.5 Scope of the Present Work

The purpose of this work is to study the effects of methane, boron and nitrogen doping on the structure and electron emission properties on the surface of CVD grown polycrystalline diamond films. In particular, the effect of methane, boron and nitrogen doping on the $sp^3/(sp^2+ sp^3)$ carbon fraction and photoelectric threshold of CVD diamond films. A series of polycrystalline diamond films were grown using hot-tungsten filament CVD on Si substrates. Using growth conditions such as methane, boron and nitrogen concentrations, $sp^3/(sp^2+ sp^3)$ carbon fraction and the photoelectric threshold were determined. The surface morphology as a function of these gas concentrations were examined using SEM. The $sp^3/(sp^2+sp^3)$ carbon fraction of the films were measured using Raman spectroscopy and x-ray photoelectron spectroscopy. The photoelectric threshold

of these diamond films grown using different methane, boron and nitrogen doping were measured. Changes in the photoelectric threshold as a function of the $sp^3/(sp^2 + sp^3)$ carbon fraction were determined.

Characterization of the electronic properties of CVD grown diamond films is important in applications of CVD diamond films in areas where high electron emission is needed such as field emission displays (FEDs). Diamond-based FEDs have the potential to be low cost, high performance alternatives to cathode ray tube and liquid crystal display technologies. In addition, diamond films with high emission efficiency can be used to make low gain electron multiplier, and ultraviolet photodetectors.

References

1. J.F.H. Cusers, *Physica* **18**, 489 (1952).

2. K.E. Spear and J.P. Dismukes, *Synthetic Diamond: Emerging CVD Science and Technology* (John Wiley & Son, New York, 1994).

3. N. Kumar, H. Schmidt and C. Xie, *Solid tate Technology*, May, 71 (1995).

4. J.C. Angus, *Proc. First Internat. Sympos. on Diamond and Diamond-like Films*, edited by J.P Dismukes, (The Electrochemical Society, Pennington, 1989), pp. 1-13.

5. N. Setaka, *J. Mater. Res.* **4**, 664 (1989).

6. F. Jansen, M.A. Mochankin and D.E. Kuhman, *J. Vac. Sci. Technol. A***8** 3785 (1990).

7. B. Singh, Y. Arie, A.W. Levine, O.R. Mesker, *Appl. Phys. Lett.* **52**, 451 (1988).

8. T. Kawato, and K. Kondo, *Jpn. J. Appl. Phys.* **26**, 1429 (1987).

9. A.R. Badzian, T.Badzian, R. Roy, R. Messier and K.E. Spear, *Mater. Res. Bull.* **23,**

531 (1988).

10. Y. Saito, K. Sato, H. Tanka, K. Fujita, S. Matuda, *J. Mater. Sci.* **23**, 842 (1988).

11. K. Suzuki, A. Sawabe and T. Inuzuka, *Jpn. J. Appl. Phys.* **29**, 153 (1990).

12. N. Furjimori,A. Ikegaya,T. Imai,K. Fukushima, N. Ohta, *Proc. First International. Sympos.on Diamond and Diamond-like Films*, edited by J.P. Dismukes, (The Electrochemical Society, Pennington, N.J. 1989) pp. 93-105.

13. K. Kobashi, K. Nishimura, and T. Horuchi, *Phys. Rev. B* **38**, 4067 (1988).

14. Y. Sato, in *New Diamond* 1988 (JNDF, Tokyo, 1988) pp.30-35.

15. Y. Sato, C. Hata, M. Kamo, *First Internatioal Conference on the New Diamond Science and Technology Program and Absr.*, 24-26 October 1988 (JNDF, Tokyo, 1988), pp. 50-51.

16. D.S. Knight and W.B. White, *J. Mater. Res.* **4**, 385 (1989).

17. J. Robertson, *Adv. in Phys.* **35**, 317 (1989).

18. S.C. Sharma, C.A. Dark, R.C. Hyer, M. Green, T.D. Black, A.R. Chourasia, D.R. Chopra and K.K. Mishra, *Appl. Phys. Lett.* **56**, 1781 (1990).

19. K.M. Mcnamara, K.K. Geason and M.W. Geis, *Mater. Res. Soc. Symp. Proc.* Vol. **162**, (1990), pp. 207-212.

20. W. Zhu, G.P. Kochanski, S. Jin, and L. Seibles, *J. Vac. Sci. Technol.* **B14 (3)**, 2011 (1996).

21. N. Fujimori, H. Nakahata, and T. Imai, *Jpn. J. Appl. Phys.* **29**, 824 (1990).

22. S. Jin and T.D. Moustakas, *Appl. Phys. Lett.* **65,** 403 (1994).

23. B.R. Stoner, J.T. Glass, L. Bergman, R.J. Nemanich, L.D. Zoltan and J.W. Vandersande, *J. Electron. Mater.* **21**, 629 (1992).

24. W. Kaiser and W.L. Bond, *Phys. Rev.* **115**, 857 (1959).

25. F.J. Himpsel, J.A. Knapp, J.A. VanVechten, and D.E. Eastman, *Phys. Rev.* **B 20**, 624 (1979).

26 J. van der Weide, Z. Zhang, P.K. Baumann, M.G. Wensell, J. Bernholc and R.J. Nemanich, *Phys. Rev.* **B 50**, 5803 (1994).

27. N.M. Miskovsky, P.H. Cutlter,and Z. H.Huang, *J. Vac. Sci. Technol.* **14**, 2037 (1996).

28. C. Nutzenadel, O.M. Kuttle, O. Groning, and L. Schlapbach, *Appl. Phys. Lett.* **69**, 2662 (1996).

29. N.S. Xu, R.V. Latham, and Y. Tzeng, *Electron. Lett.* **29**, 1596 (1993).

CHAPTER 2

THEORY OF PHOTOEMISSION FROM SOLIDS.

2.1 Introduction

The discovery of the photoelectric effect established the existence of photons [1]. For electrons to escape from the surface of a solid into the vacuum, they must recieve sufficient energy to overcome the surface potential barrier. The potential barrier depends on the material condition of the solid, and surface.

2.2 Three-Step Model of Photoelectric Emission

Photoemission can be understood in terms of a three-step process (developed by Spicer [2]) consisting of (1) photoexcitation of electrons from an intial level E_i to the final level $E_f = E_i + h\upsilon$ by means of absorption of a photon with energy $h\upsilon$, (2) transportation of the excited electrons through the crystals to the surface region with or without scattering; and (3) the escape of the electrons from the surface over the surface barrier into vacuum. These processes determine the emission yield and are responsible for a given material being a good or poor emitter. Assuming that the internally generated density of electrons is unaffected by steps (2) and (3), then those electrons whose energies exceed the surface

potential ($E_f = E_i + h\upsilon$) will be able to escape from the solid. The density of photoemitted electrons then depend on the initial density of states, $N(E_i)$, and final density of states, $N(E_f)$, and on the probabilities of transitions for $E_i \rightarrow E_f$ at a particular energy $h\upsilon$ of the radiation.

Now we consider the internal generation of excited electrons, $N_{intn}(E)$. The electronic state within an energy band of a solid is characterized by its energy E_i and its momentum K_i. The law of conservation of energy and momentum require that the excitation energy, $E_f(K_f) - E_i(K_i)$, be equal to the energy of the photon absorbed, $h\upsilon$, and that the difference in the wave vector, $K_f - K_i$, be equal to the photon wave vector, K_{ph}. Since the wave number of the photon is small, K_{ph} can be neglected, thus conservation of K is assumed, i.e. $K_f = K_i$, such transitions are characterized as direct optical transitions. However, optical transitions can also occur between states that lie at different K vectors where the change in momentum of the electrons is accommodated by a phonon which is absorbed or emitted in the transition process. Such optical transitions are characterized as an indirect transition. Representing the wave number and the phonon energy by q and $h\Omega$ respectively, momentum and energy conservation yield: $K' = K + K_{ph} \pm q$ and $E(K') = E(K) + h\upsilon \pm h\Omega$, where the plus and minus sign means absorption and emission of phonons respectively. Direct transition is a two-body process (photon, electron) while indirect transition is a three body process (photon, electron and phonon). In general, all the probability of an indirect transition is lower compared to that of direct transition. Many theoretical and experimental studies have shown that holds direct transitions are

dominant in most material [3]. The density of states, N(E), is an integration over all states with equal energy but different K values within a certain band, and summed over all bands n [4]:

$$N(E) = \frac{1}{(2n)^3} \sum_n \int d^3k \, \delta[E(k) - E_n(K)] \tag{1}$$

The quantum mechanical interaction of an electromagnetic field of vector potential A with an electron is given by [5]:

$$W = \frac{1}{2}(\boldsymbol{A}\cdot\boldsymbol{P} + \boldsymbol{P}\cdot\boldsymbol{A}) \tag{2}$$

where **P** is the momentum operator. Higher order terms in **A** are neglected (dipole approximation). Assuming that the number of electrons excited from E_i to E_f is proportional to the density of filled states at E_i, N(E_i), (where $E_i < E_f$) and proportional to the density of unoccupied states at E_f, N(E_f), ($E_f = E_i + h\upsilon > E_F$). The probability of excitation of an electron or the transition rate from an initial state $|i>$ to a final state $|f>$ is governed by the dipole matrix element [5]: $M_{if} = <f|W|i>$, Therefore, the fraction of internally excited electrons which have sufficient kinetic energy to escape for a given incident radiation is expressed as follows [4]:

$$N_{intn}(E, h\upsilon) = C\sum_{if} \int d^3K \, |M_{if}|^2 \, \delta(E_f(k) - E_i(k) - h\upsilon) \, \delta(E(K) - E_i(K)) \tag{3}$$

where C is a normalization factor and the delta function ensures energy conservation.

The density of internally excited electrons can be affected by scattering properties of the solid, such as geometric and surface properties of the solid. According to Einstein's theory of the photoelectric effect [1], the excitation rate of electrons is proportional to the incident light intensity. Optical loss caused by high surface reflectance or scattering by a rough surface can lead to absorption of a small fraction of the incident photons resulting in a low yield of internally excited electrons, which in turn leads to low electron emission. In addition, crystal size can also affect the rate of photon absorption. It has been reported that the electronic excitation shifts to higher energy with decreasing crystallite size [6]. These effects are expected to be significant for a polycrystalline material.

In order to relate the internal distribution, $N_{intn}(E, h\upsilon)$, with the measurable external energy distribution $N_{ext}(E, h\upsilon)$, consider the probability that excited electrons travel from point of origin to the surface without suffering an energy losing collision. The mean free path for photons in solids is larger than the scattering length of excited electrons [7]. Therefore excited electron originating deep inside the solid may undergo inelastic collision which may result in the loss of a large fraction of its energy and a change in momentum. These effects may reduce the probability of emission to essentially zero. Scattering mechanisms can be divided into two types: (1) phonons, impurities or imperfections in the volume or the surface. (2) Electron-electron collisions resulting in pair production or generation of cascades of secondary electrons. However, if the initial excited state is not so high as to result in pair production (impact ionization), then the

dominant electron energy lose mechanism becomes type (1) above.

Before escaping into vacuum, an electron has to overcome the surface potential barrier presented by the work function. Within the framework of the free electron approximation, this implies that the electron must have a component of its total crystal momentum K_z perpendicular to the surface which is greater than some critical value K_c [8]. The escape probability is assumed to be unity if this condition is satisfied. In general, an escape function $T(E_f, K)$ is introduced which describes the probability for an excited electron in state $E_f(K)$ to reach the surface and escape [3], thus

$$N_{ext}(E,h\upsilon) = N_{intn}(E,h\upsilon)\, T(E_f,K) \tag{4}$$

By substituting equation (3) into equation (5), the number of externally emitted photoelectrons with a specific energy for a given incident photon energy is given by:

$$N_{ext}(E,h\upsilon) = C\sum_{if}\int d^3K\,|M_{if}|^2\,\delta(E_f(K)-E_i(K)-h\upsilon)\,\delta(E-E_i(K))\,T(E_f,K) \tag{5}.$$

The transmission function ($\Gamma(E_f, K)$) is only important near the threshold and for low photon energies. If the matrix element is assumed to vary slowly, then the total transition between E_f and E_i which can take place at the energy $h\upsilon$ is called the joint density of states (JDOS), D($h\upsilon$

$$D(h\upsilon) = \frac{1}{(2n)^3}\sum_{if}\int d^3k\,\delta[E_f(K) - E_i(K) - h\upsilon] \tag{6}$$

where the range of integration is restricted to those K space for which $E_i < E_F < E_f$, and the summation is over all pairs (i, f) which can participate. The $D(h\upsilon)$ situation is characteristic of low excitation incident energies in the threshold and band structure regime. The photoemission spectrum in this energy range will exhibit an energy density of the joint density of states, therefore the matrix element will couple only to electron states vertically downward in the bands at any final state energy. Both the initial and final states play an important role. Changing the photon energy results in a corresponding change in the energy distribution spectrum due to variation in the band structure of unoccupied states. For photon energies exceeding 40 eV, the spectral feature is not strongly modulated by the matrix element effects, and the final states become available for excited electrons from all initial states. Then XPS and UPS exhibit similar features representing the density of occupied states [4].

From a quantum mechanics point of view, photoemission is explained in terms of wave functions matching at the solid-vacuum interface. In the vacuum, all states above the vacuum level are allowed (free- electron states), while inside the solid, forbidden electron state exist between the band gap. The initial electronic state E_i may be described by a delocalized Bloch state inside the solid which decays exponentially outside the solid.

Depending on the photon energy and the band structure, information on the bulk or surface properties can be obtained. Three distinctly different final states are possible. If the mean free path is large and the energy matches with an allowed band, the free electron state in the vacuum may be matched to a Bloch state inside the solid. The overlap of the initial and final states in the matrix element extends over large distances, in this case the photoelectrons carry information on the bulk properties [9]. However, if the final state energy coincides with a band gap, the wave function becomes evanescent in the solid, the matrix element vanishes everywhere except for a small region near the interface. Under this condition, photoemission is band gap emission [10] which carries information on the vicinity of the interface [11, 12]. Finally, if the mean free path is short in the solid, the free electron wave function couples with a decaying wave inside the solid and the matrix element vanishes everywhere except near the surface because of short range overlap of the initial and final state wave functions. Under this condition, photoemitted electrons carry information on the surface properties.

2.3 Threshold Energies for Electron Emission

The photoelectric threshold energy is a fundamental parameter in determining photoelectron emission characteristics of a material. Semiconductor energy levels are discussed with reference to Figure 2.1. Figures 2.1(a) and 1.1(b) show the schematics of the band structure of an intrinsic and negative electron affinity surface of a semiconductor, respectively. The vacuum level, E_{vac}, is the energy at which an electron would emerge from the semiconductor with zero kinetic energy. The electron affinity, χ, is the

energy difference between the edge of the conduction band, E_c, and the vacuum level. The work function, Φ, of an intrinsic semiconductor is the energy separating the Fermi level, E_F, from E_{vac}. The work function is a surface property of the material and depends on the electronic structure. The work function of most materials range from 3 - 5 eV. Cs has the lowest work function of about 2 eV while that of diamond is about 5.4 eV.

The work function plays an important role in determining electron emission characteristic of semiconductors. The band gap, E_g, is the difference in energy between the edge of the valence band, E_v, and the conduction band, E_c. The threshold for photoelectric emission, E_T, is the lowest photon energy required to excite an electron from the highest occupied electron energy level in the semiconductor into vacuum. For an intrinsic or non-degenerate semiconductor where the highest occupied state is the top of the valence band, E_T, is given by:

$$E_T = h\upsilon_T = \chi + E_g \tag{7}$$

In metals, $E_g = 0$, $\Phi = \chi$ and E_T is given by:

$$E_T = \Phi \tag{8}$$

In this case the Fermi level coincides with the valence band. However, doping affects the occupation of states through the Fermi distribution function. Therefore, photoelectric threshold may change with doping concentrations. For example, in degenerate p-type semiconductors, the Fermi level is ξ_p below the valence band edge, as shown in figure 2.2(a). E_T is given by:

$$E_T = \chi + E_g + \xi_p \tag{9}$$

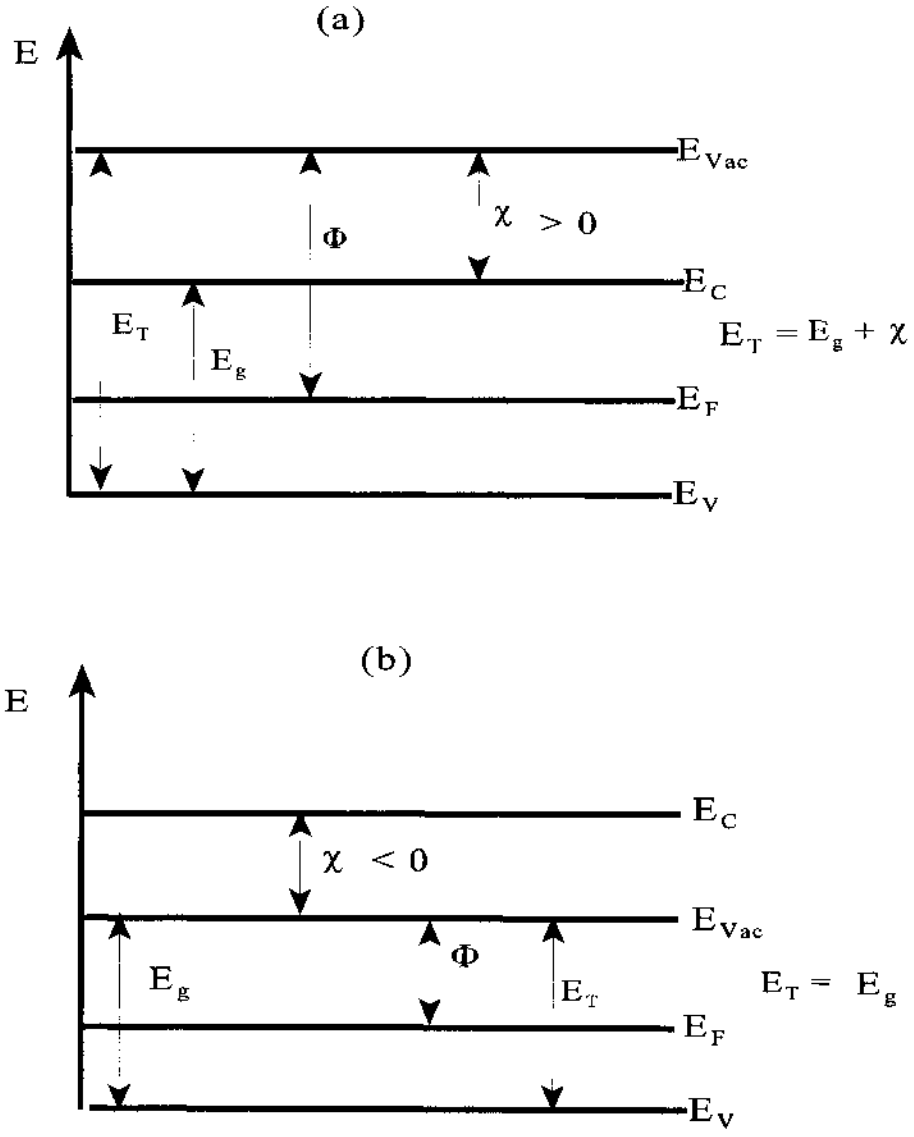

Figure 2.1. Schematic of the band structure of a semiconductor (a) an intrinsic semiconductor and definitions of symbols (b) negative electron affinity surface

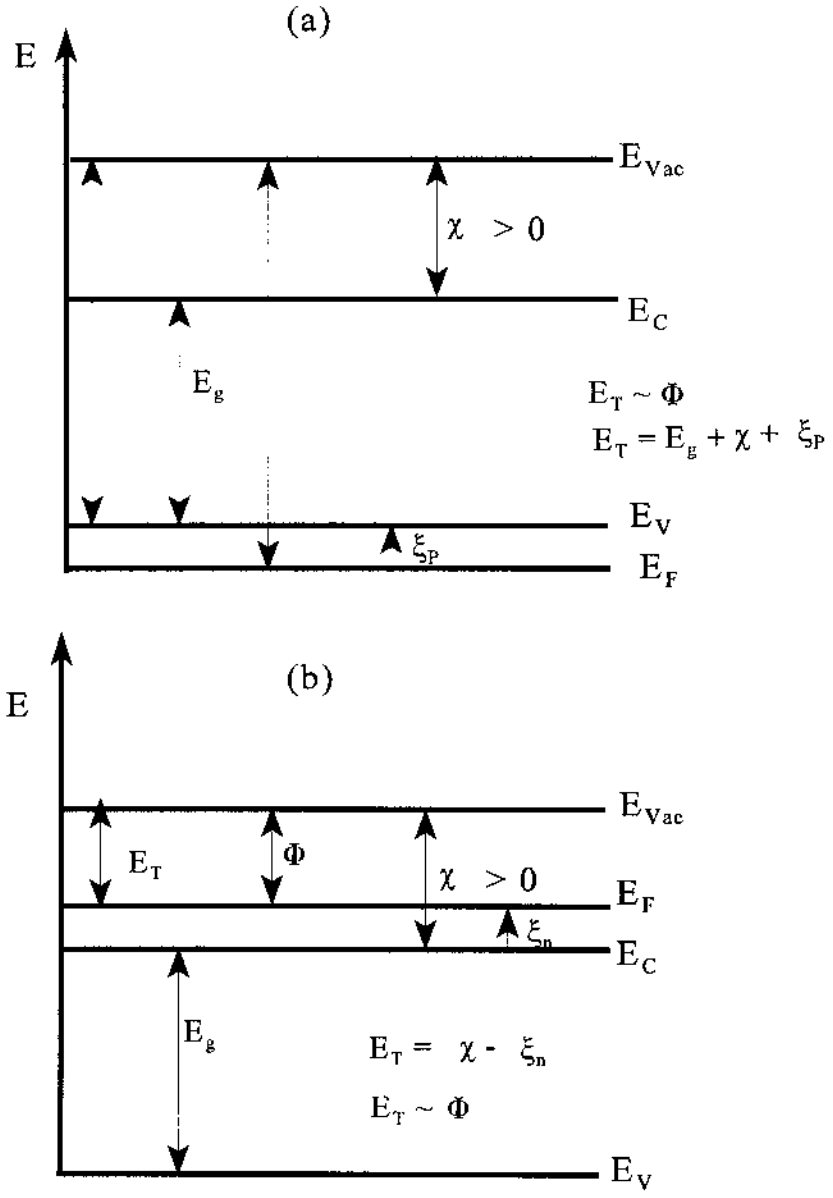

Figure 2.2. Schematic of the band diagram of a semiconductor showing dependence of threshold energy on doping (a) degenerate p-type (b) degenerate n-type semiconductors.

In a degenerate n-type semiconductor, the Fermi level is ξ_n above the conduction band edge, as shown in figure 2.2(b). E_T is given by:

$$E_T = \chi - \xi_n \tag{10}$$

It is seen from these results that the threshold energy for photoelectron emission from a semiconductor changes with the impurity contents if the impurity concentration is sufficient to produce degeneracy.

As shown in figure 2.1(b), for a negative electron affinity surface the vacuum level is lower in energy than the conduction band thus allowing electrons to easily escape from the surface into vacuum. For a NEA surface, the photoelectric threshold occurs at a photon energy equal to the band gap energy [13] ($E_T = E_g$). It is reported that CVD grown diamond films exhibit NEA [14]

2.4 Photoelectric Yield

Photoelectric yield defined as emitted electron per photon is dependent on the energy band structure, type of optical excitation and the dominant electron production mechanism in the solid as described previously. From equations (3) and (5) the photoelectric yield for electron energy distribution is given by:

$$Y = \frac{\sum_{if} \int d^3K \, |M_{if}|^2 \, \delta(E_f(K) - E_i(K) - h\upsilon) \, \delta(E - E_i(K)) \, T(E_f, K)}{\sum_{if} \int d^3K \, |M_{if}|^2 \, \delta(E_f(K) - E_i(K) - h\upsilon) \, \delta(E - E_i(K))} \tag{11}$$

Consider the case of total yield, where all emitted electron are collected as a function of incident photon energy. If the absorption ($\alpha(h\upsilon)$), reflectance (R) and the

mean free path (l) are known, then the photoelectric yield can be calculated on the basis of Spicer's model of photoemission as discussed previously. Thus, the general expression for photoemission current is given by [2]:

$$i(h\upsilon)\, d(h\upsilon) = \int \alpha(h\upsilon)\, I(x,h\upsilon)\, P(x,h\upsilon)\, dx\, d(h\upsilon) \tag{12}$$

Where i($h\upsilon$) is the photoemission current resulting from light of photon energy $h\upsilon$, d($h\upsilon$) is the band pass of the monochromator, I(x, $h\upsilon$) is the intensity of the light at a depth of x from the surface of the solid and integration is over x and P(x, $h\upsilon$) is the escape function describing the probability of electron emission through the surface. I(x, $h\upsilon$) is given by [2]:

$$I(x, h\upsilon) = I_0(h\upsilon)\,[1 - R(h\upsilon)]\, e^{-\alpha x}, \tag{13}$$

where $I_0(h\upsilon)$ is the incident photon flux and R is the optical reflectivity. The escape probability is

$$P(x, h\upsilon) = B(h\upsilon)\, e^{-x/l} \tag{14}$$

where l is the escape depth. By substituting equations (13) and (14) into (12) and integrating from 0 to ∞, assuming large sample thickness. The emission current yields [2]:

$$i(h\upsilon) = \frac{\alpha B I_0 (1 - R)}{(\alpha + 1/l)} \tag{15}$$

Therefore, the quantum yield is given by [2]:

$$Y_t = \frac{i(h\upsilon)}{I_0} = \frac{\alpha B(1-R)}{(\alpha + 1/l)} = B(h\upsilon)\,(1-R)\,P(h\upsilon) \tag{16a}$$

where [7],

$$P(h\upsilon) = \frac{\alpha(h\upsilon)\,l(h\upsilon)}{[1+\alpha(h\upsilon)\,l(h\upsilon)]} \tag{16b}.$$

Near the threshold, $d > 1/\alpha$ (light penetration depth). Therefore, $P(h\upsilon) \sim 1$ and $B(h\upsilon)$ increases smoothly with $h\upsilon$. Features in the threshold spectrum will be mainly due to changes in reflectivity through the (1-R) term. The absorption coefficient becomes important only if it leads to significant changes in the ratio of the electronic population of the final states above the vacuum level to those below the vacuum level. Changes in the photoelectric yield cause by the later effect can be employed to obtain information on states between the Fermi and the vacuum level [7].

2.5 Photoelectron Emission Characteristics near Threshold

In metals, the photoelectric threshold or work function is determined by applying Fowler's theory [15] of the yield near threshold for nearly free electron gas of a solid. According to Fowler's theory, the quantum yield near the threshold can be written as:

$$Y_t \sim (h\upsilon - \Phi)^2 \quad \text{for } (h\upsilon - \Phi) << \Phi < h\upsilon \tag{17a}$$

$$Y_t = 0 \text{ for } h\upsilon < \Phi \tag{17b}$$

From a line plot of $Y_t^{1/2}$ versus $h\upsilon$, the work function is extrapolated from the intercept at $Y_t = 0$.

A more general theoretical model of the photoelectric yield versus energy curve

near the threshold points for a variety of excitation and scattering processes was developed by Kane [16] and verified by Gobeli and Allen [17]. In this model, the photoelectric threshold yield for semiconductors are expressed as a power laws in photon energy [16]:

$$Y_t = A(h\upsilon - E_T)^n \tag{18}$$

where A and n are constants. Calculations based on density of states considerations, involving energy band expansions about the threshold point, show that the value of n can be predicted on the basis of the type of excitation and scattering mechanism operating in the bulk or at the surface of the semiconductor [16]. The processes and the predicted values of n are listed in Table 2.1. Equation (19) can be generalized to allow for the possibility of different transitions occurring over different spectral range, for example, indirect and direct transitions [17]. The threshold yield can then be described by a functional dependence of the form [17]:

$$Y_t = \sum_m A_m(h\upsilon - E_{Tm})^n m \tag{19}$$

From the fitting parameters or by extrapolation to the energy axis the value of the threshold energy is obtained.

2.6 Effect of Surface Conditions on Electron Energy Levels

Until now, the energy bands are assumed flat. The threshold energies are affected by the presence of a potential barrier at the surface of a semiconductor. Surface states are known to induce a space charge in the bulk of a semiconductor. Depending on the type and the number of the surface states (donor or acceptor states), the bands can bend either

Table 2.1. Threshold energies and energy dependence of the photoelectric yield for different excitation and scattering processes.

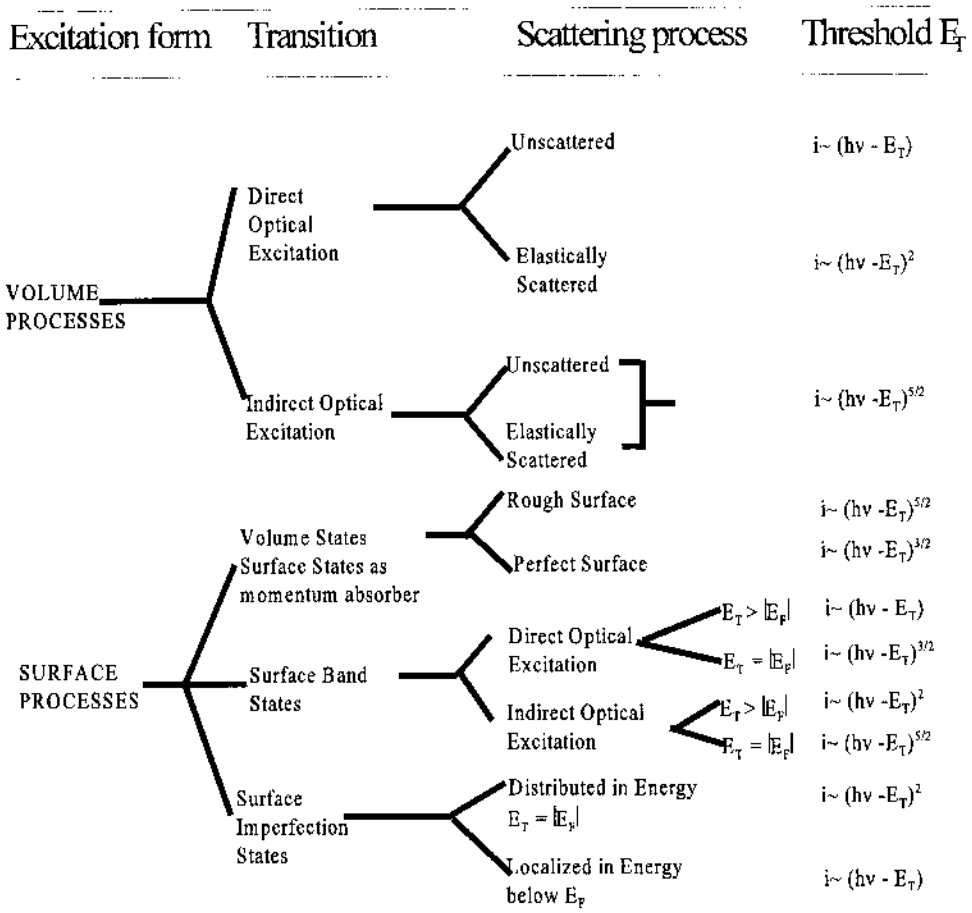

upwards or downwards near the surface. Such behavior is reflected in an effective lowering or raising of the threshold energy.

For a p-type semiconductor with a large concentration of donor levels, the donors at the surface give up electrons to the acceptors in the bulk of the semiconductor. The electron transfer creates a positive surface charge near the surface, and a negative charge region in the bulk that extends a distance W inside the bulk. The separation of charges produce an electric field located almost entirely in the semiconductor depletion layer. As a result the potential at the surface drops and the bands at the surface are bend downward as shown in figure 2.3(a). The transfer of electrons from the donor levels to the bulk continues until the Fermi level at the surface coincides with the donor level. In this case the Fermi level is said to be stabilized or pinned [18]. Thus, E_T for electron emission from the bulk is given by:

$$E_T = \chi + E_g - e\varphi_s \tag{20}$$

where φ_s is the surface potential and $e\varphi_s$ is the amount of band bending, representing reduction of electron energy in the bulk of the semiconductor.

The surface potential, φ_s, can be calculated by assuming a filled acceptor layer of a given thickness. This layer, called the Schottky layer, is characterized by a constant and finite space charge density, ρ, and outside it, ρ is zero. Solution of the Poisson equation for this charge distribution gives [19]

$$\varphi_s = 2\pi Net^2/\rho \tag{21}$$

where N is the concentration of the acceptors, the dielectric constant and t the thickness

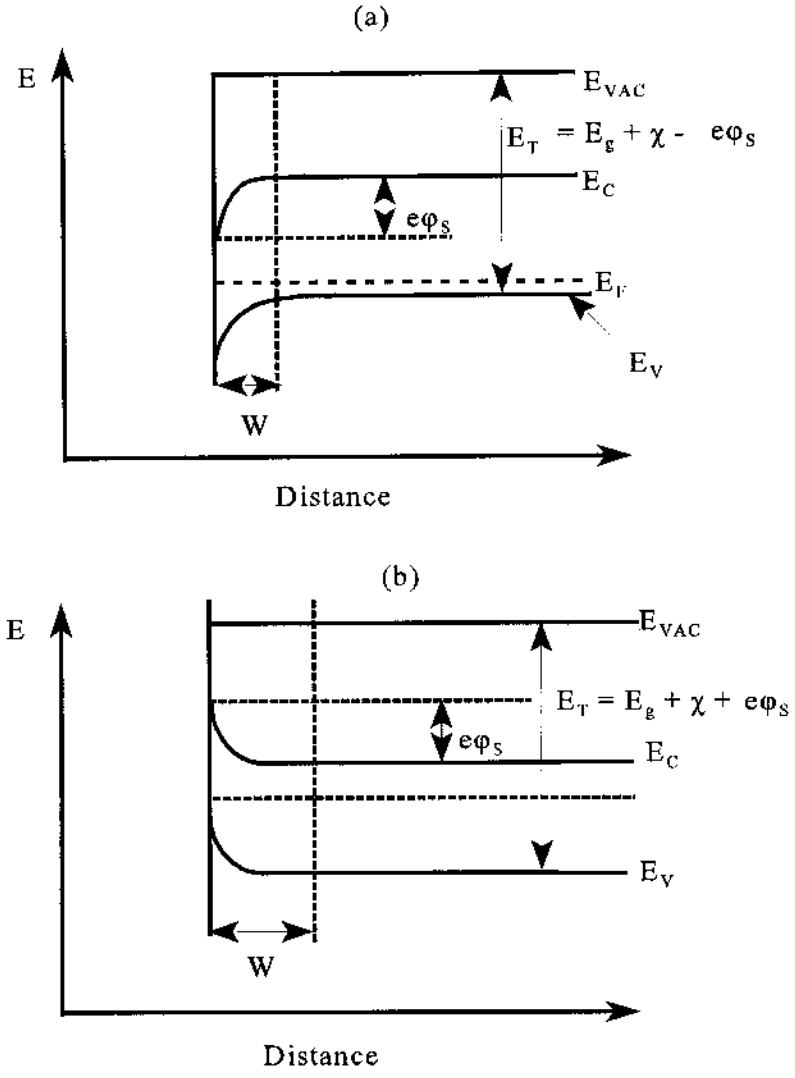

Figure 2.3. Band diagram of a semiconductor showing an amount $e\varphi_s$ of band bending at the surface (a) donor surface states (b) acceptor surface states.

of the space charge layer. It follows that the amount of band bending is dependent upon the concentration of the acceptor levels.

Similarly, for an n-type semiconductor with acceptor surface states, the electrons from the bulk donor states flow into the acceptor states creating a positive charge space in the bulk, and a negative surface charge. The electrostatic potential is higher in the bulk than at the surface by an amount equal to $e\varphi_s$. As a result the electron energy is degraded at the bulk more than at the surface. The energy bands are bent upward at the surface as shown in figure 2.3(b). In this case the threshold, E_T, is given by

$$E_T = \chi + E_g + e\varphi_s \tag{22}$$

Based on this energy band model, an n-type surface on a p-type bulk will have a lower threshold energy, therefore a higher yield than a p-type surface on an n-type bulk. The higher the doping, the narrower the space charge layer within the escape depth, thereby allowing more of the bulk to be effective for electron emission. Furthermore, the internal electric field within the depletion region will facilitate electron emission for the p-type case, since the field tends to accelerate excited electron into vacuum.

2.7 Atomic and Electronic structure of carbon based materials

Knowledge of the atomic structure of a material is essential for the understanding of the physical properties of the material. The primary goal in the theory of the structure which is beyond the scope of the present work, is to understand both how different materials are formed and how the resultant structure controls the properties of the

material.

Crystalline semiconductor materials such as diamond exhibit a long range order and well defined band gaps. In contrast, amorphous materials are characterized by lack of long range order. One of the effects of disorder on the electronic structure of a semiconductor material is the introduction of band tailing or pseudogap [20] which alters the optical and electrical properties of a semiconductor material.

Carbon forms a number of crystalline and non-crystalline solids with diverse properties [21]. The two crystalline forms of carbon are diamond (a wide band gap sp^3 bonded semiconductor), and graphite (a layered sp^2 bonded metal with no band gap). In the sp^3 configuration, each of the four valence electron of the carbon atoms is tetrahedrally bonded to an adjacent atom, forming strong σ bonds. In the sp^2 configuration, only three out of the four electrons form strong intra-layer σ bonds, the fourth electron is in a π orbital which lies normal to the σ bonding plane. The π states are more weakly bonded than the σ states, and are situated close to the Fermi level. This difference in the bonding configuration between diamond and graphite is responsible for the differences in their properties.

A variety of non-crystalline carbon due to the allotropic nature of carbon are intermediate structures between diamond and graphite, with varying amounts of sp^3 and sp^2 bonded carbon depending on deposition conditions. The sp^2 forms of non- crystalline carbon are the best known. This includes amorphous carbon with high concentration of sp^2 carbon. Under appropriate deposition conditions, it is possible to produce diamond-

like carbon (DLC), which is characterized by a high content of sp^3 bonded carbon. DLC exhibit properties similar to diamond (high band gap, high atomic density, high hardness, chemical inertness, optical transparency and a low coefficient of friction [21]), and consists of both amorphous carbon and diamond crystallites.

The electron structure of diamond and graphite has been widely investigated and are well established [22]. Recently, electronic structure calculations of a-C and a-C:H has been performed on a number of model structure containing different concentrations of sp^3 and sp^2 bonded carbon [23]. These studies concluded that the π states form the valence and the conduction band edge that control the electronic properties, such as band gap, whereas, the σ bands control the extended states and the mechanical properties of the material. The degree of disorder in a σ bonded system such as variation in coordination number, bond length and bond angle determines the σ band gap (tailing of localized states) [20]. While, disorder in a π system results in a range of band gap depending on the medium range correlation between π states [23]. Experimentally, it is found that the band tail broadens into the gap region with increasing levels of structural disorder, causing a shift in the optical gap towards lower energies [24, 20, 23, 25].

References

1.. A. Einstein, Ann *Physik* **17**, 132 (1905)

2. W.E. Spicer, *Phys. Rev.* **112**, 114 (1958).

3. N.V. Smith, *Phys. Rev.* **B3**, 1862 (1971).

4. D.A. Shirley, ed.: *Electron spectroscopy. Proc. of the Int. Con.*, Asilomar (calif.) Sept.

1997, North Holland, Amsterdam 1972, pp. 487.

5. B.H. Bransden and C.J. Joachain, *Physics of Atoms and Molecules,* John Wiley & Sons, Inc., New York (1990), pp. 155-193.

6. A.P. Alivsatos, *J. Phys. Chem.* **100**, 13226 (1996).

7. H. Ibach, *Electron Spectroscopy for Surface Analysis, (Topics in Current Physics*; V. **4**), Springer- Verlag Berlin Hiedeberg, 19977, pp. 4.

8. C.N. Berglund and W.E. Spicer, *Phys. Rev.* **136**, 1030 (1964).

9. J.T. Devreese, A.B. Kunz, T.C. Collins, *Elementary Excitations in Solids, Molecules, and Atoms* (Plenum Press, London 1974).

10. P.J. Feidelman, D.E. Eastman, *Phys. Rev.* **B 10**, 4932 (1974).

11. N.E. Christensen, B. Feuerbacher, *Phys. Rev.* **B 10**, 2349 (1974).

12. B. Feuerbacher, N.E. Christensen, *Phys. Rev.* **B 10**, 2373 (1974).

13. C.Bandis and B.B. Pate, *Rev.* B **52,** 12056 (1995).

14. J.van der Weide, Z. Zhang, P.K. Baumann, M.G. Wensell, J. Bernholc, and R.J. Nemanich, *Rev.* **B 50**, 5803 (1994).

15. R.H. Fowler, *Phys. Rev.* **38**, 45 (1931).

16. E.O. Kane, *Phys. Rev.* **127**, 131 (1962).

17. G.W. Gobeli and F.G. Allen, *Phys. Rev.* **127**, 141 (1962).

18. D.Long, *Energy Bands in Semiconductor*, John Wiley, New York (1968) pp. 197.

19. R. Dalven, *Introduction to Applied Solid State Physics*, Plenum Press, New York, (1980) pp. 145.

20. D. Das Gupta, F. Demichelis, C.F. Pirri, R. Spagnolo and A. Tagliaferro, *Diamond and Diamond-Like Films and Coating*, Edited by R.E. Clausing, Plenum Press, New York, (1991), pp. 427.

21. J. Robertson, *Diamond and Diamond-Like Films and Coating*, Edited by R.E. Clausing, Plenum Press, New York, (1991), pp. 331.

22. F.J. Himpsel, J.F. van der Veen, and D.E. Eastman, *Phys. Rev.* **22**, 1967 (1980).

23. J. Robertson and E.P. O'Reilly, *Phys. Rev.* **B 35**, 2946 (1986).

24. R.A. Street, T.M. Searle, I.G. Auatin, and R.S. Sussmann, *J. Phys.* C **7**, 1582 (1974).

25. T. Tiedje, and J.M. Cebulka, *Phys. Rev.* B **28** 7075 (1983).

CHAPTER 3

EXPERIMENTAL TECHNIQUES AND SET-UP FOR THE GROWTH AND CHARACTERIZATION OF CHEMICAL VAPOR DEPOSITION GROWN DIAMOND FILMS

3.1 Introduction

In this chapter, a description of the experimental techniques and experimental set-up for the growth and characterization of chemical vapor deposition (CVD) grown diamond films are described. Polycrystalline diamond films were grown on single crystal p-type silicon substrates using the hot tungsten filament CVD technique from a mixture of methane and hydrogen gases. Also, boron and nitrogen doped polycrystalline diamond films were grown using a gas mixture of diborane and nitrogen gases, respectively. Abrasion and bias enhanced nucleation methods were used to increase the nucleation density of diamond crystallites on the Si substrates. The effects of methane, boron and nitrogen concentrations on the photoelectron emission properties of the grown films were investigated using different characterization techniques. Laser Raman spectroscopy and x-ray photoelectron spectroscopy (XPS) were used to characterize the sp^2 and sp^3 carbon

content of the diamond films, and determine the sp^3/sp^2 carbon fraction. Scanning electron microscope (SEM) was used to characterize the surface morphology. The photoelectric threshold of the CVD diamond films were determined by measuring the energy distributions of photoemitted electrons using ultraviolet photoelectron spectroscopy (UPS), and by measuring the photoelectric current as a function of incident photon energy.

3.2 Chemical Vapor Deposition Growth System

The pioneering work by Augus [1] and Spitsyn [2] on deposition of diamond films using a CVD process has led to considerable interest in the use of diamond for semiconductor applications. Many different techniques are employed to grow diamond films using CVD, but all have some basic features in common. For example, in CVD growth of diamond films, it is essential to activate the mixture of hydrocarbon and hydrogen gases to generate atomic hydrogen and carbon radicals, as described below. The means by which such activation is accomplished varies considerably. Examples of activation techniques include thermal [3], plasma [4,5], and use of a combustion flame [6].

Atomic hydrogen is produced by catalytic dissociation of the hydrogen molecule on the hot-tungsten filament surface [7]. It has been reported that atomic hydrogen prevents the formation and growth of graphitic carbon by etching sp^2 carbon [8], and also stablizes the diamond surface preventing surface reconstruction into sp^2 bonded carbon [9]. In addition, it is theorized that atomic hydrogen can create a radical sites by

abstraction of hydrogen atom on the surface carbon atoms [10]. In general, the ratio of carbon radicals to atomic hydrogen determines diamond film quality. An increase in methane concentration is known to result in a higher percentage of non-diamond forms of carbon [11].

As discussed above, CVD growth of diamond involves high concentrations of atomic hydrogen and carbon radicals. The concentrations of these growth species on the surface of the substrate or growing film depend on growth conditions, such as gas pressure, filament and substrate temperatures and geometry of the reactor. It is obvious that the results of diamond deposition are subject to a large number of growth conditions [12]. For this reason experimental results from one deposition system to another are not easily reproducible. The CVD process used in our experiments uses a hot-tungsten filament at approximately $2{,}000^0$ C to activate the hydrogen and methane gases.

The nucleation of diamond crystallites on a non-diamond substrate is necessary for the growth of diamond films. The density of diamond nucleation on non-diamond substrates is extremely low. For a mirror polished Si substrate, a nucleation density of less than 10^{-5} cm is typical, resulting in the growth of separate crystallites rather than a continuous diamond film [13,14]. In order to increase the nucleation density of Si substrates, one applies surface pretreatment. A common surface pretreatment technique is abrasion of the substrates using diamond grit. Using this technique nucleation densities are found to increase by several orders of magnitude and continuous polycrystalline diamond films can be easily grown [15]. In our experiments, the abrasion technique was

used to enhance diamond nucleation on Si substrates for the growth of boron and nitrogen doped polycrystalline diamond films. This was accomplished by polishing the substrate using diamond powder having approximately 1 μm particle size. After polishing, the substrate was cleaned by ultrasonic agitation using acetone and methanol, and then rinsed in triple distilled water. This method produced a rough surface with a high nucleation density. However, a disadvantage of the this method is that it cannot be performed with the sample in-situ in the growth chamber. Another method that has been successful in enhancing diamond nucleation on Si substrates is ion bombardment of the substrate, also referred to as bias enhanced nucleation (BEN) [16, 17, 18]. In general, BEN is performed by applying a negative bias of a 100-200 V to the substrate with respect to the filament as described below. This process is reproducible, controllable, and can be performed in-situ. Under certain growth conditions, BEN followed by the growth process has produced highly oriented diamond films on silicon (100) substrates [19, 20].

A series of polycrystalline diamond films were grown in a CVD system designed and constructed at the University of North Texas Scanning Tunneling Microscopy laboratory. In this system, diamond films were grown on a heated substrate from a mixture of methane and hydrogen gases activated by a hot-tungsten filament placed approximately 1" from the substrate. This simple technique offers excellent control of film morphology and reproducibility. This technique is a well known CVD method in wide use by the semiconductor industry. Figure 3.1 shows the hot-tungsten filament CVD system used in our studies. The CVD system consists of a growth chamber equipped with

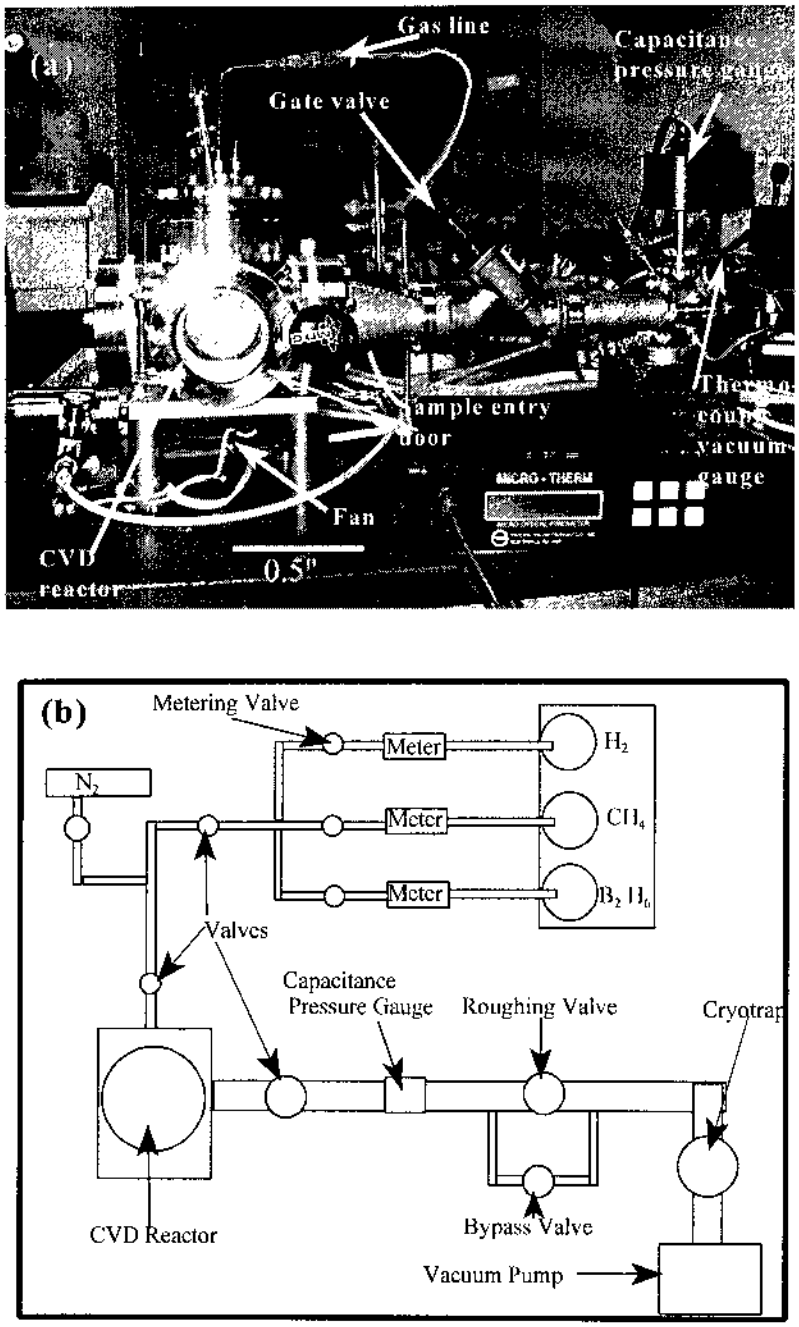

Figure 3.1. CVD growth system: (a) A photographic picture of the CVD growth system showing details of the experimental setup (b) a schematic diagram of the CVD growth system.

gas feed throughs and controllers, coaxial water cooled copper power leads for substrate heating, a liquid nitrogen trap and a two stage rotary pump. The cooling of the copper power leads is necessary to prevent them from overheating at growth temperatures that are typically 600-900^0 C. A glass window located in front of the growth chamber allows the sample to be viewed by a pyrometer for non-contact substrate and filament temperature measurements.

The substrates used for our studies were p-type Si wafers with (100) crystallographic orientation. The wafer was cut with a diamond scribble into a rectangular pieces of approximately 0.04" in width and 0.06" in length. The Si substrate was wrapped with molybdenum foil and then attached to a sample holder. The sample holder consists of a quartz plate with four copper electrodes attached on each side with a copper screw, as shown in figure 3.2. These electrodes provide power to heat the filament and substrate. A tungsten filament wire approximately 0.001" in diameter and 1.5" in length was mounted parallel to and approximately 1" above the substrate. The sample holder was then mounted inside the growth chamber with four copper screws.

After the substrate was loaded into the growth chamber, the chamber was evacuated to $< 9 \times 10^{-3}$ Torr using a rotary vacuum pump. High purity hydrogen gas having a purity of 99.99% was introduced into the chamber. The gas pressure in the growth chamber was controlled by a bypass valve and maintained at a constant pressure of approximately 30 Torr to 38 Torr depending on the growth conditions. The gas pressure was monitored using a capacitance-type manometer.

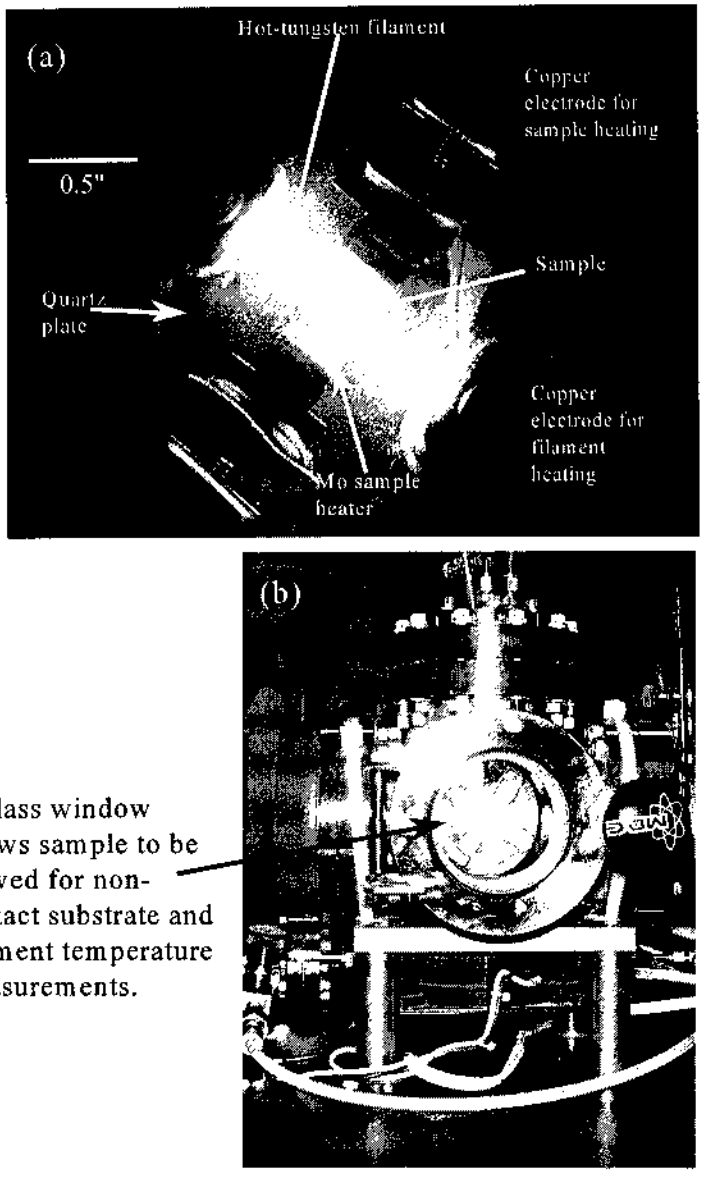

Figure 3.2. Detailed picture of the sample holder taken during diamond growth. (a) The filament and substrate temperatures were approximately 2200^0 C and 800^0 C, respectively (b) Shows the sample holder inside the CVD system.

In order to apply a negative bias voltage to the substrate for BEN, the substrate electrode was connected to the negative terminal of a dc power supply and the entire chamber was grounded. The substrate was heated by resistively heating the molybdenum foil that was wrapped around the substrate, as described previously. This arrangement maintained adequate thermal contact between the substrate and the molybdenum foil. The substrate was gradually heated until the operating temperature of approximately 800^0 C was reached. The tungsten filament was then turn on and maintained at approximately 2200 ^{0} C by adjusting the current to 6 A. The temperature of the filament and substrate were measured using a disappearing type optical pyrometer. High purity methane gas having purity of 99.99% was then introduced into the growth chamber at a flow rate that depended on growth condition.

Prior to diamond growth the BEN process was performed by applying a negative bias of about 320 V to the substrate relative to the chamber for 30 minutes. This subjected the substrate to positive ion bombardment. The distance between the substrate and the filament during the BEN process was approximately 1". When the voltage was first applied, no emission current between the filament and the sample was observed. As the voltage was increased to -284 V, an emission current of approximately 10 mA was observed and the gas began to visibly glow blue. Further increase in voltage resulted in an increase in emission current, and an increase in the intensity of the glow discharge. The emission current at -320 V was approximately 100 mA. Due to the flatness of the substrate, confining the plasma to the region between the substrate and the filament was

problematic. As the bias voltage was increased, the plasma preferentially forward at sharp points inside the growth chamber where the electric field strength was high [21]. To overcome this unwanted effect, a tungsten wire approximately 1 mm in diameter was wound in the shape of a circular disk with a surface area approximately to that of the substrate. The circular disk was attached to the grounded inlet gas tubing inside the growth chamber. The position of this circular disk was aligned between substrate and the filament so as confine the plasma above the substrate.

After the BEN step, the negative bias on the substrate was turned off and a continuous diamond film was deposited for approximately 4-6 hours at a substrate temperature of 870 ^{0} C. The flow rate of hydrogen in all the experiment was 200 standard cubic centimeter per minute (sccm) and the methane flow rate was varied from 0.20 to 1.60 sccm depending on the experimental specification. To achieve doping of the diamond films, diborane or nitrogen gas was introduced into the gas mixture during the growth process. Temperatures of the tungsten filament and the substrate were monitored with an optical pyrometer. The growth process was terminated by first shutting of the methane flow while maintaining the sample, filament, and hydrogen settings. Then the filament, sample heater and hydrogen flow were turned off, respectively.

3.3 Scanning Electron Microscope (SEM)

The effects of methane, boron and nitrogen concentrations on the surface morphology of polycrystalline diamond films were examined using SEM. An examination of the surface structure of CVD diamond films is important in explaining the properties of such films.

A Jeol T-300 Scanning Electron Microscope, operating at a maximum voltage of 25 keV was used to obtain SEM images of the diamond films. It consists of an electron column, vacuum pumping system, sample chamber and electronic control and imaging systems. The operational principle of the scanning electron microscope is illustrated in figure 3.3. The electron column consists of the electron gun that produces a beam of electrons by thermionic emission from a tungsten filament. These electrons are accelerated by a voltage in the range of 5-25 KeV down the center of the electron column and through magnetic lenses. These lenses reduce the diameter of the electron beam to less than 1 μ size, which is then focused and scanned across the surface of the diamond film. Incident electron beam on the diamond surface generates a large number of secondary electron emission. The secondary electrons are collected at a positively biased collector coated with a scintillator material that generates photons in proportion to the number of electrons. The photons pass down to a photomultiplier detector that produces an electrical signal in proportion to the number of photons. The signal is displayed on a cathode ray tube or photographically using a polaroid type 52 film.

3.4 Raman Spectroscopy

Raman spectroscopy utilizes inelastic scattered light from lattice collisions to characterize the phonon energies of materials. It is also sensitive to internal stress [22]. Electron energy loss spectroscopy (EELS) [23] and nuclear magnetic resonance (NMR) [24] have all been used to show the presence of diamond in CVD diamond films. However, they provide little or no information on the various nanocrystalline or highly

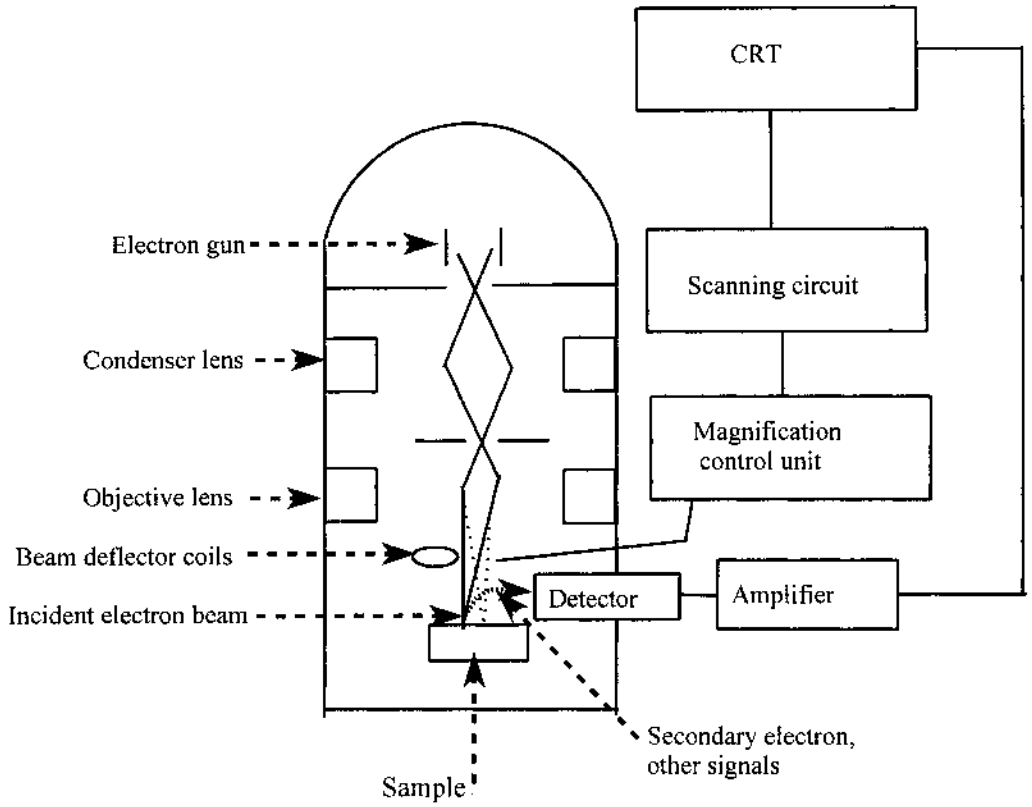

Figure 3.3. Principle of Scanning electron microscope.

disordered carbon phases that are often present in CVD diamond films. It is because of these difficulties that Raman spectroscopy is commonly used in characterizing carbon materials.

The Raman spectra for this study were obtained by using a combination of Ar laser, spectrometer and a photomultiplier. Figures 3.4 show a schematic of the experimental set-up. It consists of a Innova 90 Ar ion laser capable of operating at a

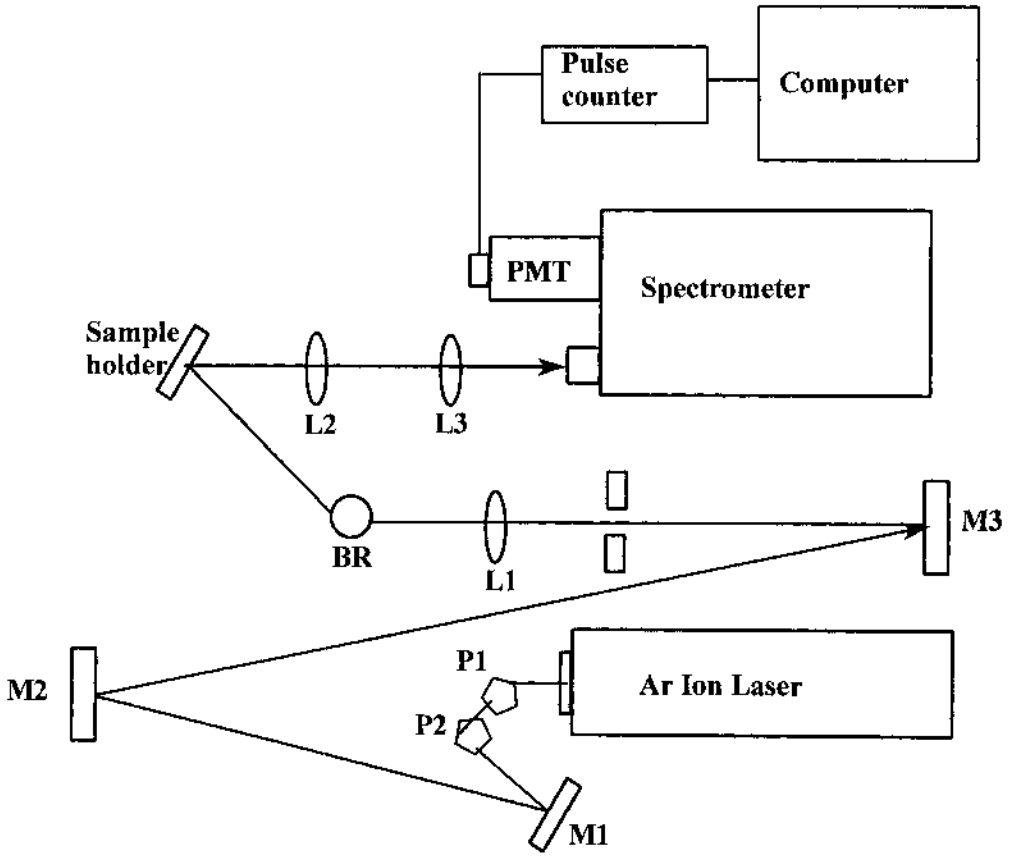

Figure 3.4. Schematic of Raman spectroscopy system. M, L and BR represent mirrior, Lens and beam reflector, respectively.

maximum power of 5 watts, with a range of visible lines from 4579 Å to 5145 Å. With this variety of laser lines a broad range of incident photon energies from 2.70 to 2.41 eV can be selected by using a prism located at the focus of the laser beam within the laser cavity. The incident laser beam emerging from the cavity passes through two prisms and a long optical path to the spectrometer. This configuration is necessary to suppress unwanted laser lines or plasma frequencies from the incident laser beam. Using a lens of 50 cm focal length (Lens 1), the laser beam is focused onto the diamond sample through a

beam reflector (BR). The resulting scattered radiation is gathered by the collecting lens (Lens 2) and focused to another lens (Lens 3). This lens then direct the scattered radiation to the entrance slit of the Spex 1404 double monochromator with 1200 grooves/mm grating. The spectrometer separates the scattered radiation spatially on the basis of the frequency. The double monochromator is essential to separate the Raman photons from large number of Rayleigh photons. At the exit slit of the spectrometer the Raman signal forms an image of a series of faint lines. By scanning the spectrometer, these lines move in succession across the exit slit and are detected by using a Hamamatsu GaAs photomultiplier tube attached to the exit port. The Raman signal generate photoelectron from the photocathode of the photomultiplier which is accelerated and amplified through a series of dynodes to a pulse of about 10^{10} electrons. The electrons are converted into voltage pulse which is processed and displayed by a computer.

. The Raman data were analyzed with a commercial software program called peakfit [25]. The Raman spectra are peak fitted with Gaussian and Lorentzian line shape to identify contributing peaks to the spectrum. From the fitting parameters, the peak position, half-width, intensity ratio, and the area under each peak were obtained. These parameters provide information about the material properties of the polycrystalline diamond films.

3.5 Photoelectron Spectroscopy (PES)

In photoelectron spectroscopy (PES) photons of well defined energy (hv) are absorbed by the sample resulting in excitation of the sample. If the photon energy is

greater than the work function of the sample, electron emission will occur. Information about the sample electronic structure can be extracted by analyzing the energy distribution of the emitted electrons for a fixed incident photon energy or the photoelectron current as a function of incident photon energy. The emitted electrons can come from the core, valence band or conduction band depending on the type of radiation used for the excitation process. For example, with ultraviolet radiation, only electrons from the valence or conduction band states are observed, while with X-ray, emission of electrons from the core levels is possible.

A Vacuum Generator Scientific, VG ESCA LAB Mark 11 system was used to obtain the spectra of the electron energy distribution of the polycrystalline diamond films. With the UPS and XPS, the mode of operation is to fix the incident energy and measure, as a function of energy the number of emitted photoelectrons. A schematic of the experimental apparatus is shown in figure 3.5. CVD diamond samples were loaded from the preparation chamber with a load lock into the analytical chamber. The preparation chamber was evacuated with a turbor molecular pump to a pressure of 1 x 10^{-6} torr. XPS and UPS measurements were done in an ultra-high vacuum (UHV) at a base pressure of 1 x 10^{-9} torr. This pressure was achieved by using an ion pump and a Ti-sublimation pump.

The photoelectron spectra were collected by irradiating the diamond film with Mg K_{α} X-rays (1253.5 eV) photons from a dual anode X-ray source or ultraviolet light (4.89, 5.64, 5.90 eV) from a discharge lamp operated with xenon. A hemispherical electrostatic energy analyzer with analyzer pass energy typically set at 10 eV. After passing through

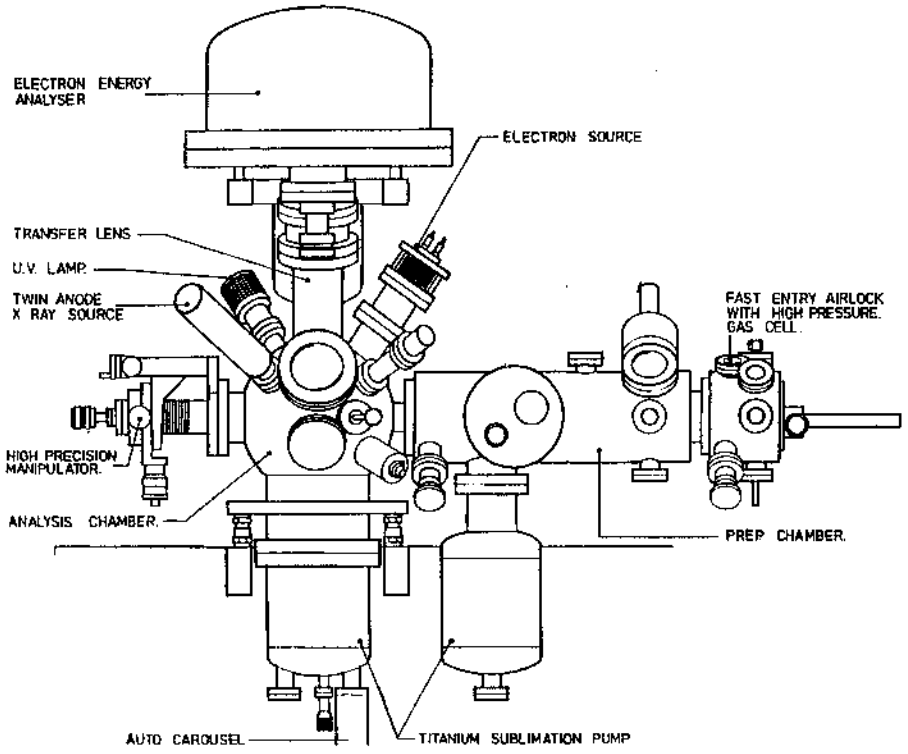

Figure 3.5. Schematic of the XPS and UPS apparatus. (Adapted from the VGS ESCA LAB Mark 11 system manual)

the analyzer, the electrons are detected by using an electron channel multiplier (channeltron).

For the XPS spectra, survey scan were collected in the 1000 to 0 eV binding energy region. The analyzer pass energy was set to 10 eV. The dwell time was set at

0.85 s with a step size of 0.5 eV. Regional scans, 283-290 eV for the core carbon spectra and 295-325 eV for the associated characteristic loss spectra (plasmon peaks) were obtained. XPS and UPS spectra were analyzed using a peakfit [25]. From the fitting parameters the peak positions, hence the binding energies were obtained which are identify with sp^3 and sp^2 form of carbon. Since the ionization cross section for XPS core level spectra are dependent on atomic factor, when the incident radiation is well above the absorption egde of the core level [26]. The intensity of the core level peaks is then directly proportional to the concentration of atomic species in the film. On this basis, the ratio of sp^3 to (sp^3 + sp^2) were quantified from area ratios of the XPS core level. The same procedure was applied to the plasmon loss spectra to obtain a semi-quantitative analysis.

For UPS spectra, the analyzer pass energy was set at 20 eV. The dwell time was maintained at 0.85 s with a step size of 10 meV. The same peak fitting procedure was the concentration of atomic species in the film. On this basis, the ratio of sp^3 to (sp^3 + sp^2) were quantified from area ratios of the XPS core level. The same procedure was applied to the plasmon loss spectra to obtain a semi-quantitative analysis.

For UPS spectra, the analyzer pass energy was set at 20 eV. The dwell time was maintained at 0.85 s with a step size of 10 meV. The same peak fitting procedure was used as in XPS spectra. The photoelectric work function of the polycrystalline diamond films were obtained by using the following equation: $\Phi = h - E_{max}$.

3.6 Photocurrent Measurements

In this experiment, all photoelectrons were collected as a function of the incident photon energy to obtain the photoelectric threshold. The basic experimental set-up is shown in figure 3.6. CVD diamond film was placed at the center of an analytical chamber equipped with quartz silica window. The chamber was evacuated and maintained at about 10^{-8} torr by a turbomolecular pump. The photoelectric measurements were carried out by exciting electron emission from the diamond surface using ultraviolet light from a 150 watts xenon high pressure arc lamp in combination with a grating monochromator as shown in figure 2.8. The energy of the incident photons was varied from 3.0 to 6.0 eV in 0.07 eV increments using the monochromator. The light was chopped with a mechanical chopper at a frequency of 167 Hz in order to improve the signal to noise ratio. The Light was focused with a lens through a quartz window on the sample at normal incidence. This way the scattered light in the chamber is reduced by allowing reflected beam to pass out the same window through which it entered. The photoelectrons were collected using 0.01 inch diameter tungsten wire grid positioned approximately 2 mm from the diamond sample. All other surfaces in the chamber also serve as collectors. The photocurrent leaving the sample were converted to voltage and pre-amplified by a factor of 10^7. The voltage was measured using a Stanford Research SR850 lock-in amplifer.

Data of photocurrent versus incident photon energy in the region near the threshold were analyzed by fitting it to a polynomial of the order 3/2. The onset of photoemission (threshold) was obtained by extrapolating the curve to zero and the

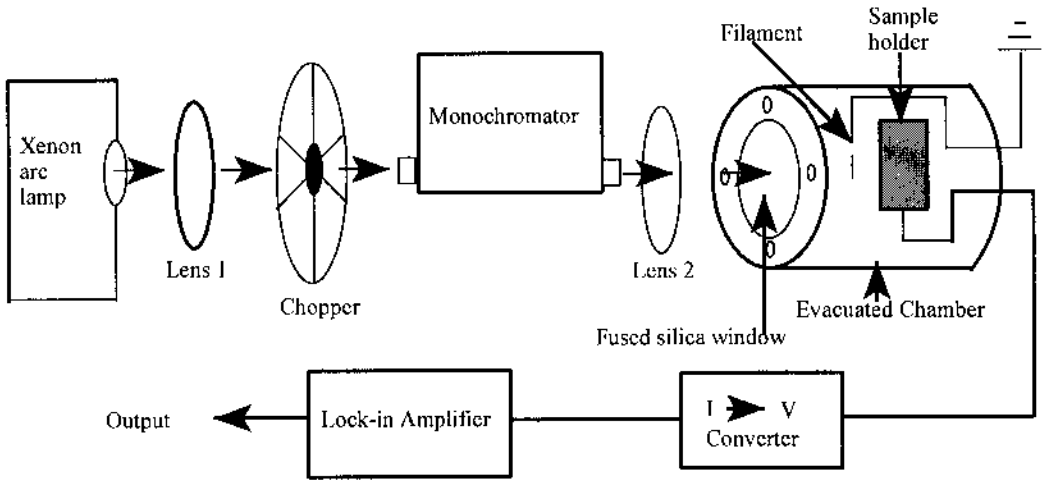

Figure 3.6 Schematic of the experimental setup for photocurrent measurements.

functional form of the curve was used to determine the emission mechanism.

References.

1. J.C. Augus, *Proc. First Internat. Sympos. on Diamond and Diamond-like Films*, edited by J.P. Dismukes, The Electrochemical Society, Pennington, N.J.,(1989), pp. 1-13.

2. B.V. Spitsyn, L.L. Bouilov, and B.V. Derjagin, *J. Crystal Growth* **52**, 219, (1981).

3. S. Matsumoto, Y. Sato, M. Kamo, and N. Setaka, *Jpn. J. Appl. Phys.* **21**, L183 (1982).

4. M. Kamo, Y. Sato, S. Matsumoto, and N. Setaka, *J. Cryst. Growth* **62**, 642 (1983).

5. A. Badzian, T. Badzian, R. Roy, R. Messier, and K. Spear, *Mat. Res. Bull.* **23**, 531

(1988).

6. L.M. Hanssen, W.A. Carrington,J.E. Butler, and K.A. Snail. *Mater. Lett.* **7**, 289 (1988).

7. I. Langmuir, *J. Am. Chem. Soc.* **37**, 417, (1915).

8. Y. Saito, K. Sato, H. Tanaka, K. Fujita, and S. Matsuda, *J. Mater. Sci.* **23,** 842 (1988).

9. B.B. Pate, *Surf. Sci.* **165**, 83 (1986).

10. M. Frenklach, *Diamond and Diamond-Like Films and Coatings*, Edited by R.E. Clausing et al., Plenum Press, New York, (1991). pp. 499-523.

11. T.D. Moustakas, *Solid State Ionics* **32/33**, 861 (1989).

12. R.T. Anthony, *Diamond and Diamond-Like Carbon and Coatings*, edited by R.E. Clausing, L.L. Horton, J.C. Augus, and P. Koidl (Plenum Press, New York, 1991).

13. P.K. Bachmann, W. Drawl, D. Knight, R. Weimer, and R.F. Messier, in Extented Abstracts No. **15**, *Diamond and Diamond-like Material Synthesis*, edited by G.H. Johnson, A.R. Bazdzian, and M.W. Geis (Material Research Society, Pittsburgh, PA, 1988), pp. 99-102.

14. E. Molinari, R. Polini, M.L. Terranova, P. Ascerelli, and S. Fontana, *J. Mater. Res.* **7**, 1778-1787 (1992).

15. B.R. Stoner, G.H. Ma, S.D. Wolter, and J.T. Glass, Phys. Rev. B, 11067 (1992).

16. S. McGinnis, M. Kelly, and S. Hagstrom, Appl. Phys. Lett. 66, 3117 (1995).

17. Q. Chen, J. Yang, and Z. Lin, *Appl. Phys. Lett.* **67**, 1853 (1995).

18. F. Stubhan, M. Ferguson, and H.J. Fusser, *Appl. Phys. Lett.* **66**, 1900 (1995).

19. B. Stoner and J. Glass, *Appl. Phys. Lett.* **60**, 698 (1992).

20. S. McGinnis, M. Kelly, and S. Hagstrom, and R. Alvis, *J. Appl. Phys.* **79**, 170 (1996).

21. J.D. Jackson, *Classical Electrodynamics*, Second Edition, John Wiley and Sons Inc, New York, (1975), pp. 75-78.

22. M. Yoshikawa, G. Katagiri, H. Ishida, A. Ishitani, M. Ono, and K. Matsumara, *Appl. Phys. Lett.* **55**, 2608 (1989).

23. J. Buruley, and P.E. Batson, *Mat. Res. Soc. Symp. Proc. Vol.* **162**, 255 (1990).

24. K.M. Mcnamara, K,K, Gleason, and M.W. Geis, *Mat. Res. Soc. Symp. Proc. Vol.* **162**, 207 (1990).

25. Peakfit, Jandel Scientific, San Rafeal, CA.

26. E.M. Purcell, *Phys. Rev.* **54** 818 (1938).

CHAPTER 4

VARIATION OF THE PHOTOELECTRIC THRESHOLD OF POLYCRYSTALLINE CHEMICAL VAPOR DEPOSITION GROWN DIAMOND FILMS WITH $SP^3/(SP^3+SP^2)$ CARBON FRACTION

4.1 Introduction.

The effect of methane (CH_4) concentration on the $sp^3/(sp^3+sp^2)$ carbon fraction and photoelectron emission properties of CVD grown polycrystalline diamond films was investigated. Different $sp^3/(sp^3+sp^2)$ carbon fractions were obtained by varying the CH_4 concentration used during growth. We observed a continuous and significant decrease in the photoelectric threshold of the CVD grown diamond films as the fraction of sp^3 bonded carbon in the film decreases, where the fraction of sp^3 bonded carbon is defined as the ratio of sp^3 bonded carbon to sp^3 plus sp^2 bonded carbon ($sp^3/(sp^3+sp^2)$).

Field emission (FE) and secondary emission of electrons from CVD grown diamond films have been reported to occur at room temperature and low electric field [1, 2]. However, the mechanism responsible for the high electron emission is not clearly understood. Since diamond has a high work function, a number of mechanism have been

proposed to explain the field emission including: surface hydrogenation [3], defects [2], enhancement of the local electric field due to the sharpness of the diamond crystallites edges [4] and negative electron affinity (NEA) [2]. Attempts to lower the work function of diamond films include covering them with alkali metals such as Cs [5, 6], however alkali metals easily oxidize resulting in degradation of the field emission current.

Changes in the relative concentration of the sp^3 and sp^2 bonded carbon. Our main focus is to understand the effects of CH_4 concentration on the $sp^3/(sp^3+sp^2)$ carbon fraction and the resulting changes in photoelectric threshold energies. In the following sections, experimental procedure and the results of Scanning electron microscopy (SEM), Raman spectroscopy, x-ray photoelectron spectroscopy (XPS) and photoelectric measurements are presented.

4.2 Experimental

Polycrystalline diamond films were grown on polished Si substrates using a hot tungsten filament CVD reactor previously described. Smooth substrates, each about .5 x .25 x .025" in dimension were cut from a mirror-polished p-type silicon wafer with a diamond scribble (100) crystallographic orientation. The substrates were cleaned ultrasonically in acetone and rinsed in distilled water. The substrate was wrapped at each end by a molybdenum foil and then mounted on a sample holder in the deposition chamber, as shown in figure 3.2. The sample temperature was controlled by resistive heating of the molybdenum foil by passing a current of about 48 A through it. Hydrocarbon radicals were produced by using a hot tungsten filament wire of about

0.001" in diameter and 1.6" long, positioned approximately 1.2" from the substrate. The temperature of the tungsten filament and the substrates were monitored by an optical pyrometer corrected for emissivity. The growth chamber was evacuated by a two-stage rotary pump to about 10 milliTorr. A high purity hydrogen gas (99.99%) was introduced into the chamber. Then followed by introduction of CH_4 gas. The gas flow was monitored by mass flow meters and controlled using needle valves.

Initial diamond nucleation was achieved using bias enhanced nucleation. The substrates were dc biased at -320 volts for 30 minutes, relative to the filament and the vacuum chamber which were electrically grounded. The emission current was typically 100 mA. After this step, the bias was turned off and thin diamond film was deposited for 6 hours at a substrate temperature of 870^0 C and a pressure of 30 Torr using methane and hydrogen gases. The hydrogen flow rate was 200 standard cubic centimeters per minute (sccm) and the methane flow rate was varied from 0.40 to 1.60 sccm. The tungsten filament temperature was 2200^0 C.

The growth experiment was terminated by first shutting off the methane flow while maintaining the sample, filament, and hydrogen settings for 2 minutes. Then the filament, sample heater and hydrogen flow were turned off in the that order. The sample was transferred in air and mounted in a chamber equipped with a fused silica window. The chamber was evacuated by a turbomolecular pump to a pressure of about 10^{-8} Torr.

The photoelectric measurements were obtained by exciting electron emission from the surface using ultraviolet light from a 150 Watt Xenon arc lamp and

monochromator. The energy of the incident photons was varied from 3.0 to 6.0 eV in 0.07 eV increments using a monochromator. The light was chopped with a mechanical chopper at a frequency of 167 Hz and focused with a lens on the sample surface. Photoelectrons were collected using a 0.01 inch diameter tungsten wire grid positioned approximately 7.87 x 10^{-3} inches from the sample, and the photocurrent was measured using modulation techniques and a lock-in amplifier.

The Raman spectra were measured in the standard backscattering configuration using the 5145 Å line of an argon ion laser. The XPS measurement were made using a VG ESCALAB MARKII system with an energy resolution of 0.08eV in a vacuum $<10^{-10}$ Torr. The XPS spectra were acquired in the pulse-counting mode using Mg K_{α} line (1253.5 eV). A JEOL JSM-T300 scanning electron microscope (SEM) was used to examine the surface morphologies of the films. Details of the experimental procedure are described in previous chapter.

4.3 Surface Morphology

Figures 4.1-4.3 show the scanning electron micrographs of polycrystalline diamond films grown using CH_4 concentrations of 0.10%, 0.20%, 0.30%, 0.45%, 0.60% and 0.70%, respectively. Changes in surface morphology and crystallinity of the films are observed. As the CH_4 concentration increases, the film morphology is characterized by varying from non-continuous diamond crystals to a continuous diamond film with a decrease in average diamond crystallite size, consistent with previous report [7]. The average diamond crystallite size estimated from the SEM images is 1.25 μm, 0.75 μm,

0.54 μm and 0.25 μm, for the films grown using 0.20%, 0.30%, 0.45% and 0.07% CH_4 concentration respectively. As the crystallite size decreases, the number of grain boundaries between the crystallites increases.

The diamond film grown using 0.10% CH_4 concentration consists of well defined, randomly oriented (100) faces of diamond crystals as shown in fig. 4.1(a). The film is not continuous but shows a number of clusters because of the low density of crystals. This is due to the fact that after the initial nucleation, formation of new nuclei on the substrate does not occur [8]. The nuclei grow vertically and laterally as isolated crystals grow until they join neighbouring crystals to form a continuous film. As the CH_4 concentration is increased to 0.20%, a mixture of square (100) and triangular (111) faces are observed and the film coalesces into a continuous film, as shown in fig. 4.1(b). For a CH_4 concentration of 0.30%, the film becomes predominantly (111) orientation with large diamond facets, as shown in fig. 4.2(a). At higher CH_4 concentrations within the range of this study, the crystalline morphology become smaller and less defined. For example, for CH_4 concentrations greater than 0.30%, the crystallite size and surface roughness decreases. The films consist of continuous and densely populated small diamond crystals with a pyramidal shape (figs 4.2(b) and 4.3(a). At the highest CH_4 concentration (0.70%) the morphology is characterized by a small diamond crystals with no obvious crystallographic orientation, as shown in fig. 4.3(b).

4.4 Raman Spectroscopy Results

Figures 4.4 show the Raman spectra of diamond films grown using CH_4 concen-

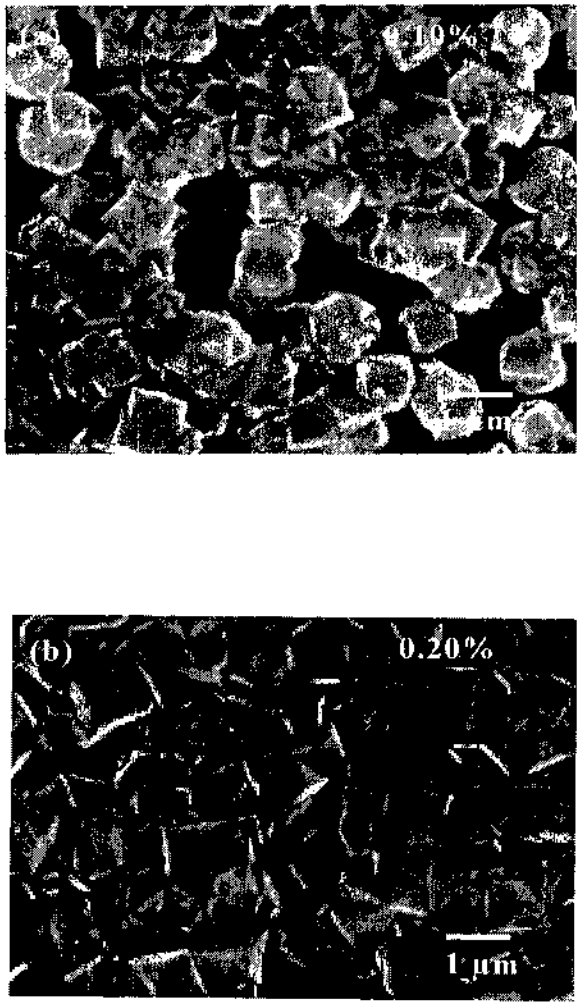

Figure 4.1. Scanning electron micrographys of chemical vapor deposition grown polycrystalline diamond films grown on Si substrates using (a) 0.10% (b) 0.20% CH_4 concentration.

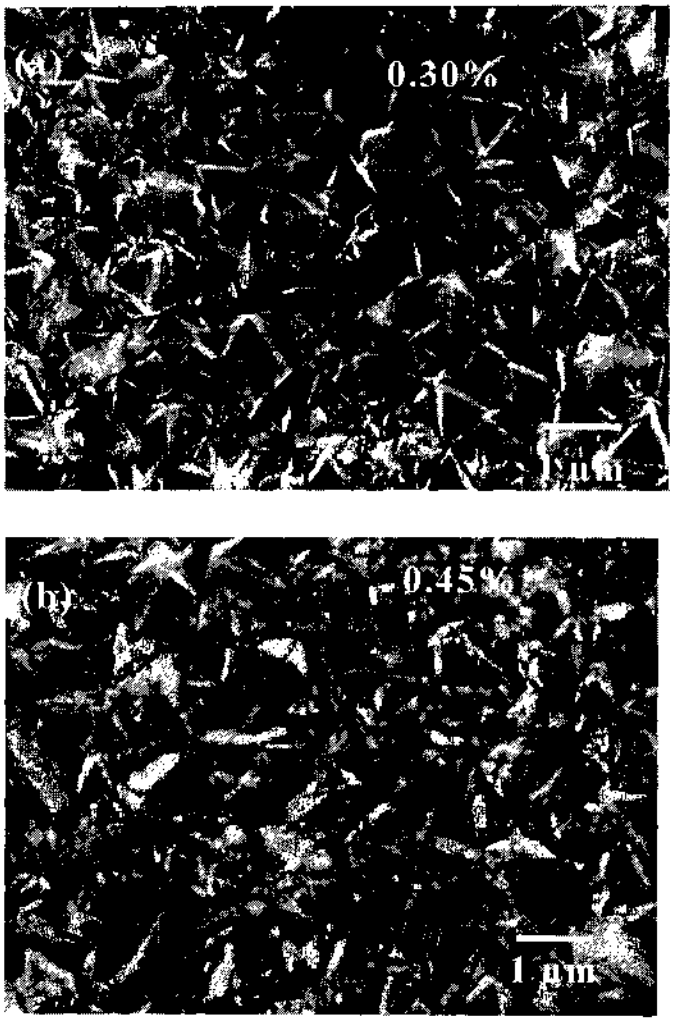

Figure 4.2. Scanning electron micrographys of chemical vapor deposition grown polycrystalline diamond films grown on Si substrates using (a) 0.30% (b) 0.45% CH_4 concentration.

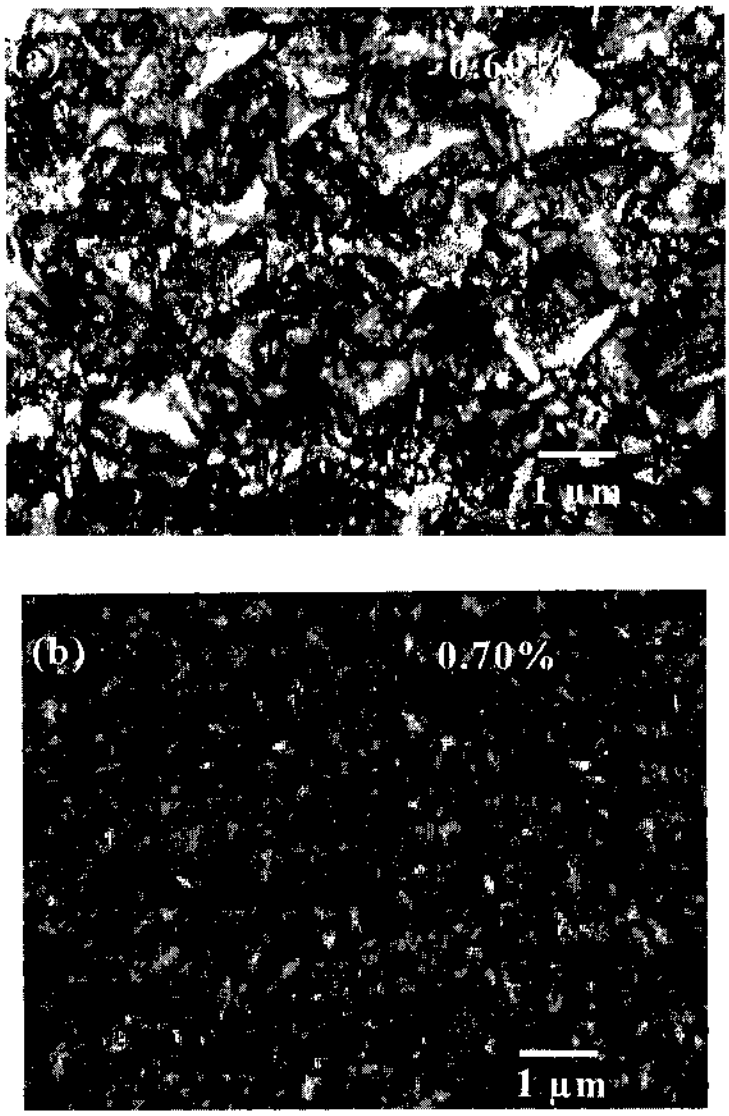

Figure 4.3. Scanning electron micrographys of chemical vapor deposition grown polycrystalline diamond films grown on Si substrates using (a) 0.60% (b) 0.70% CH_4 concentration.

trations of 0.10%, 0.20%, 0.30%, 0.45%, 0.60% and 0.70%, respectively. It is seen from figure 4.4 that the shape of the spectra vary as a function of the CH_4 concentration used during growth. The Raman spectra of the films show a sharp peak at about 1332 cm^{-1}, characteristic of single-crystal diamond (sp^3) [9,10] and a broad peak extending from around 1544 cm^{-1} to 1579 cm^{-1} that is attributed to sp^2 carbon or a random network of $sp^3$and sp^2 carbon [11]. The diamond peak is observed to decrease with increasing CH_4 concentration, while the sp^2 carbon peak increases with increasing CH_4 concentration, indicating structural changes.

In order to obtain numerical analysis of the Raman data, the Raman spectra are peak fitted with Gaussian and Lorentzian line shapes to identify contributing peaks to the spectrum. A numerical fitting program [12] was used to determine the intensities, peak positions, and Full width at half maxinium (FWHM) of the individual diamond line as well as the areas under each peak. The percentage of sp^3 bonded carbon in the films were determined from the ratio of the area under the single-crystal diamond peak at 1332 cm^{-1} to the total area under the spectrum.

A fit to the Raman spectrum of the film grown using a CH_4 concentration of 0.70% shows five characteristic peaks, as shown in figure 4.4(f). In fig. 4.4(f), Peak 1 at 1150 cm^{-1} is due to disordered or nanocrystalline diamond and a breakdown of the Raman selection rule for small crystallites [11]; Peak 2 at 1332 cn^{-1} is the single-crystal diamond; Peak 3 at 1350 cm^{-1} is due to disordered or nanocrystalline graphite, similar to the nanocrystalline diamond (peak 1), As long-rang translational symmetry is lost, the

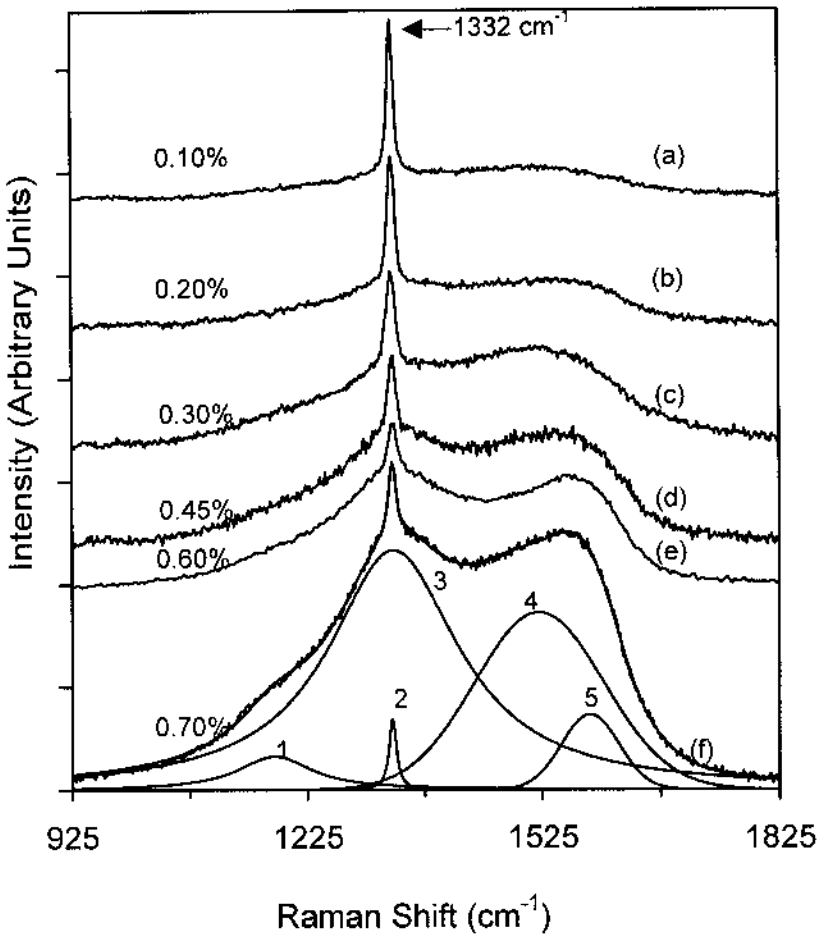

Figure 4.4. Compilation of the Raman spectra of chemical vapor deposition grown polycrystalline diamond films grown on Si substrate using 0.10%, 0.20%, 0.30%, 0.45%, 0.60% and 0.70% CH_4 concentrations. The percentage of CH_4 concentrations is indicated beside each spectrum. The peaks labeled 1-5 in the fit are discussed in the text.

crystal momentum may no longer be conserved, and phonons with any **K** vector may contribute to the spectrum. Peak 4 at 1527 cm^{-1} is due to sp^3-sp^2 carbon networks; and Peak 5 at 1579 cm^{-1} is due to single-crystal graphite [7, 11]. Peaks 1, 3, 4 and 5 are Gaussian because these transitions involves exchange of phonons. Peak 2, corresponding to crystal diamond, is Lorentzian because the excitation laser line has a Lorenzian profile. This line is determined by the lifetime of the excited Ar ions and does not involve exchange of phonons. When phonon interactions occur, the Lorentizan line broadens and becomes Gaussian. However, with the exception of peak 2 the particular line shapes used to fit the experimental data do not affect the results. These results show that CVD diamond films exhibit a range of structures consisting of sp^3, sp^2 and sp^3-sp^2 carbon.

The Raman integrated intensity was analyzed as a function of CH_4 concentration to show the structural properties of the films. Figure 4.5 shows a plot of the intensity as a function of CH_4 concentration used during growth. Figure 4.5 shows that the intensity of the sp^3 carbon with respect to sp^2 carbon decreases sharply from 1.34 to 0.24 as the CH_4 concentration increases from 0.10% to 0.45% and then decreases slowly at higher CH_4 concentrations. The increase in the proportion of the sp^2 bonded carbon with increasing CH_4 concentrations is consistent with structural phase transformation. The high intensity ratio observed for films grown at lower CH_4 concentrations is a characteristic of good quality diamond film.

Area analysis of the Raman spectra shows that, as the CH_4 concentration increases, the area under the sp^3 peak at 1332cm^{-1} decreases with respect to the total area

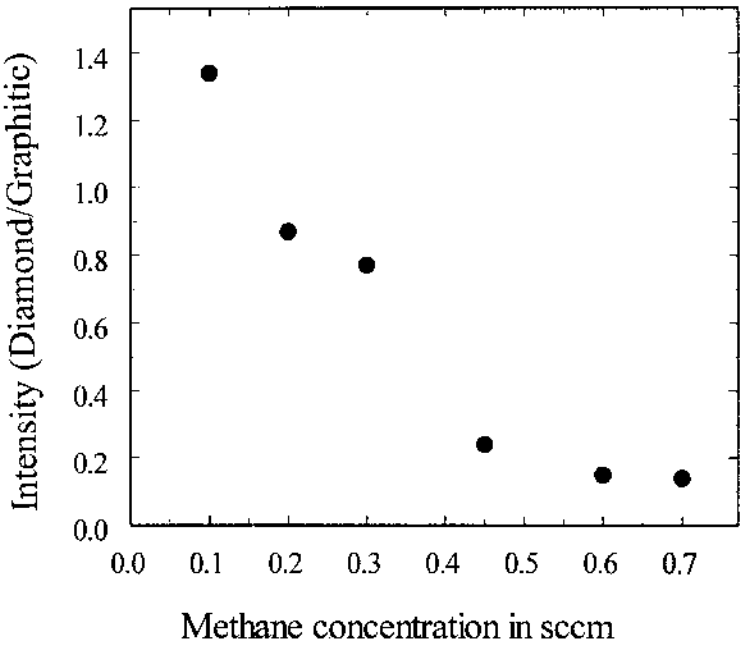

Figure 4.5. Raman integrated intensity as a function of methane concentration used during growth.

under the peaks, as shown in figure 4.6. It is seen from figure 4.6 that the fraction of sp^3 bonded carbon decreases from 15.1 to 1.06 or, equivalently, that the fraction of sp^2 bonded carbon increases from 1.06 to 15.1 as the CH_4 concentration increases from 0.10% to 0.70%. It is important to note that the decrease of sp^3 carbon as the CH_4 concentration increases coincides with the decrease in the intensity ratio. These results strongly suggest that the films grown at lower CH_4 concentration contain mostly sp^3

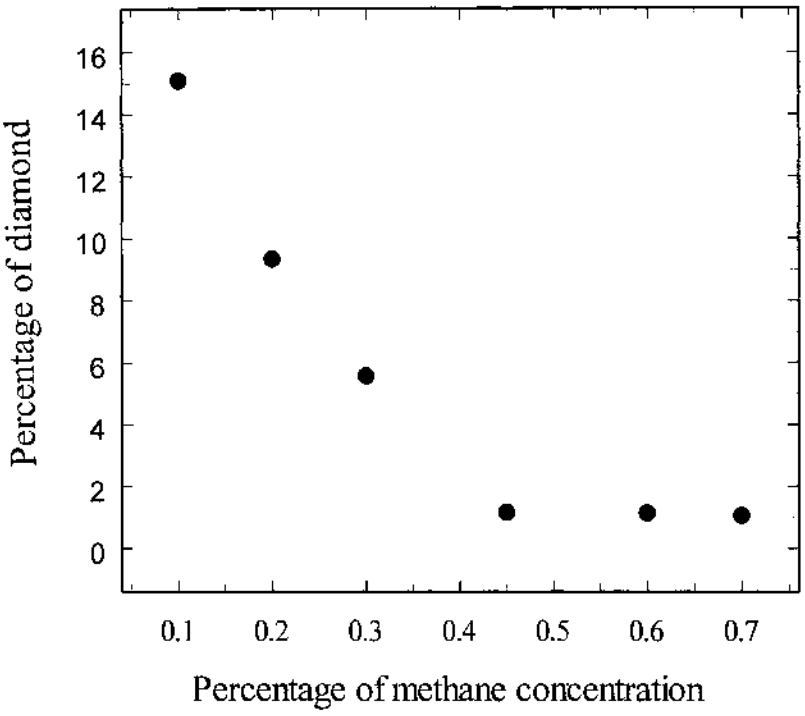

Figure 4.6. Percentage of diamond content Raman as a function of methane concentration used during growth.

carbon, with only a very small fraction of the sp^2 bonded carbon, indicating good crystallinity. This is consistent with the SEM images that show large diamond crystals at lower CH_4 concentrations.

The FWHM of the diamond peak is a qualitative measure of the perfection of the diamond structure [13, 14]. In order to determine the structural quality of the CVD

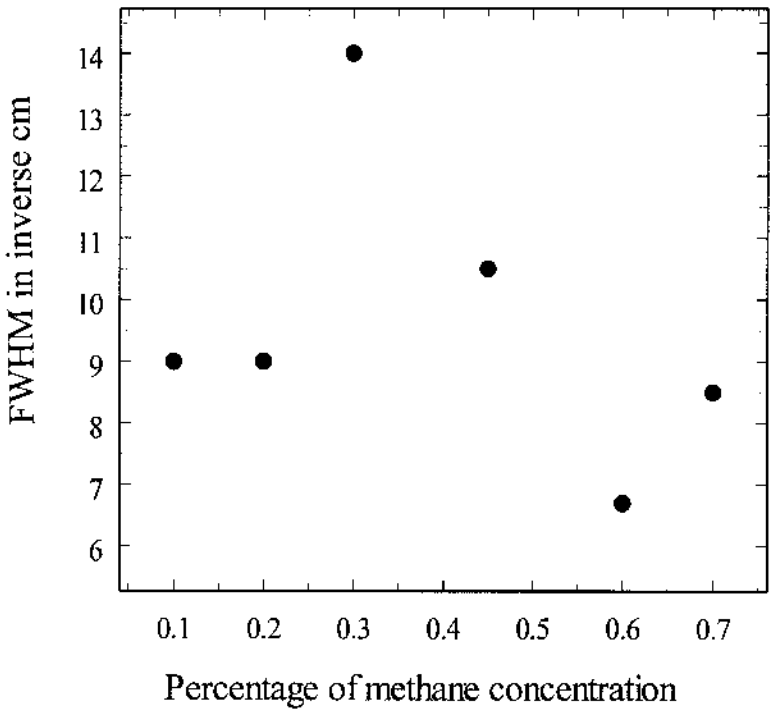

Figure 4.7. FWHM of the Raman diamond peaks as a function of methane concentration used during growth. The FWHM shows no correlation with the methane concentration.

polycrystalline diamond films, the diamond linewidth was analyzed as a function of CH_4 concentration. The FWHM of the Raman diamond peak at 1332 cm^{-1} of the above films is shown in figure 4.7 as a function of CH_4 concentration. Interestingly, closer examination of the FWMH revealed no apparent correlation with the CH_4 concentration used during growth. As can be seen in figure 4.7, the FWHM of the diamond peak varies

inconsistently with CH_4 concentration. The FWHM is about 9.0 cm^{-1} for the films grown using 0.10% and 0.20% of CH_4 concentrations, and then increases to maxinium value of about 14.0 cm^{-1} for the film grown at 0.30% CH_4 concentration, then decreases to a minimum value of about 6.7 cm^{-1} for the film grown at 0.60% CH_4 concentration and then increased slightly to 8.5 cm^{-1} for the film grown at 0.70% CH_4 concentration. The FWHM of the diamond peak at 1332 cm^{-1} has been reported to increase as defect concentration increases [2]. Therefore the observed variation of the FWHM in the present study indicates that the films contain varying degree of structural imperfections or defect concentrations.

The Raman peak position of a single-crystal diamond is about 1332 cm^{-1} as previously described. Comparison of the Raman peak position of a single-crystal diamond to those of the films under studies show a shift, ranging from 0.70 cm^{-1} to 1.90 cm^{-1}, as shown in Table 4.1. This provides further evidence to support the fact that the structural quality of the grown films are different from that of single-crystal diamond. The shift of the diamond Raman peak is attributed to an increase in defect density that is related to strain and/or the size of the diamond crystallites [15]. Stress can occur in the films due to a difference in the coefficient of thermal expansion or a lattice mismatch between the substrate and the grown film. The magnitude of the stress is estimated by measuring the peak frequency shift of the diamond line. It is well known that a material under tensile stress exhibits a Raman peak shift to lower frequency, while a Raman peak shift to higher frequency is observed under compressive stress [15]. According to the

results presented in Table 4.1, the peak shift of the diamond line is consistent with compressive stress. If the experimental shift is assumed to be entirely due to stress effects, the degree of this stress can be estimated from $S = (1.08GPa/cm^{-1})\Delta P$, for stress parallel to <100> and $S = (2.63GPa/cm^{-1})\Delta P$, for stress parallel to <111>, where the ΔP is the peak shift in cm^{-1} and S is the stress in GPa [14]. However, in a polycrystalline diamond film with randomly oriented crystals, crystals of different orientations develop different levels of stress. For example, stress will be parallel to <111> for some crystals, parallel to <100> for others, and intermediate direction for many others. From the maximum peak shift of 1.9 cm^{-1} in the present study, the average stress is roughly estimated to be about 1.38 GPa corresponding to the most highly stressed film (0.30%). Not surprising, since the level of stress in (111) crystallographic orientation is expected to exhibit a maximum value.

A general observation is that under the conditions for formation of high-quality diamond, the intensity ratio and the sp^3 carbon content are higher and the morphology is characterized by large and well defined facets. Under the conditions that lead to the co-deposition of non-diamond carbon the intensity ratio and carbon content are low. The morphology of the film displays smaller diamond crystals.

Raman spectroscopy is good for qualitative analysis. Since diamond films are transparent, Raman spectroscopy also give information about the bulk of the film. However, it is difficult to obtain a quantitative characterization of the fraction of sp^3 carbon from the Raman data because the probability for Raman scattering from sp^2

carbon is approximately 50-80 times greater than that from sp^3 carbon [7]

4.5 X-ray Photoelectron Spectroscopy Results

To obtain a quantitative measure of the $sp^3/(sp^3+sp^2)$ carbon fraction at the surface of the films, we used XPS of the C 1s line, as reported by Waite and Shah [16]. Figure 4.8 shows the XPS spectra of the C 1s line for binding energies from 282 to 289 eV, for polycrystalline diamond films grown using CH_4 concentrations of 0.10%, 0.20%, 0.30%, 0.45%, 0.60% and 0.70%, respectively. All of the spectra in the energy domain can be fitted with two peak. The two peaks occur at binding energies of 285.75 eV and 284.7 eV respectively. The peak at 285.75 eV is attributed to sp^3 bonded carbon and the peak at 284.7 eV is due to sp^2 bonded carbon as reported in Ref. 16. The $sp^3/(sp^3+sp^2)$ carbon fraction is determined by calculating the ratio of the area under the sp^3 peak to the total area under both peaks. We observed that, as the CH_4 concentration increases, the $sp^3/(sp^3+sp^2)$ carbon fraction decreases from 91% to 55%, as shown in Table 4.1 and graphically presented in figure 4.9. The relative low intensity of the graphitic structure observed in the spectrum of the film grown with 0.10% CH_4 concentration, is consistent with high quality diamond film in correlation with the Raman and SEM results.

In addition, we obtained a qualitative measure of the sp^3 carbon content at surface of the films by studying the bulk plasmon loss peaks associated with the C 1s line, as reported by Haq et. al. [17]. A computer line shape analysis was used to determine the peak position of the individual plasmon features. As shown in figure 4.10, the region from 295 eV to 325 eV contains a peak at about 320 eV, which is attributed to bulk

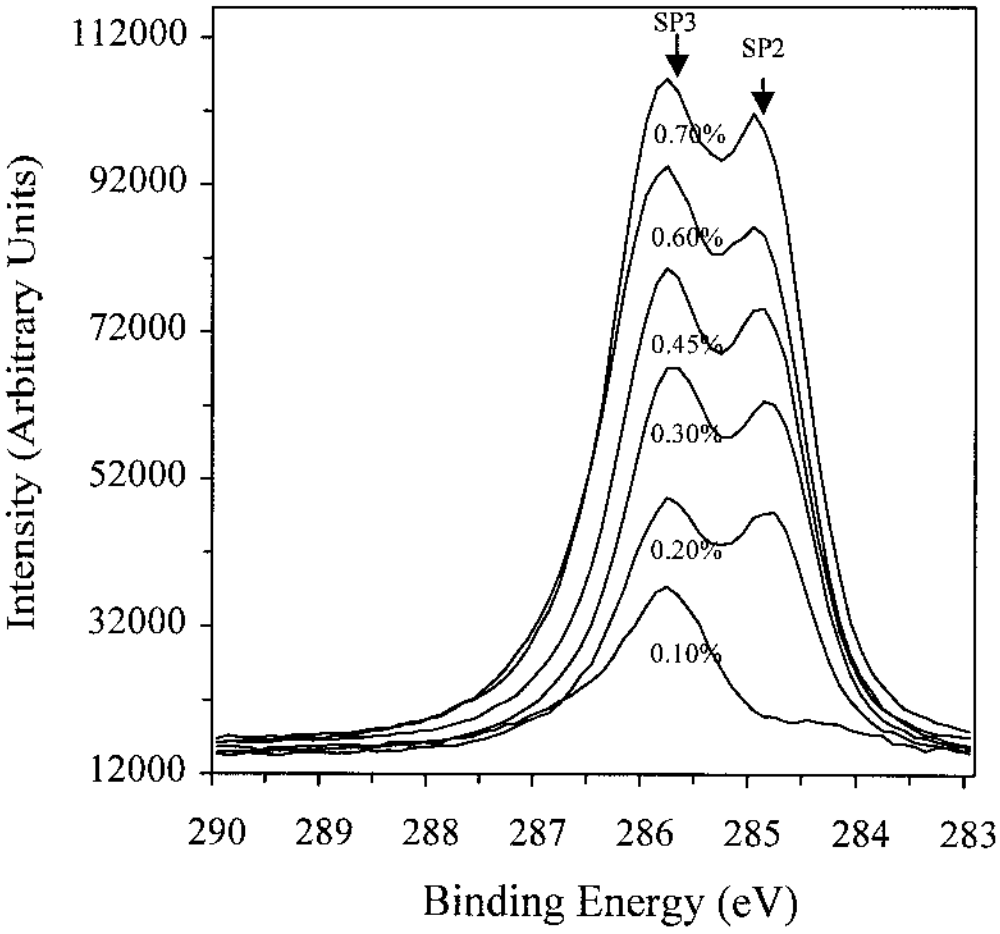

Figure 4.8. X-ray photoelectron spectra of the C 1s line of a chemical vapor deposition grown polycrystalline diamond film grown using 0.10%, 0.20%, 0.30%, 0.45%, 0.60%, and 0.70% methane concentrations.

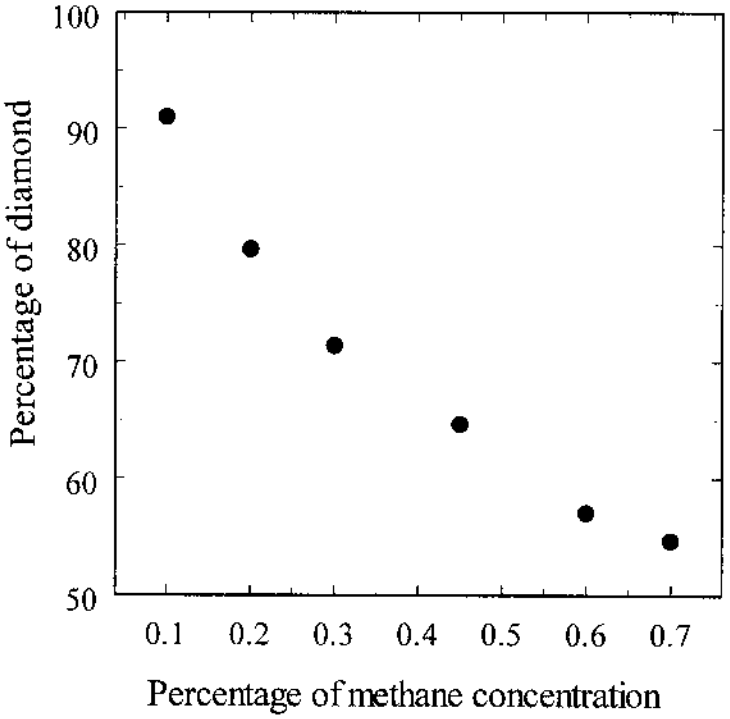

Figure 4.9. Percentage of diamond content as a function of methane concentration used during growth.

plasmons in sp^3 carbon, a band centered at about 310 eV, which is due to plasmons in the amorphous carbon and surface plasmons in the diamond, and a small peak at about 300 eV, which is believed to be residual signal from the Carbon 1s line [17]. The ratio of the area under the sp^3 peak to the total area is observed to decrease with an increase in CH_4 concentration as shown in Table 4.1, in agreement with the C 1s, SEM and Raman results.

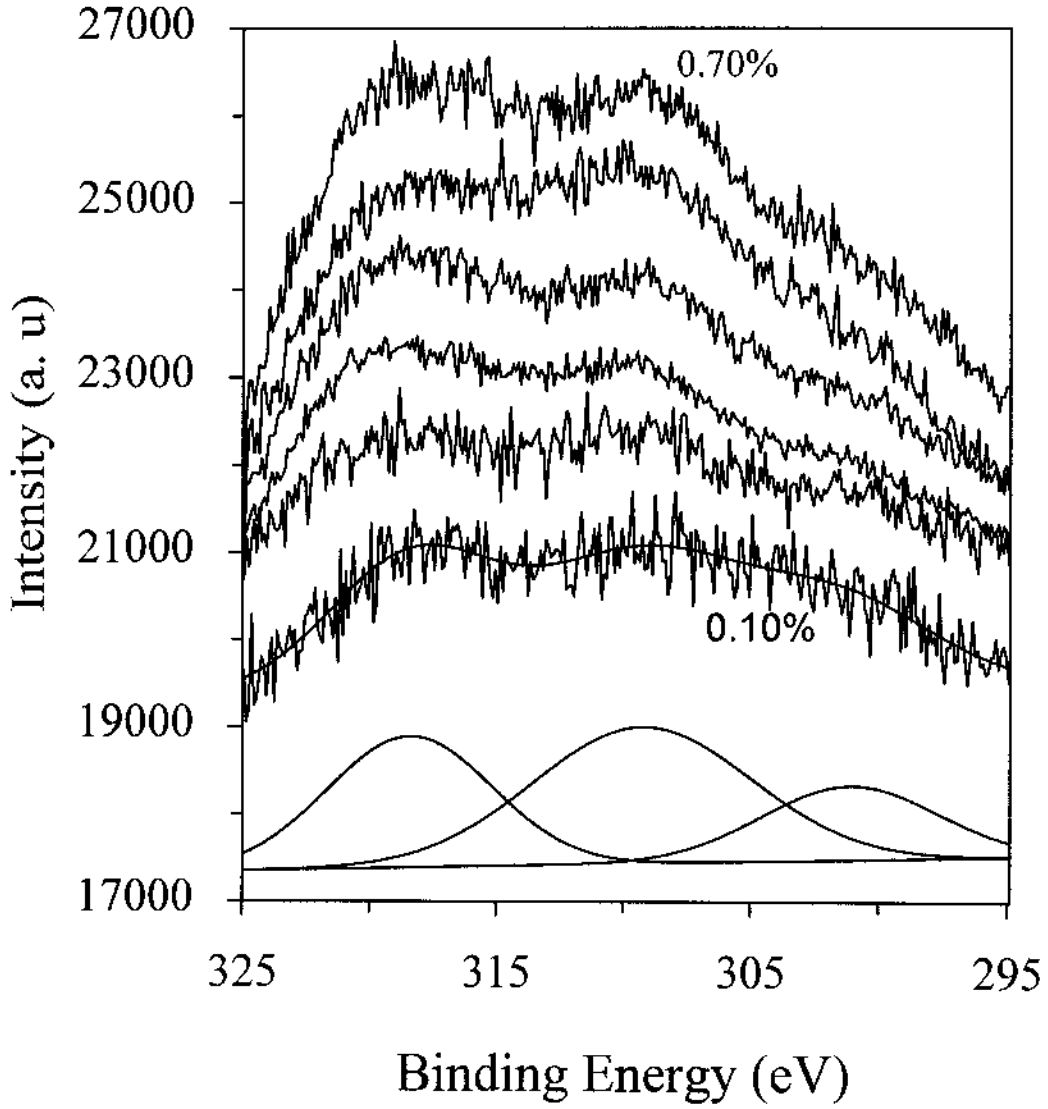

Figure 4.10. Plasmon loss peaks associated with the C 1s for the films shown in Fig. 4.8, and a fit to the data for the film grown using a methane concentration of 0.10%.

4.6 Photoelectric Threshold Results

Figures 4.11 shows the photoelectric response of the films discussed above. The data are corrected for the dependence of the intensity of the light source on photon energy, and the band pass of the monochromator that was approximately 0.03 eV. All the curves are seen to be of the same general form and follow a threshold tailing characterized by a dependence of the form $Y = A(E-E_T)^{3/2}$, where A and the photoelectric threshold, E_T, are adjustable parameters. This is functional form expected for excitation of an electron from the valence band to vacuum [18]. The values of E_T is given in Table 4.1. We observed that, as the $sp^3/(sp^3+sp^2)$ carbon fraction decreases from 91% to 55%, the photoelectric threshold decreases from approximately 4.8 to 3.9 eV. The highest values of the threshold energy were observed for films grown at low CH_4 concentrations, when the structure exhibits high quality diamond film (large crystal size and high content of sp^3 carbon). The smallest values of the threshold energy were observed for films with an amorphous structure (small crystallite size and high content of sp^2 carbon). This result shows that the threshold energy is strongly dependent on the $sp^3/(sp^3+sp^2)$ carbon fraction at the surface of the film.

4.7 Discussion

All of the results are summarized in Table 4.1 as a function of the percent CH_4 concentration used during the growth. All of our results are consistent with the photoelectric threshold being dependent on the surface and near surface fraction of sp^3 carbon.

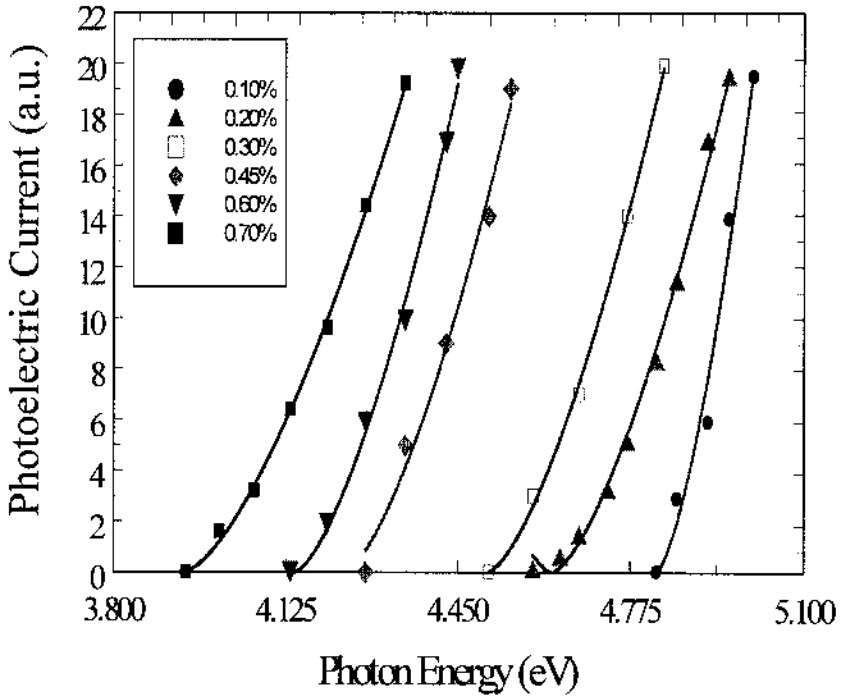

Figure 4.11. Photoelectric responses near threshold for diamond films grown using CH_4 concentrations of 0.10%, 0.20%, 0.30%, 0.45%, 0.60% and 0.70%. The curves are fiited to functions of the form $A(E-E_T)^{3/2}$.

TABLE 4.1. Properties of diamond films as a function of percent methane. A_D/A_T is the ratio of the area under the diamond peak to the total area in Raman and plasmon spectra. The FWHM is of the Raman peak at 1332 cm^{-1}. The percent sp^3 is determined from the C 1s line as described in the text. E_T is the photoelectric threshold.

Percent Methane	Raman A_D/A_T	FWHM (cm^{-1})	Diamond peak shift (cm^{-1})	XPS data Percent sp^3	Plasmon A_D/A_T	E_T (eV)
0.10	15.1	9.0	0.66	91.0	46.8	4.8
0.20	9.35	9.0	0.69	79.7	36.6	4.6
0.30	5.57	14.0	1.90	71.4	33.1	4.5
0.45	1.17	10.5	0.70	64.7	31.3	4.3
0.60	1.15	6.7	1.49	57.1	24.2	4.1
0.70	1.06	8.5	1.52	54.7	18.8	3.9

Recently, it has been reported that an increase in field emission from diamond films occurs as the CH_4 concentration, doping level and ion irradiation increases [2]. This report observed no correlation between the field emission current and the sp^3 content, which was characterized using Raman spectroscopy. The increase in field emission was attributed to an increase in defects in the diamond crystallites because the FWHM of the Raman peak at 1332 cm^{-1} was observed to increase as the field emission increased [2]. Recent theoretical studies have shown that vacancy defects in diamond lie in an energy range 1-2 eV above the valence band [19]. However, we do not believe that the decrease in photoelectric threshold that we observed is due to an increase in defects in the diamond crystallites because the FWHM of the diamond peak at 1332 cm^{-1} showed no correlation with the photoelectric threshold.

Ultraviolet photoelectron spectroscopy of CVD polycrystalline diamond films have been shown to exhibit NEA surface [20]. For an NEA surface, the photoelectric threshold occurs at a photon energy equal to the band-gap [21]. Therefore,the decrease in photoelectric threshold as the fraction of sp^3 carbon at the surface decreases may be due to a decrease in the band gap of the films. This is consistent with recent theoretical calculations that predict that the band gap of sp^3 carbon networks decreases with a decrease in the fraction of sp^3 carbon to sp^3 plus sp^2 carbon [22]. The diamond films consists of diamond crystallites separated by grain boundaries that contain sp^3 and sp^2 bounded carbon. Therefore, the band gap of the diamond crystallites can remain unchanged and the band gap of the disordered and sp^2 carbon at the grain boundaries can

change. We note that the band gap of amorphous carbon has been shown to decrease with a decrease in the fraction of sp^3 carbon [23]. Therefore, we propose that the decrease in threshold energy is due to the decrease in the $sp^3/(sp^3+sp^2)$ carbon fraction of the sp^3-sp^2 networks at the grain boundaries that results in a decrease in the band gap of such networks.

4.8 Conclusion

The $sp^3/(sp^3+sp^2)$ carbon fraction have been correlated to the photoelectric threshold energy. We found that CH_4 concentration has a significant effect on the $sp^3/(sp^3+sp^2)$ carbon fraction and photoelectric threshold for electron emission. Electron emission from CVD polycrystalline diamond film is due to valence band emission. We observed a significant decrease in the photoelectric threshold of CVD grown polycrystalline diamond films from 4.8 to 3.9 eV as the $sp^3/(sp^3+sp^2)$ carbon fraction at the surface decreases from 91% to 55%. We propose that the decrease in threshold is due to a decrease in the band gap of the sp^3-sp^2 networks at the grain boundaries. This effect can be used to tailor the electronic properties of diamond films for applications such as photocathodes and field emission.

References

1. W.Zhu, G.P. Kochansk, S. Jin, and L. Seibles, *J. Vac. Sci. Technol.* B **14**, 2011 (1996).

2. D.P. Malta, J.B. Posthill, T.P. Humphreys, *Appl. Phys. Lett.* **64**, 1929 (1994).

3. A. Breskin, R. Chechik, E. Shefer, D. Bacon, Y. Avigal, R. Kalish, and Y. Lifshitz, *Appl. Phys. Lett.* **70**, 3446 (1997).

4. C. Nutzenadel, O.M. Kuttel, O. Groning and L. Schlapbach, *Appl. Phys. Lett.* **69**, 2662 (1996).

5. G.T. Mearini, I.L. Krainsky, J.A. Dayton, Y.Wang, C.A. Zorman, J.C. Angus and D.F. Anderson, *Appl. Phys. Lett.* **66**, 242 (1995).

6. M.W. Geis, J.C. Twichell, J. Macaulay and K. Okano, *Appl. Phys. Lett.* **67**, 1328 (1995).

7. W.A. Yarbrough and R. Messier, *Science* **247**, 688 (1990).

8. R.C. Hyer, M. Green, k.K. Mishra, S.C. Sharma, *J. Mater. Sci Lett.*, Vol. **10**, 515 (1990).

9. S.A. Solin and A.K. Ramdas, *Phys. Rev.* **B1** (1970).

10. V.L. Humphreys and J. Khachan, *Electron. Lett.* **31**, 1018 (1995).

11. C. Wild, N. Herres, P. Koidl and T. Anthony, Electrochem. Soc. Proc. **89**, 283 (1989).

12. Peakfit, Jandel Scientific, San Rafeal, CA.

13. S.A. Stuart, S.Prawer and P.S. Weiser, *Appl. Phys. Lett.* **62**, 1227 (1993).

14. M. Yoshikawa, G. Katagiri, H. Ishida, A. Ishitani, M. Ono, and K. Matsumara, *Appl. Phys. Lett.* 55, 2608 (1989).

15. Y. H. Le Grice, R. J. Nemanich, J. T. Glass, Y. H. Lee, R.A. Rudder, and R. J. Markunas, in Diamond, Silicon carbide and Related Wide Bandgap Semiconductors, edited by J. T. Glass, R. Messier, and N. Fujimori, Mater. Res. Soc. Symp. Proc. **162**. Pittsburgh, PA, 1990, p. 219.

16. M.M. Waite and S.I. Shah, *Appl. Phys. Lett.* **60**, 2344 (1992).

17. S. Haq, D.L. Tunnicliffe, S. Sails, and J.A. Savage, *Appl. Phys. Lett.* **68**, 469 (1996).

18. E.O. Kane, *Phys. Rev.* **127**, 131 (1962).

19. N.M. Miskovsky, P.H. Cutler, and Z.H. Huang, *J. Vac. Sci. Technol.* **14**, 2037 (1996).

20. I.L. Krainsky, V.M. Asnin, G.T. Mearini, and J.A. Dayton, *Phys. Rev. B* **53**, R7650 (1996).

21. C. Wild, P. Koidl, W. MullerSebert, H. Walcher, R. Kohl, N. Herres, R. Locher, R. Samlenski, and R. Brenn, *Diamond Relat. Mater.* **2**, 158 (1993).

22. R. Sen, R. Sumathy, and C.N.R. Rao. *J. Mater. Res.* **11**, 2961 (1996).

23. S.Kaplan, F. Jansen, and M. Machonkin, *Appl. Phys. Lett.* **47**, 750 (1985).

CHAPTER 5

PHOTOELECTRON EMISSION PROPERTIES OF BORON DOPED CHEMICAL VAPOR DEPOSITION GROWN DIAMOND FILMS

5.1 Introduction

In this chapter, detailed investigation of the structural and photoelectron emission properties of polycrystalline diamond films as a function of boron doping are presented. Diamond films were grown on p-type single-crystal Si substrates using hot tungsten filament chemical vapor deposition techniques. The grown films were characterized with SEM, Raman spectroscopy, XPS, UPS and photoelectric current measurements. Measurements of the photoelectric current and electron energy distribution show that the photoelectric threshold is insensitive to the boron concentrations used during growth. Although the boron doping modified the surface morphology and photoemission intensity. The photoemission intensity increases with microcrystalline diamond content and the photoelectric threshold is about 4.4 eV, in agreement with previous measurements (chapter 4). In addition, there are evidence of emission bands centered at about 4.63, 4.92, 5.12 and 5.30 eV.

Electron emission from undoped [1-2] and boron doped [3] CVD grown diamond films has been observed under relatively low electric field (3-40 V/um). However, the mechanism responsible for the high electron emission from these materials is not entirely clear. Diamond is a wide band gap material. The quantum photoyield measurement on natural single crystals of diamond is reported to give photoemission threshold of 5.5 eV [4], which theoretically will require high threshold energy for electron emission. Energy levels in the band gap generated by doping/impurities or surface/defect states have been suggested to be responsible for the low field electron emission from undoped and boron doped diamond [1-3]. In order to understand the origin of electron emission from CVD polycrystalline diamond films, electronic energy levels of undoped and boron doped diamond films were studied using photoemission techniques. By analyzing the energy distribution of photoemitted electrons and the energy dependence on emitted electrons, information about electronic energy levels of the films is revealed. This data is essential for development of diamond film technology in the areas of flat panel displays and photodectors.

5.2 Experimental

Boron doped polycrystalline diamond films were grown on p-type single-crystal Si substrates by hot filament chemical vapor deposition technique using a gas mixture of hydrogen (H_2), methane (CH_4) and diborane (H_2B_6). The Si substrate surface was preseeded with diamond powder in order to obtain continuous diamond films. This was done by polishing the substrate surface with diamond powder of about 1 μm particle size.

After polishing, the substrate was cleaned ultrasonically in acetone, methanol and rinsed with distilled water.

The substrate was mounted on a molybdenum heater and loaded into the deposition chamber, and the system was evacuated down to 10 mTorr. High purity hydrogen gas was introduced into the deposition chamber. The substrate was heated resistively via molybdemum foil. A tungsten filament maintained at about 2220^0 C was used in close proximity to the substrate surface to promote film growth. As mentioned in chapter 2, the hot tungsten filament produces atomic hydrogen and carbon radicals necessary for the diamond film growth. A mixture of high purity methane and diborane gas was introduced into the growth chamber. The gas flow was monitored with electronic mass flow meters and controlled with needle gate valve. Hydrogen and methane flow rates were 200 sccm and 0.5 sccm, respectively. Different concentrations of boron in different films were achieved by adding 4, 6, 8 and 10 sccm into the gas mixture during the growth of individual films. Diamond film was deposited for 4 hours at a substrate temperature of 860^0 C and a pressure of 38 torr. Temperatures of the filament and the substrate were measured with an optical pyrometer corrected for emissivity.

The surface morphologies of an undoped and boron doped diamond films were investigated using JEOL T-300 scanning electron microscope (SEM). Characteristic feature of diamond crystals were observed in all the films. Identifications of the carbon phases as well as a qualititative determination of the ratio of $sp^3/(sp^3+ sp^2)$ carbon fraction present in the films were obtained using Raman spectroscopy. The Raman spectra were

obtained by exciting the diamond film with the 5145 Å line of an argon ion laser, and measured in the backscattering configuration on a SPEX 1404 double monochromator with computer data acquisition.

The electronic structures of the polycrystalline grown diamond films were investigated using XPS and UPS techniques. The XPS was used to obtain a quantitative ratio of the $sp^3/(sp^3+ sp^2)$ carbon fraction at the surface of the film, and the UPS was used to characterize the electronic energy levels or states of the films. These were accomplished by measuring the electron energy distribution (EDC) of photoemitted electrons using a VG ESCALAB MARK11 system equipped with hemispherical electron analyzer ($\Delta E = 0.08$ eV) in a vacuum of about 5×10^{-9} torr. From the electron energy distributions of the XPS and UPS spectra, values of the $sp^3/(sp^3+ sp^2)$ carbon fraction and the photoelectric threshold energies were determined, respectively. The XPS spectra were acquired in the pulse counting mode, at a constant analyzer pass energy of 10 eV. The excitation source for the XPS measurements was Mg K_a radiation of energy 1253.6 eV. The UPS spectra was acquired at a constant pass energy of 1 eV. The excitation source for the UPS measurements was a 150 watts xenon high pressure arc lamp. A grating monochromator was used to select three different incident photon energies (4.87, 5.38 and 5.64 eV) to obtain three different spectrum for each diamond film.

Measurements of the emission current as a function of incident photon energy were performed for films grown with 0, 4, 6 and 8 sccm of boron concentrations. The values of the photoelectric threshold obtained by using this techniques are close

to those determined using ultraviolet photoelectron spectroscopy. Details of the experimental procedure is presented in chapter 3.

5.3 Morphology of the film surfaces

Figures 5.1- 5.3 show the scanning electron microscopy images of polycrystalline diamond films grown using boron concentrations of 0, 4, 6, 8, and 10 sccm, respectively. Figure 5.3(b) is a compilation of the sem images of all the diamond films to facilitate comparison. As shown in figure 5.3(a), the surface morphology and crystallinity are functions of boron concentrations. In general, as the boron concentration increases the average crystalline size decreases, consistent with previous report [5]. Also, the crystal orientation tends to be predominantly (111) faces with the presence of large grains of (100) faces depending on the boron concentration. The morphology of the undoped film contains (100) faces of diamond crystals, as shown in figure 5.1(a). The film grown at 4 sccm of boron has a highly faceted morphology, and contain large diamond crystals with (100) orientation, as shown in figure 5.1(b). The surface morphology changes significantly at 6 sccm of boron. At this concentration, the film surface morphology shows a more uniform microcrystalline diamond with predominantly (111) crystallographic orientation, as shown in figure 5.2(a). However, at 8 sccm of boron, although the microcrystalline features persist, also large crystals of (111) faces are observed, about the same size as that of the film grown at 4 sccm of boron (fig. 5.2(b). As the boron concentration is increased to 10 sccm, the majority of crystallographic orientation appearing on the film surface are (111), as shown in figure 5.3(a). Also, small

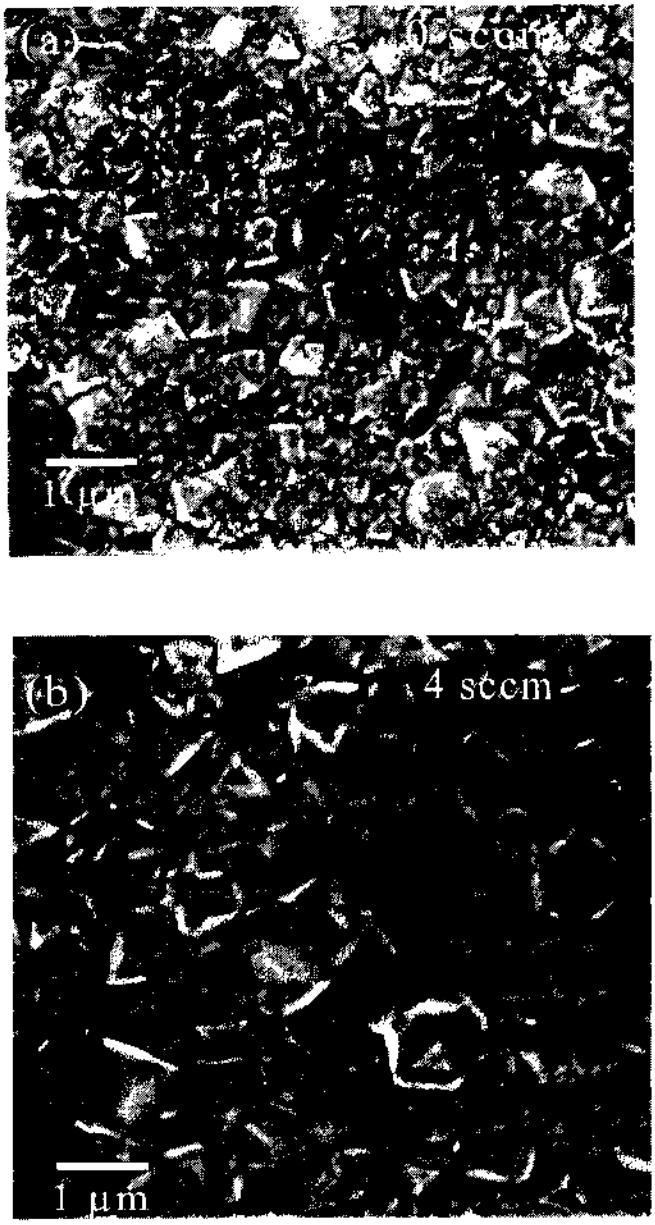

Figure 5.1. Scanning electron micrographs of chemical vapor deposition grown polycrystalline diamond films grown on Si substrates using (a) 0 sccm (b) 4 sccm of boron.

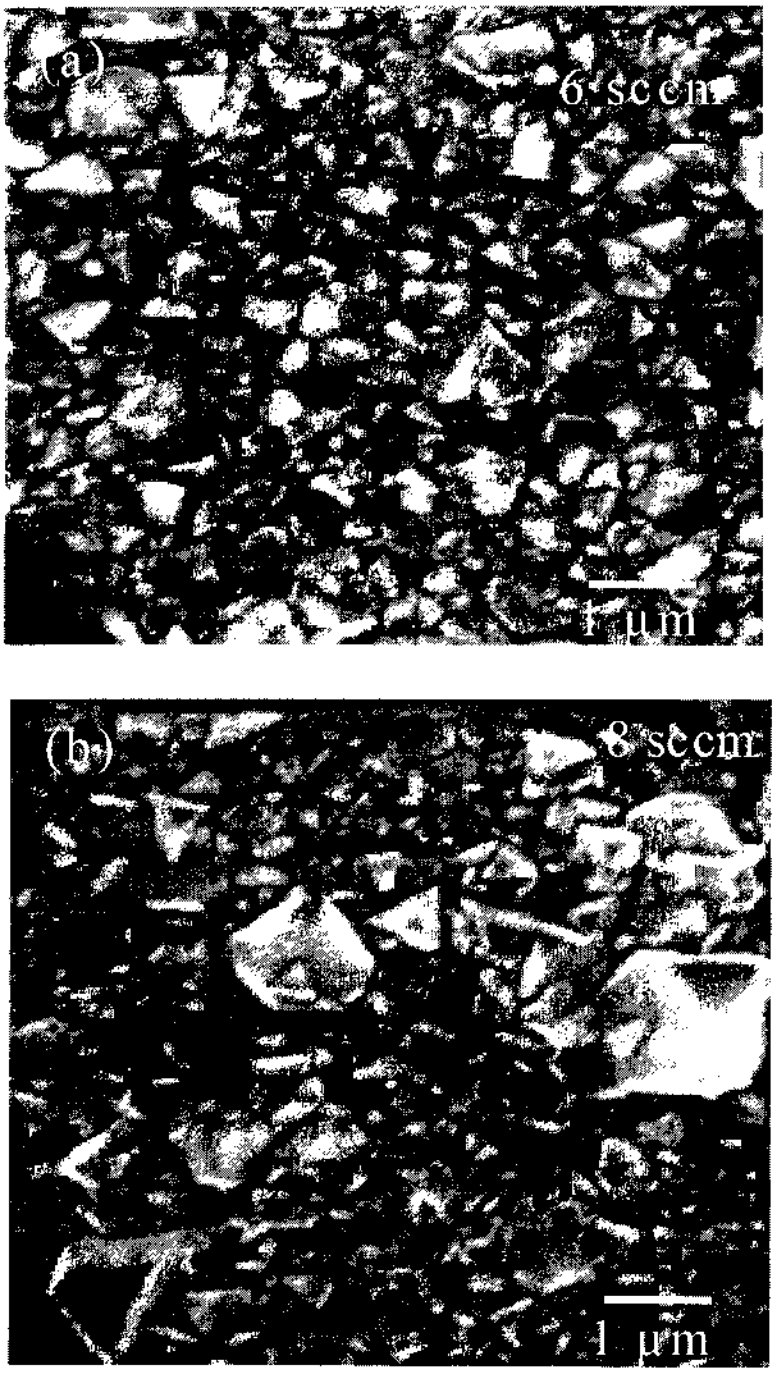

Figure 5.2. Scanning electron micrographs of chemical vapor deposition grown polycrystalline diamond films grown on Si substrates using (a) 6 sccm (b) 8 sccm of boron.

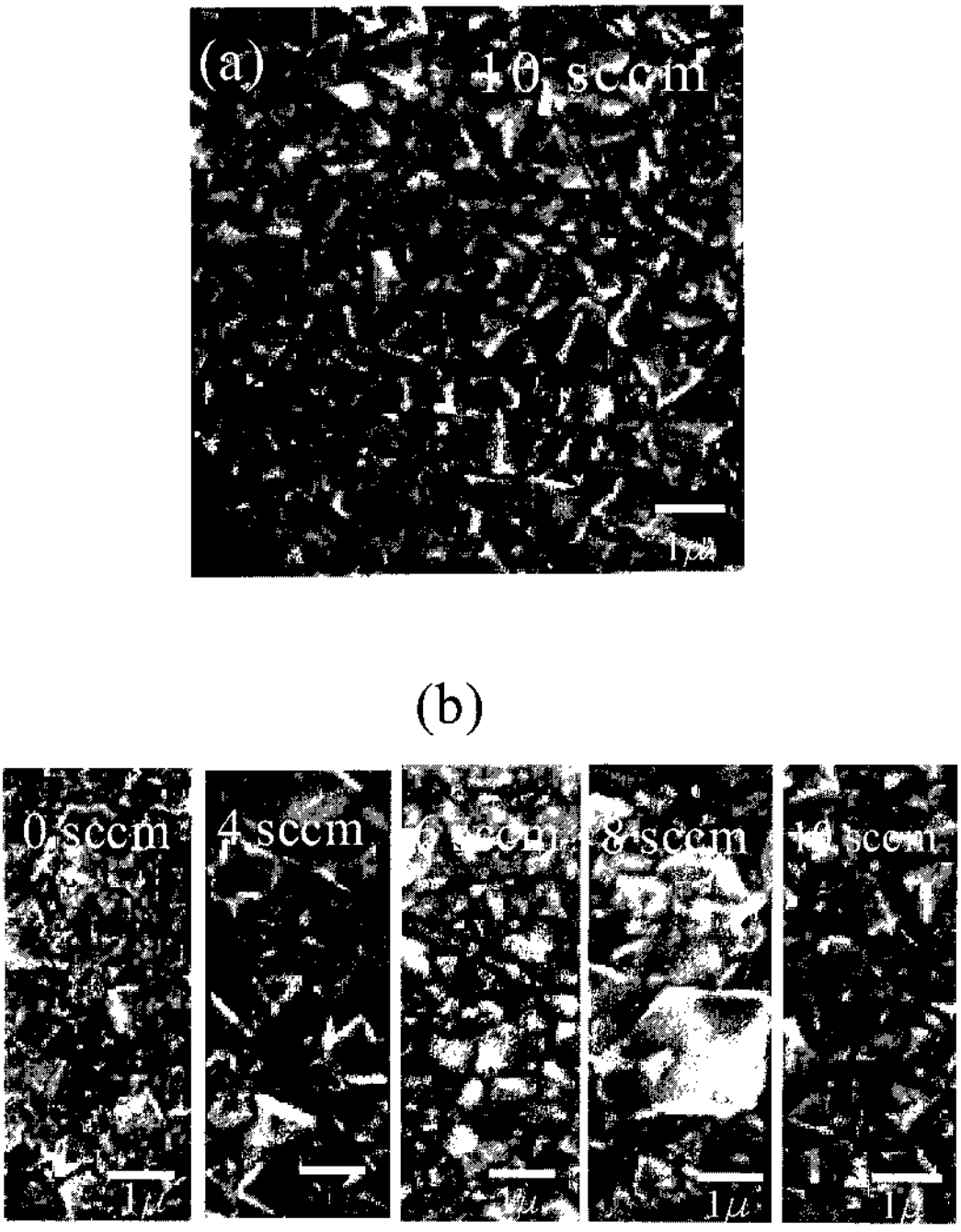

Figure 5.3. Scanning electron micrographs of chemical vapor deposition grown polycrystalline diamond films grown on Si substrates using (a) 10 sccm of boron (b) compilation of all the boron doped diamond films for comparison.

diamond crystallites with no clear crystallographic orientation are observed. The appearance of such a structure is common for CVD diamond films exhibiting (111) orientations. This is in part due to the fact that (111) faces have a defective structure. It has been shown by Tsai et al using TEM that the (111) growth faces contained much greater defect density than (100) faces [6].

It is evident from the SEM results that addition of 4 sccm of boron significantly improved the crystal quality of the diamond film, whereas higher boron concentrations deteriorate the crystal quality of the film.

5.4 Raman Spectroscopy Results.

Figures 5.4-5.8 show the Raman spectra of polycrystalline diamond films grown under different concentrations of boron (0, 4, 6, 8, and 10 sccm). For comparison, the Raman spectra of all the diamond films are compiled in Figure 5.9, arranged from bottom to top in the order of increasing boron concentrations. In general, all the spectra show a sharp peak at about 1333 cm^{-1} characteristic of single-crystal diamond and a broad peak extending from about 1540 to 1580 cm^{-1}. This peak arises from graphite and other forms of carbon including amorphous carbon. The slight widening of the characteristic 1333 cm^{-1} peak of diamond is probably due to lattice strain caused by incorporation of boron into the diamond lattice [6, 7]. However, the most striking feature of fig. 5.9 is the appearance of an additional peak at about 1207 cm^{-1} for films grown at 0, 6, and 10 sccm of boron concentrations. This peak is more evidence in figures 5.4, 5.6, and 5.8, and has been identified previously with nanocrystalline or microcrystalline diamond [8].

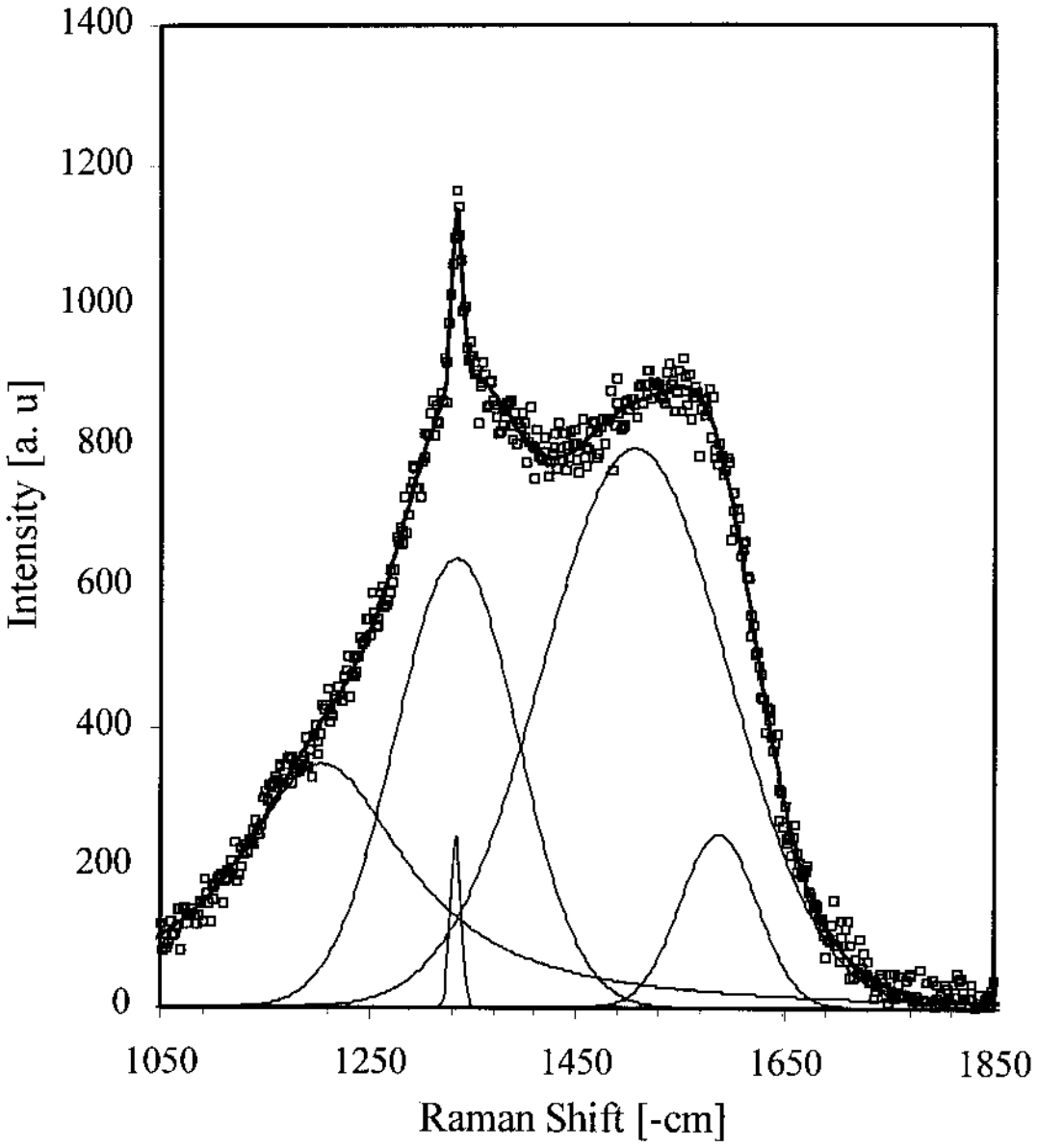

Figure 5.4. Raman spectrum of a chemical vapor deposition grown polycrystalline diamond film grown on Si substrate using 0 sccm of boron.

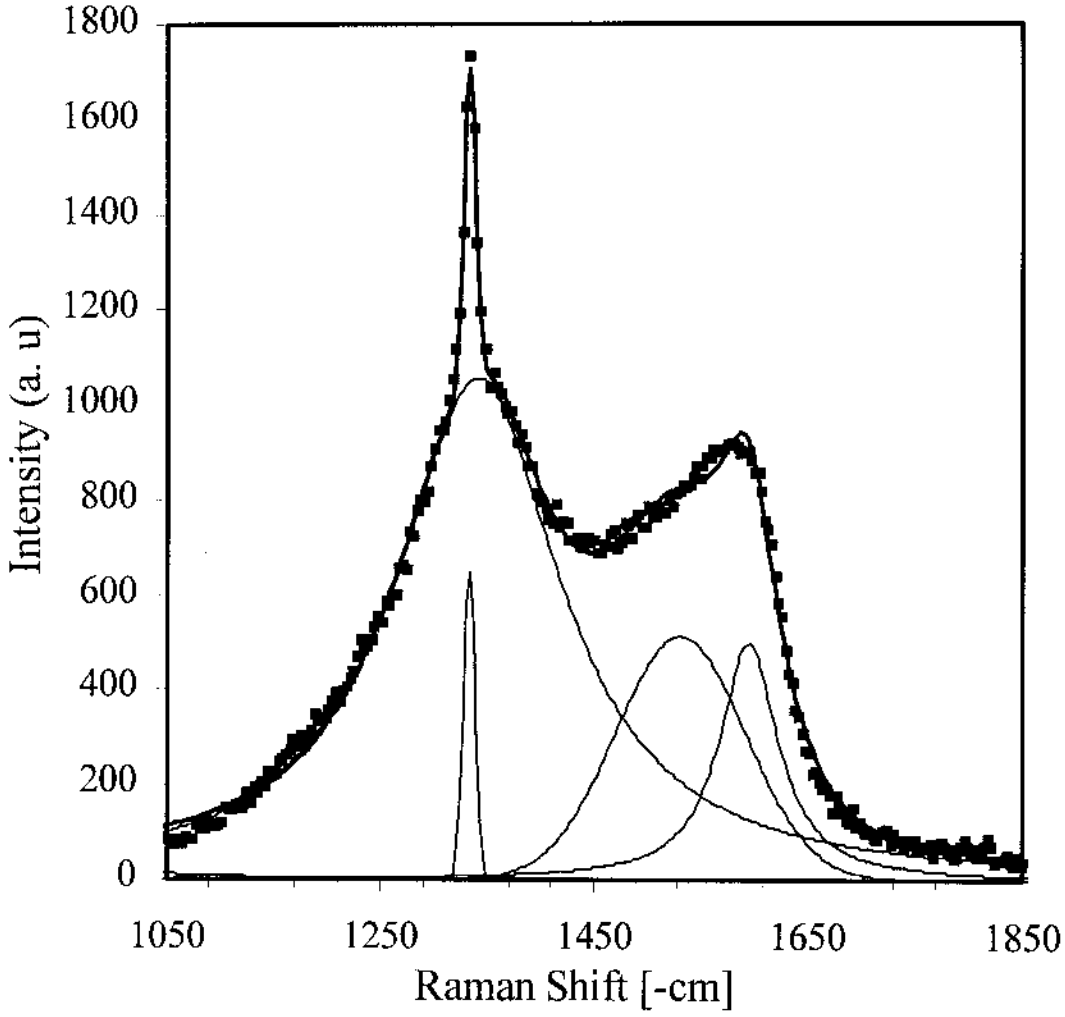

Figure 5.5. Raman spectrum of chemical vapor deposition grown polycrystalline diamond film grown on Si substrate using 4 sccm of boron.

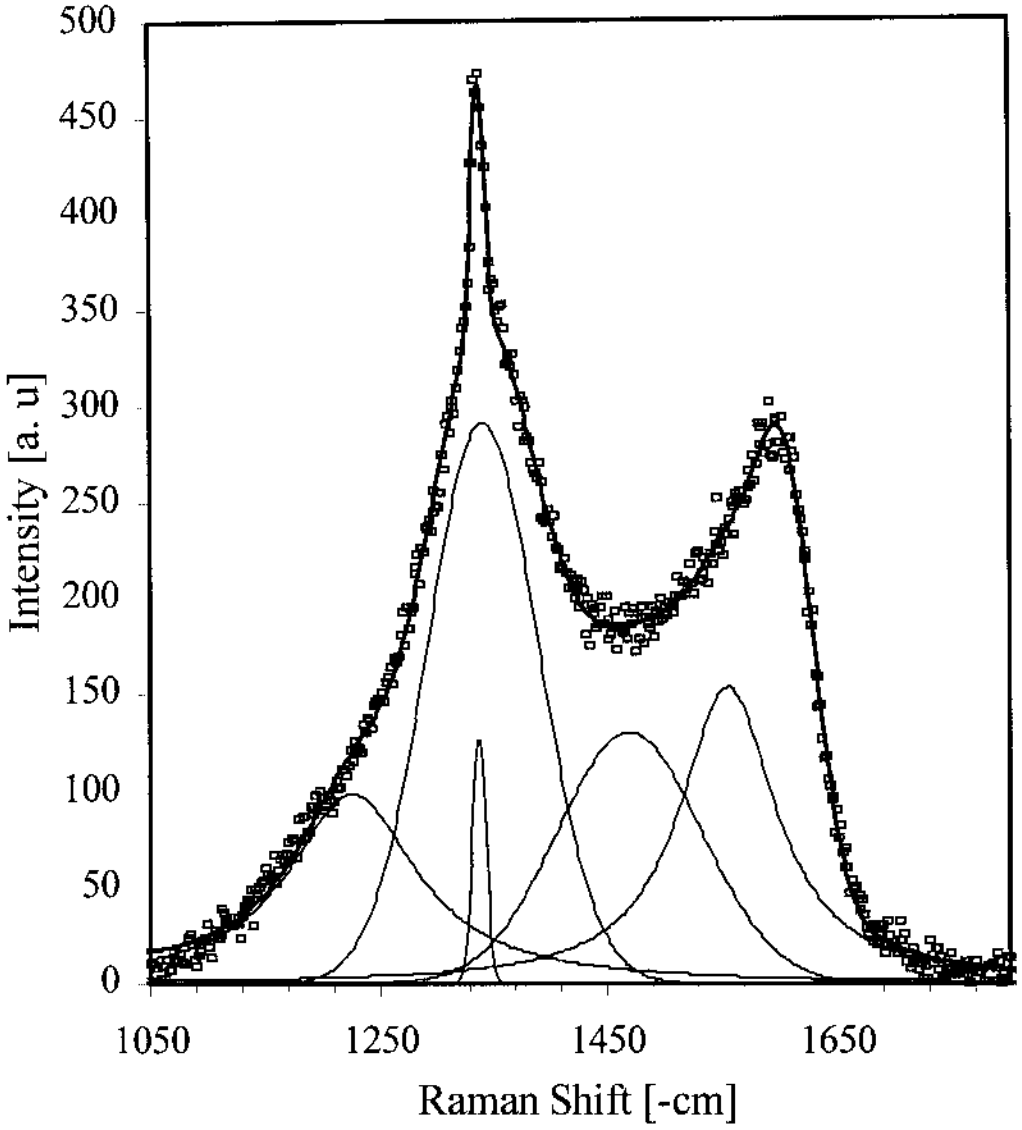

Figure 5.6. Raman spectrum of a chemical vapor deposition grown polycrystalline diamond film grown on Si substrate using 6 sccm of boron.

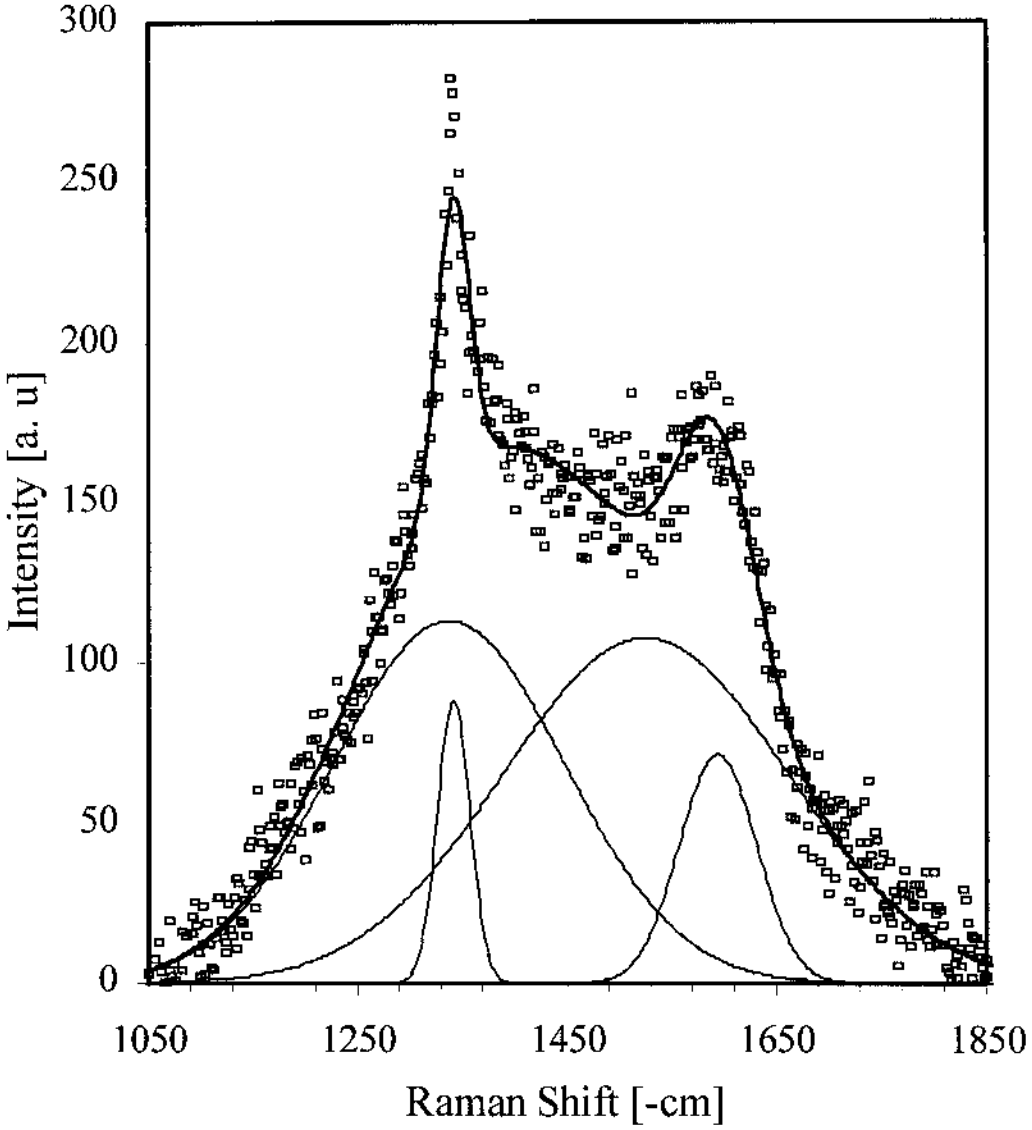

Figure 5.7. Raman spectrum of a chemical vapor deposition grown polycrystalline diamond film grown on Si substrate using 8 seem of boron.

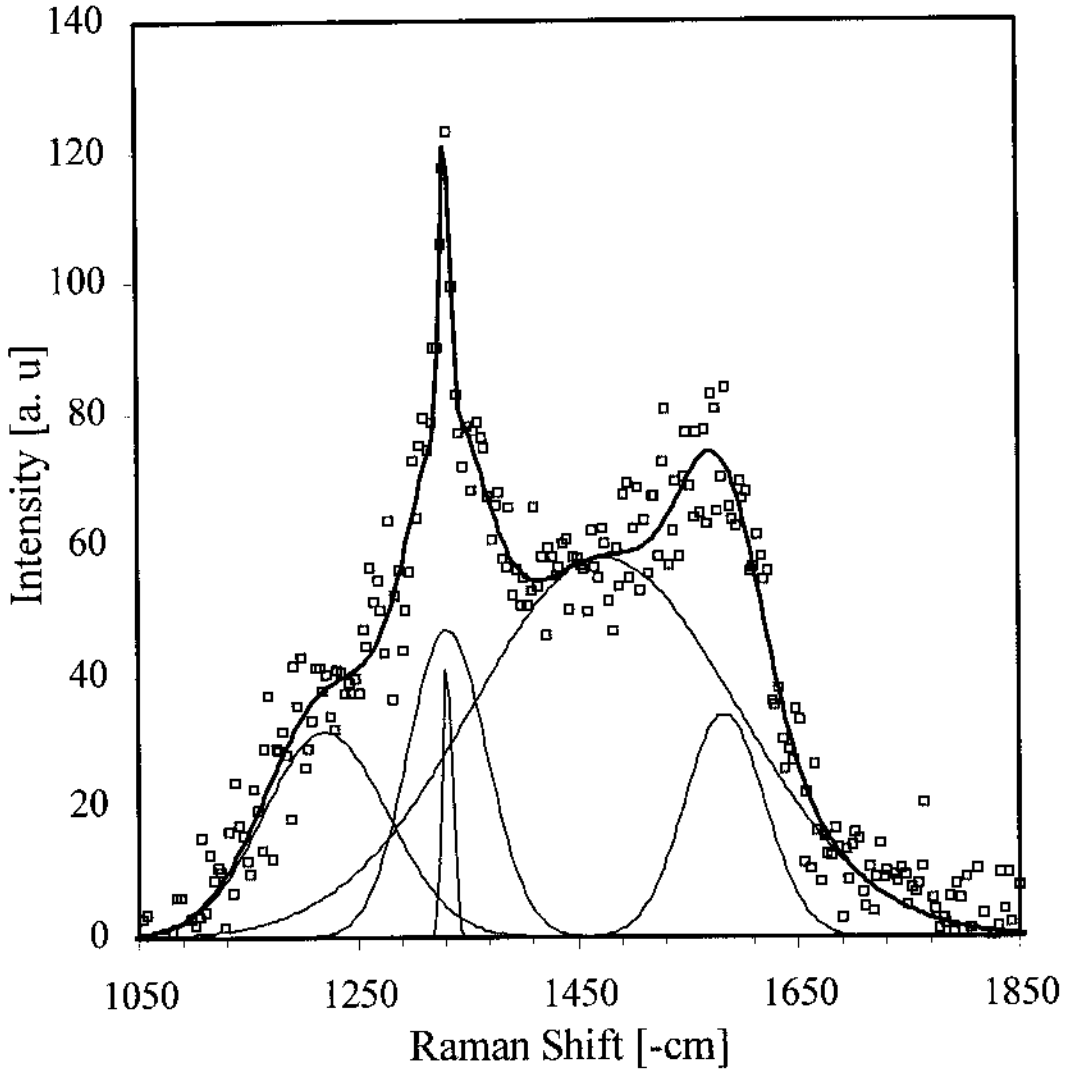

Figure 5.8. Raman spectrum of a chemical vapor deposition grown polycrystalline diamond film grown on Si substrate using 10 sccm of boron.

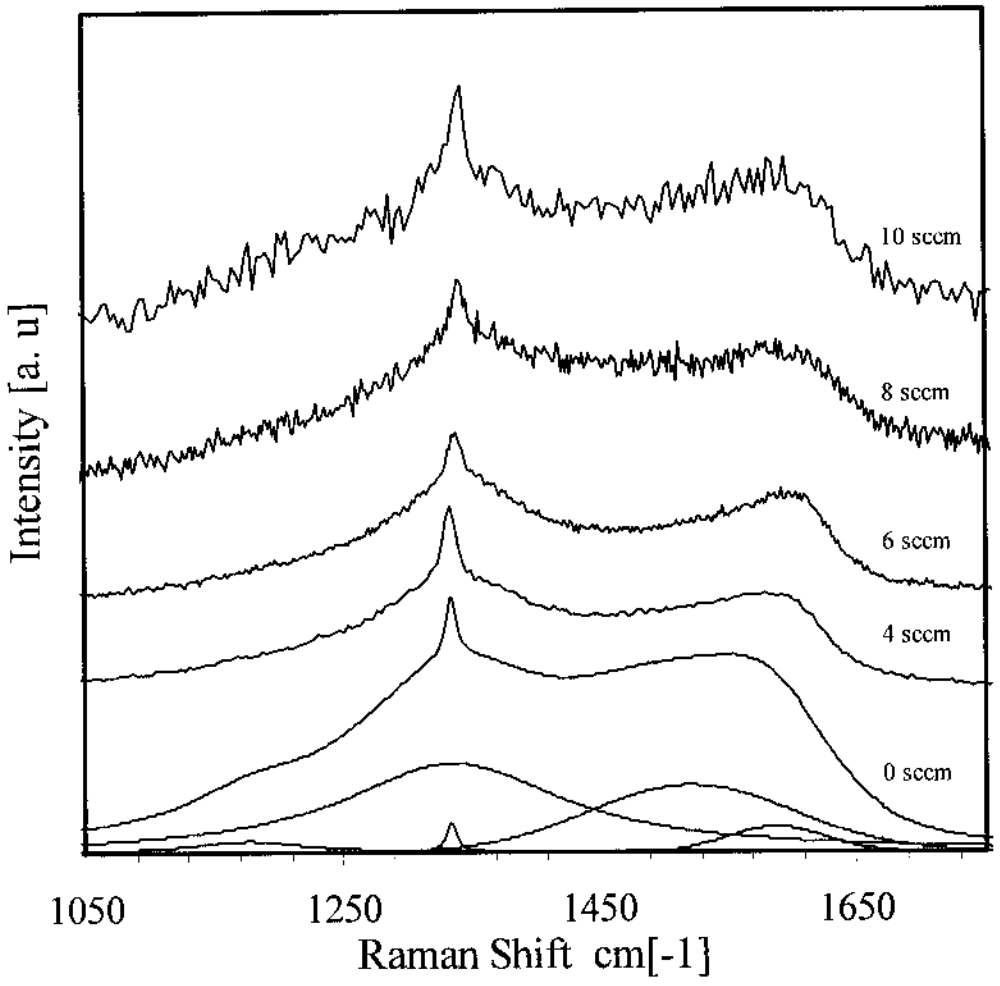

Figure 5.9. Raman spectra of chemical vapor deposition grown polycrystalline diamond films grown on Si substrate using 0, 4, 6, 8 and 10 sccm of boron.

The presence of this peak implies that the polycrystalline diamond films grown with 0, 6 and 10 sccm of boron contain more smaller diamond crystals than those grown at 4 and 8 sccm of boron, consistent with the SEM results.

The diamond line peak at 1333 cm^{-1} increases slightly with addition of 4 sccm of boron into the reaction gas, indicating better crystal quality in correlation with the SEM result. This result is consistent with the general observation on boron doped polycrystalline diamond films. Miyata el at [9] Nishimur el at [10] and Won el at [11] have shown that addition of small amount of boron to a CVD gas mixture during diamond film growth results in an increase of the diamond Raman peak, thus better crystal quality.

In order to obtain a numerical analysis of the Raman data, the Raman spectra were peak fitted. From the fitting parameters the integrated intensities, full width at half maximum (FWHM) of the individual diamond lines and the area under each peak were determined. A qualitative determination of the ratio of $sp^3/(sp^3+ sp^2)$ bonded carbon fraction in the films were obtained by comparison of the area under the diamond peak at 1333 cm^{-1} to the sum of areas of individual peak in each spectrum.

Figure 5.10 shows the integrated intensity ratio as a function of boron concentrations. As can be seen from figure 5.10 and Table 5.1, except for the slight increase at 4 sccm of boron, the intensity ratio does not appear to be influenced by boron concentration. This result is an indication that there is no significant increase in

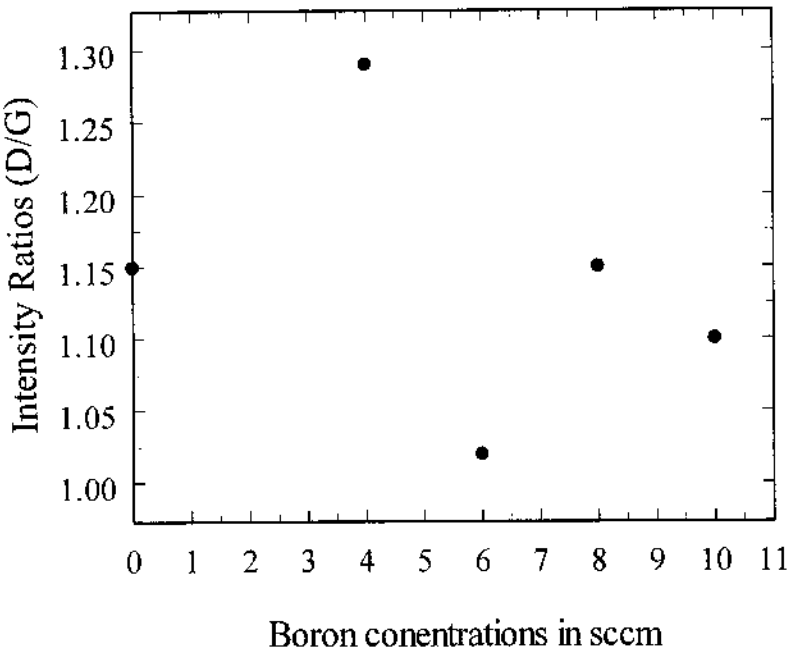

Figure 5.10. Raman integrated intensity as a function of boron concentrations used during growth.

concentration of the sp^2 bonded carbon as a result of an increase in boron concentrations used during growth.

A plot of the FWHM of the boron doped polycrystalline diamond line as a function boron concentration shows no significant change, as displayed figure 5.11. The value of the FWHM varies from approximately 9.69 to 13.06 cm^{-1}, corresponding to a maximum change of about 3.37 cm^{-1}. Since the FWHM of CVD diamond films is known to increases with defect density. Therefore, defect density is essentially the same

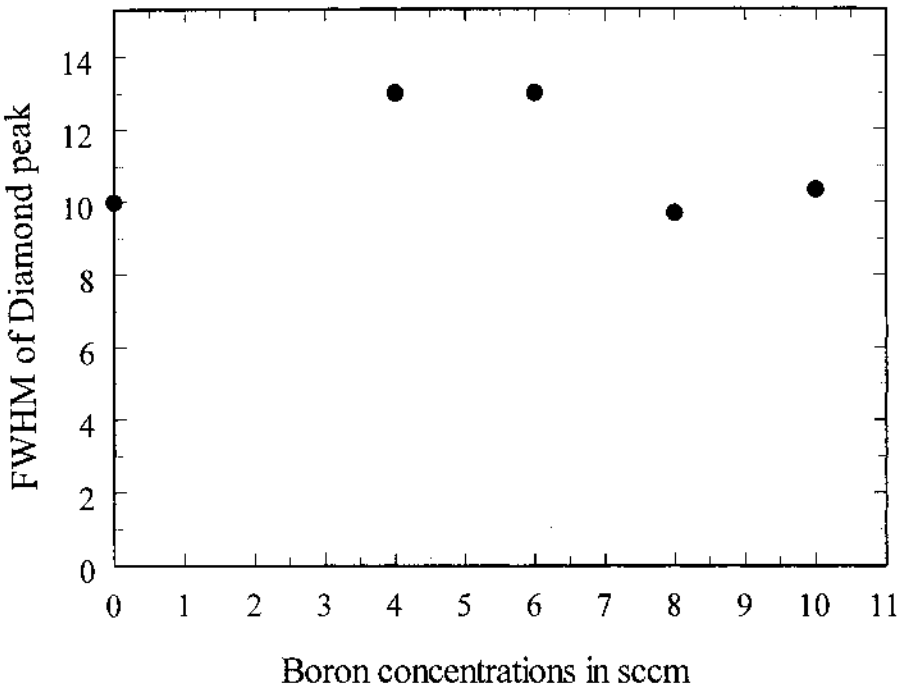

Figure 5.11. FWHM of the Raman diamond peaks as a function of boron concentrations used during growth.

in all films, independent of boron concentration for the range studied.

Further analysis of the boron doped Raman spectra is shown in figure 5.12. This figure represents percent ratio of the area under the diamond line at 1333 cm^{-1} to the total area under all peaks as a function of boron concentrations. As can be seen, no significant change (maximum change of about 0.52%) is observed indicating that the boron doped films contain approximately the same fraction of sp^3 bonded carbon for the range of boron concentrations studied.

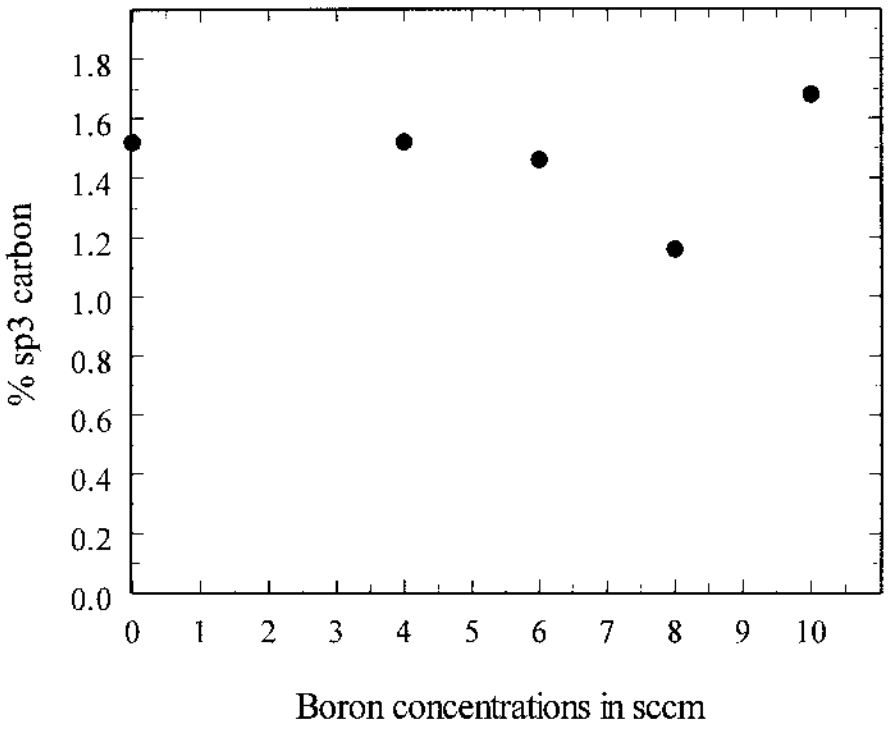

Figure 5.12. Percentage of sp^3 carbon fraction as a function of boron concentrations used during growth.

Overall, the main observations is that the diamond and sp^2 bonded carbon peak positions, the intensity ratio, FWHM of the diamond line and the carbon area ratios do not exhibit any significant change. Therefore are considered to be independent of boron concentrations within the dopant range studied. These results are summarized in Table 5.1 below.

Table 5.1 Structural properties of CVD diamond films as a function of boron concentrations.

Boron Conc. (sccm)	Raman data % sp^3	Intensity Ratio (I_D/I_G)	FWHM (cm^{-1})	XPS data % sp^3
0	1.52	1.15	10	73.4
4	1.52	1.29	13	73.5
6	1.46	1.02	13	84.7
8	1.16	1.15	9.69	80.0
10	1.68	1.10	10.34	79.5

5.5 X-Ray Photoelectron Spectroscopy Results.

Figure 5.13 show XPS spectra of the C 1s line in binding energies from 278 eV to 290 eV, of polycrystalline diamond films grown using 0, 4, 6, 8, and 10 sccm of boron. The XPS data for the boron doped films are shifted by about 0.25 eV relative to the undoped film. This shift is attributed to incorporation of boron atoms into the diamond which alters the chemical environment of the core levels, thus their binding energies. The XPS data were analyzed by fitting the spectra with three Gaussian lines that are centered at about 283.8, 284.5 and 284.6 eV. These peaks are believed to be due to sp^2 carbon, and sp^3 carbon with a diamond peak and microcrystalline diamond peak separated by about 0.1 eV, respectively. This extra diamond peak gave a small contribution to the total diamond content and was most prominent for boron concentrations of 0, 6 and 10 sccm. The line shown represents the best fit to the data. For 10 sccm data, the three Gaussian

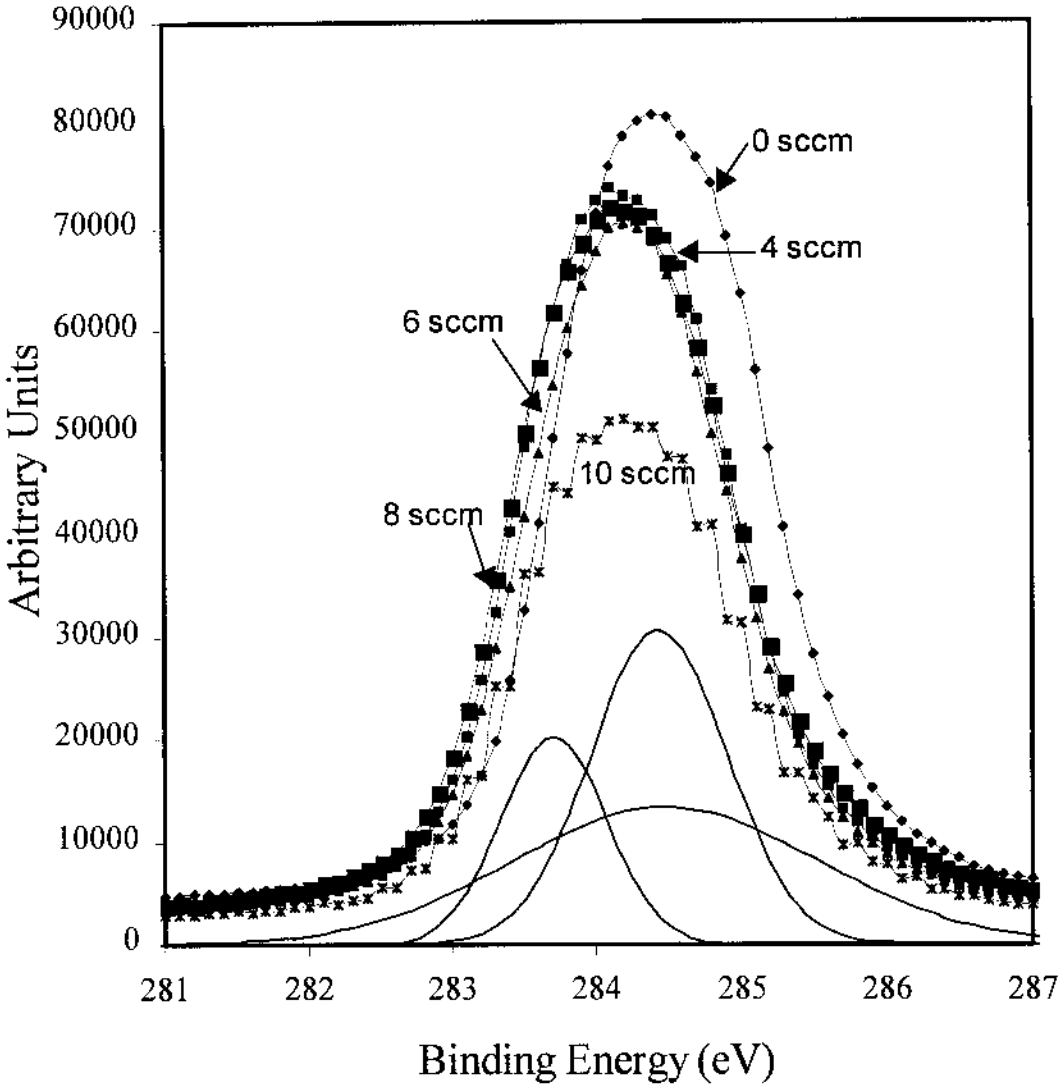

Figure 5.13. Compilation of the XPS spectra of chemical vapor deposition grown polycrystalline diamond film grown using 0, 4, 6, 8 and 10 sccm of boron.

lines used to fit the data are shown as well. The value of $sp^3/(sp^3+ sp^2)$ carbon fraction at the surface of the film is determined by calculating the ratio of the area under the sp^3 peak to the total area under the peaks. We observed that as the boron concentration increases, the $sp^3/(sp^3+ sp^2)$ carbon fraction remains basically the same at an average value of about 78%, indicating that the films are predominantly sp^3 bonded carbon. The values of $sp^3/(sp^3+ sp^2)$ carbon fraction are shown in Table 5.1 and graphically presented in figure 5.14. This result is in corroboration with the Raman results.

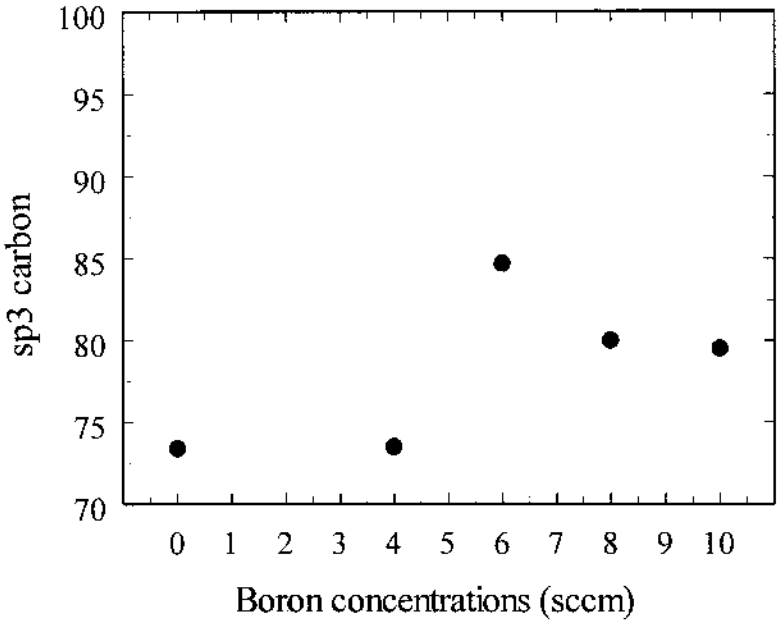

Figure 5.14. Percentage of sp^3 carbon fraction as a function of boron concentrations used during growth.

5.6 Ultraviolet Photoelectron Spectroscopy Results.

UPS was used to characterize the electronic energy levels and emission characteristic of the polycrystalline diamond films by measuring the energy distribution of photoemitted electrons from the surface of the film. Figures 5.15 and 5.16 show the energy distributions curves in binding energy at different incident photon energies (from 4.87 to 5.63 eV), for films grown with boron concentrations of 0 and 4 sccm. From these figures, it can be seen that the spectra depend strongly on the excitation energy. The broadening of the curves and the simultaneous shift of the peaks to higher binding energy, as well as a drastic decrease in emission intensity as the photon energy is increased are apparent. This broadening suggests that the lifetime for scattering is strongly dependent on the electron energy consistent with previous experimental and theoretical work [12]. The decrease in emission intensity at higher source energies is due to a corresponding decrease in the intensity of the light source and the variation in the escape probability of higher energy electrons [12]. The shift of the peak position to higher binding energies with an increase in photon energy is attributed to a valence optical transition, where momentum is preserved [13]. Therefore the structure in the UPS spectra is produced by structure in the valence band of the films, and the energy of the initial states responsible for the observed structure is a function of the excitation energy.

For comparison, figures 5.17-5.19 show the normalized energy distributions of emitted electrons of all the boron doped diamond films at excitation energies of 4.87, 5.38 and 5.63 eV respectively. Clearly, variation in emission intensities with boron

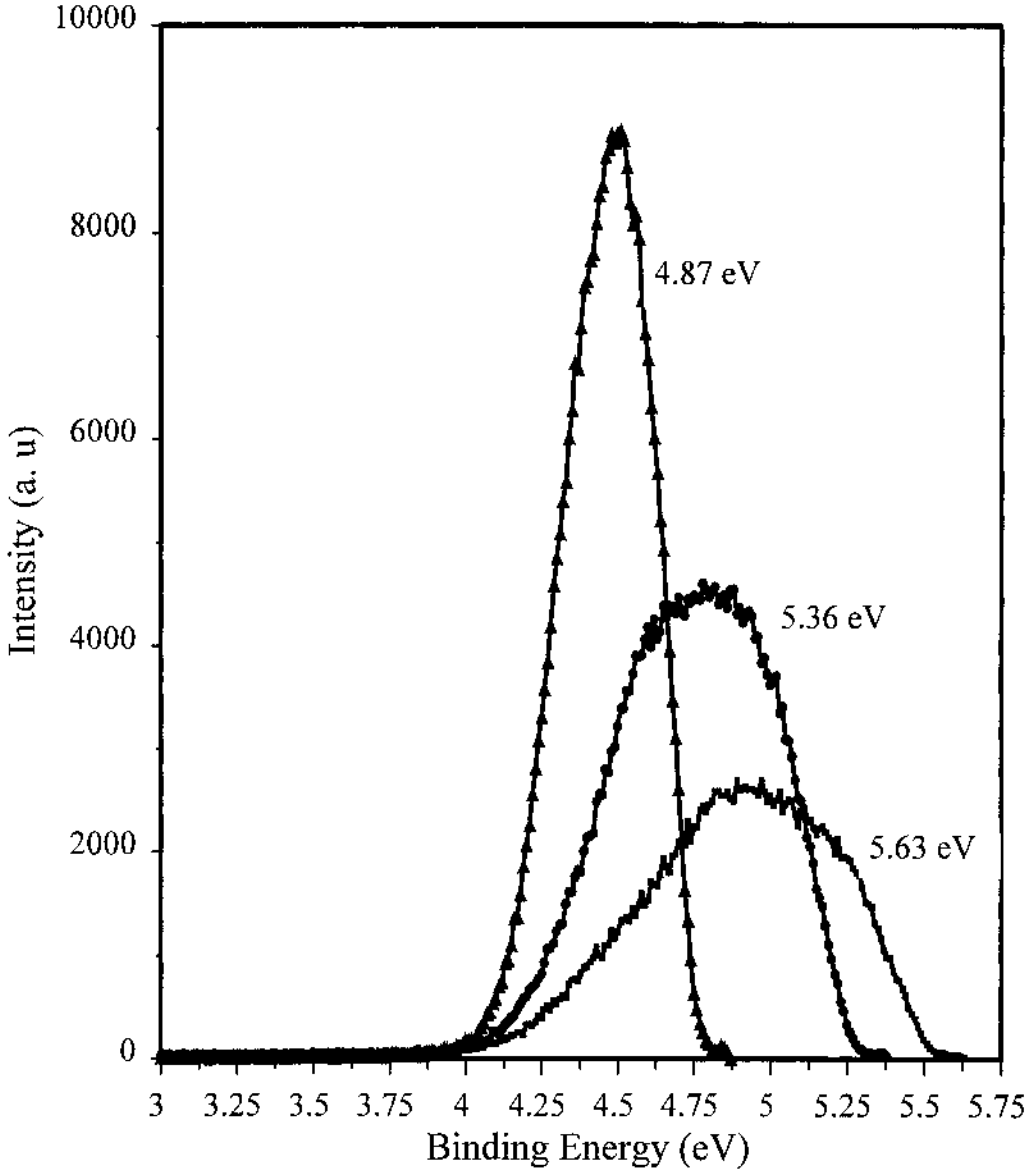

Figure 5.15. Energy distributions of photoemitted electrons from chemical vapor deposition polycrystalline diamond film grown using 0 sccm of boron. The figure shows a shift of the main peak to higher binding energy with increasing photon energy. The energy of the exciting photons is shown for each spectrum.

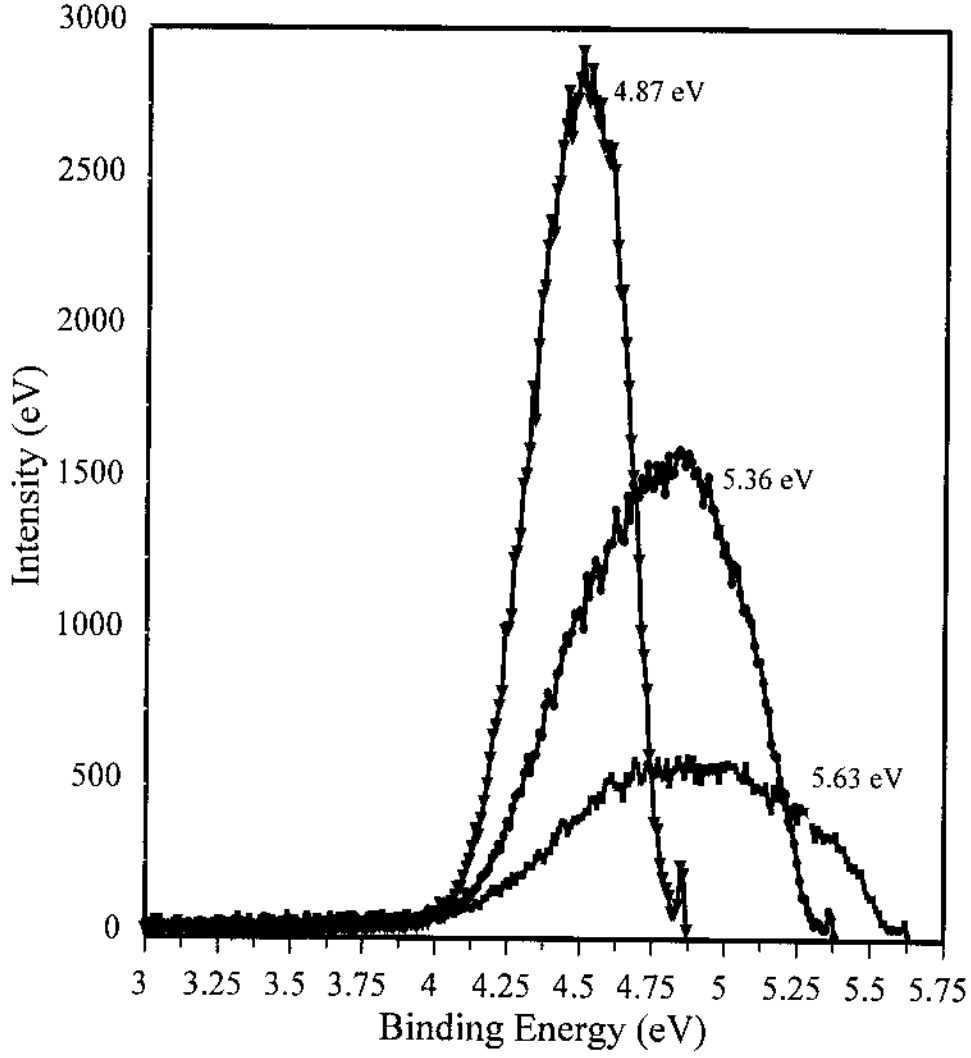

Figure 5.16. Energy distributions of photoemitted electrons from chemical vapor deposition polycrystalline diamond film grown using 4 sccm of boron. The figure shows a shift of the main peak to higher binding energy with increasing photon energy. The energy of the exciting photons is shown for each spectrum.

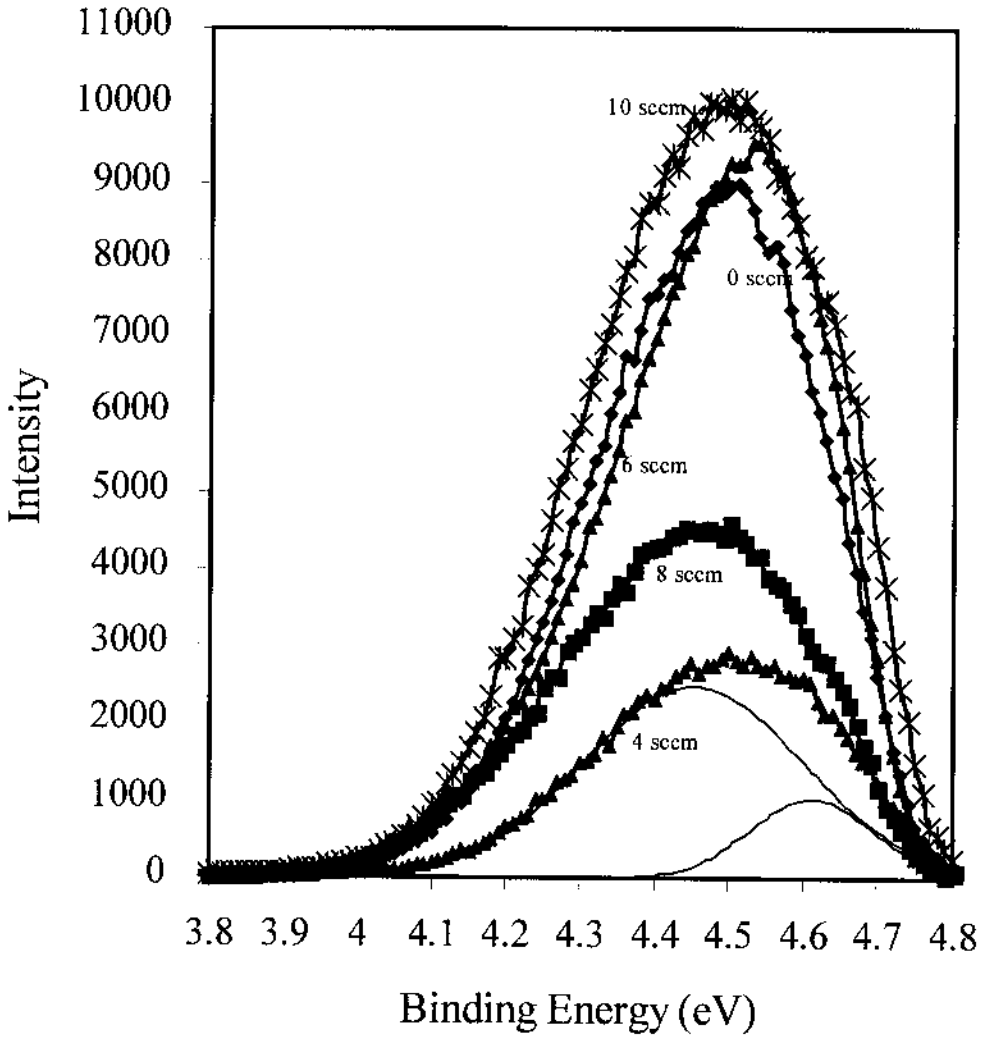

Figure 5.17. Energy distributions of photoemitted electrons from chemical vapor deposition polycrystalline diamond film grown using 0, 4, 6, 8, and 10 sccm of boron. The energy of the exciting photons is 4.87 eV.

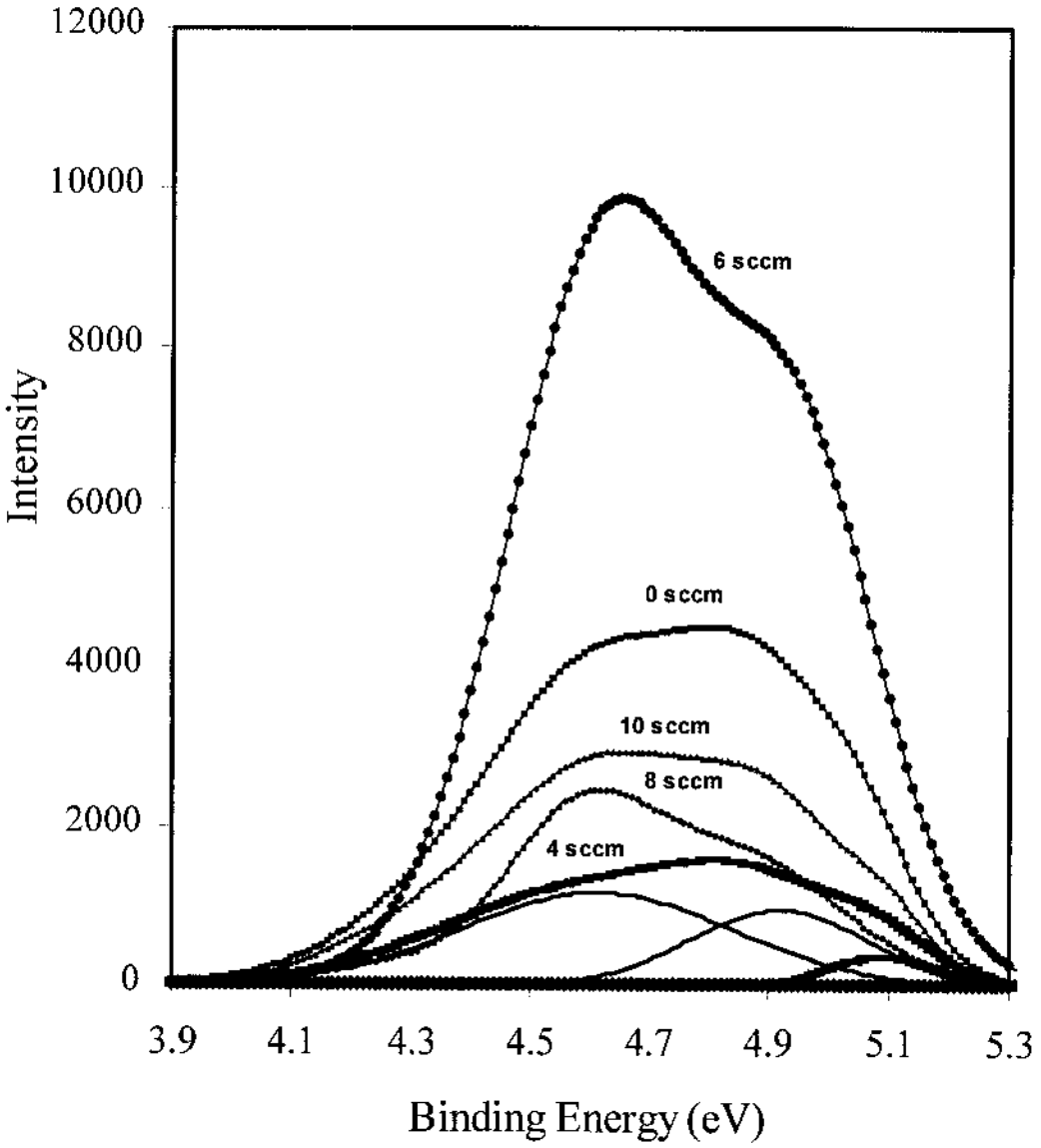

Figure 5.18. Energy distributions of photoemitted electrons from chemical vapor deposition polycrystalline diamond film grown using 0, 4, 6, 8, and 10 sccm of boron. The energy of the exciting photons is 5.36 eV.

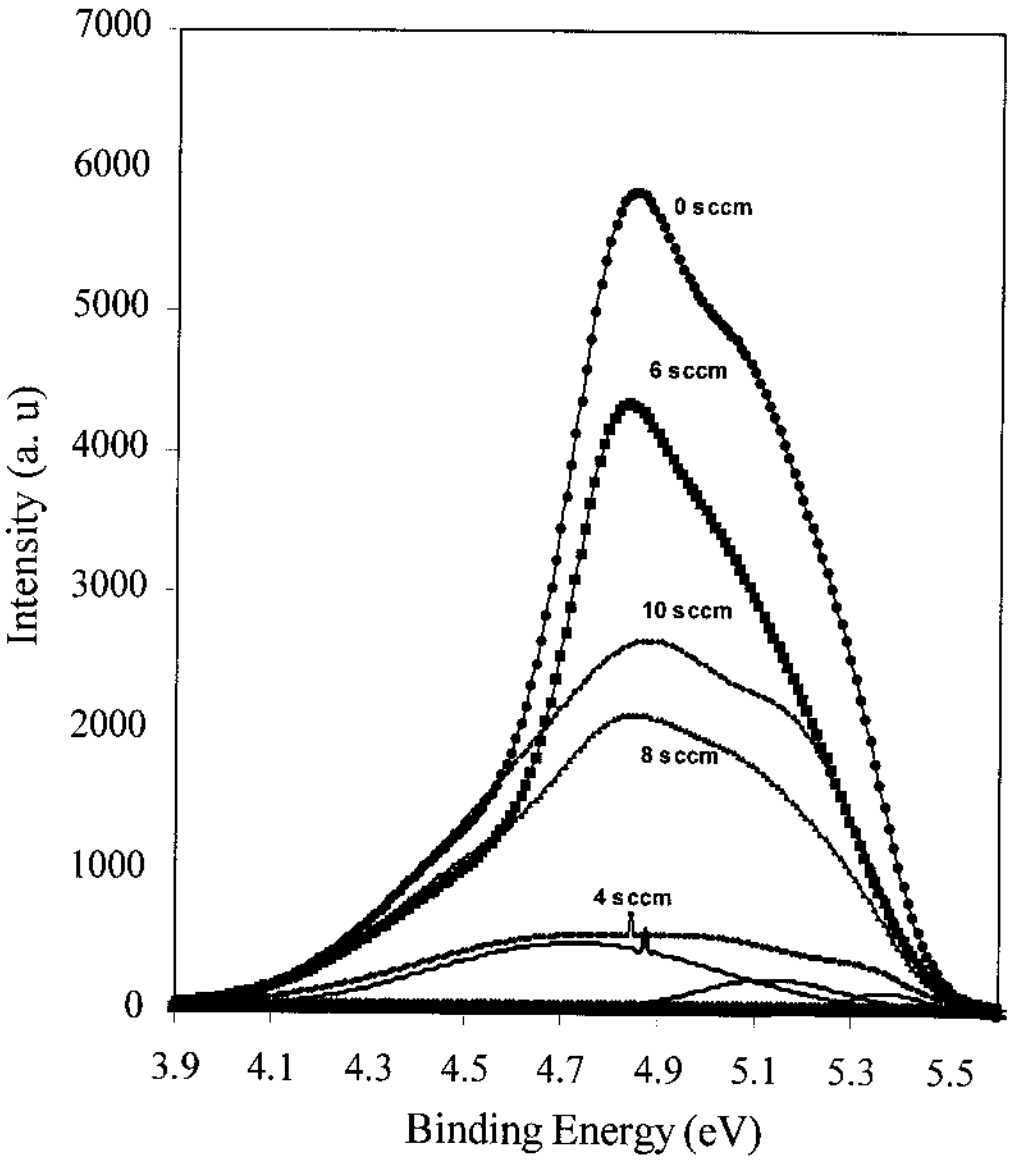

Figure 5.19. Energy distributions of photoemitted electrons from chemical vapor deposition polycrystalline diamond film grown using 0, 4, 6, 8, and 10 sccm of boron. The energy of the exciting photons is 5.63 eV.

concentrations is evident at the different photon energy. The film grown at 6 sccm of boron appears to exhibit the most emission intensity while that of film grown at 4 sccm of boron tends to exhibit the least emission intensity. In general, however, the emission intensity is found to vary strongly from sample to sample depending on the photon energy. This reflects the sensitivity of electron emission to the polycrystalline nature of the films. The observed differences in emission intensity appear to be correlated to the surface roughness and the crystal size of the films. These effects are discussed later.

In contrast to variation in relative emission intensities, similarity in the structure of the spectra at a particular photon energy for films grown with different boron doping levels is evident (figs. 5.17-5.19). Therefore, it is expected that the origin of the electronic energy levels responsible for the observed structure are closely similar. To confirm this, it is first noted that with an increase in photon energy, the UPS spectra change from slightly asymmetric (fig. 5.17) to more asymmetric (fig. 5.19). This asymmetry is probably due to unresolved emission bands. Therefore, a computer line shape analysis of these spectra was undertaken to identify the electronic energy bands contributing to photoelectron emission. These results obtained by fitting the experimental spectra into Gaussian curves are shown in figures 5.17, 5.18 and 5.19, respectively. A fit to the low-energy spectra resolved peaks at binding energies of 4.38 and 4.63 eV. At a photon energy of 5.36 eV, additional peaks at 4.92 and 5.12 eV also contribute. At a photon energy of 5.63 eV, an additional peak at 5.30 eV also contributes. It is interesting to note that at different photon energies all the spectra at each energy domain can be resolved into the peaks described

above including undoped film. These results show that a series of emission bands with different initial energies or states contribute to electron emission. And the initial states are independent of boron concentrations used during growth.

Of special interest is the lack of structure in the low energy region of the UPS curves, such as would result if a well defined localized energy or surface states were present in the films. From the fitting parameters of the energy distribution curves, the lowest or observed threshold energy for undoped and boron doped films is about 4.38 eV, and no structure was found below this energy in all the film. These observations coupled with a sharp onset of photoemission and the fact that the curves exhibit a broad feature that moves monotonically to higher binding energy as the photon energy is increased, suggest that the electron emission is due to valence band states. To verify this, measurements of the photoemission current was performed as a function of photon energy in the threshold region as presented below.

5.7 Photoelectric Measurements

The emission current was measured as a function of photon energy for films grown with 0, 4, 6 and 8 sccm of boron. Employing this method, we found that the photoelectric threshold does not change with boron concentration consistent with the UPS data.

Figure 5.20 shows a plot of the photoelectric current near threshold as a function of incident photon energy for polycrystalline diamond films grown with 0, 4, 6 and 8 sccm of boron. The data have been analyzed on the basis of the Kane's theory [14], by

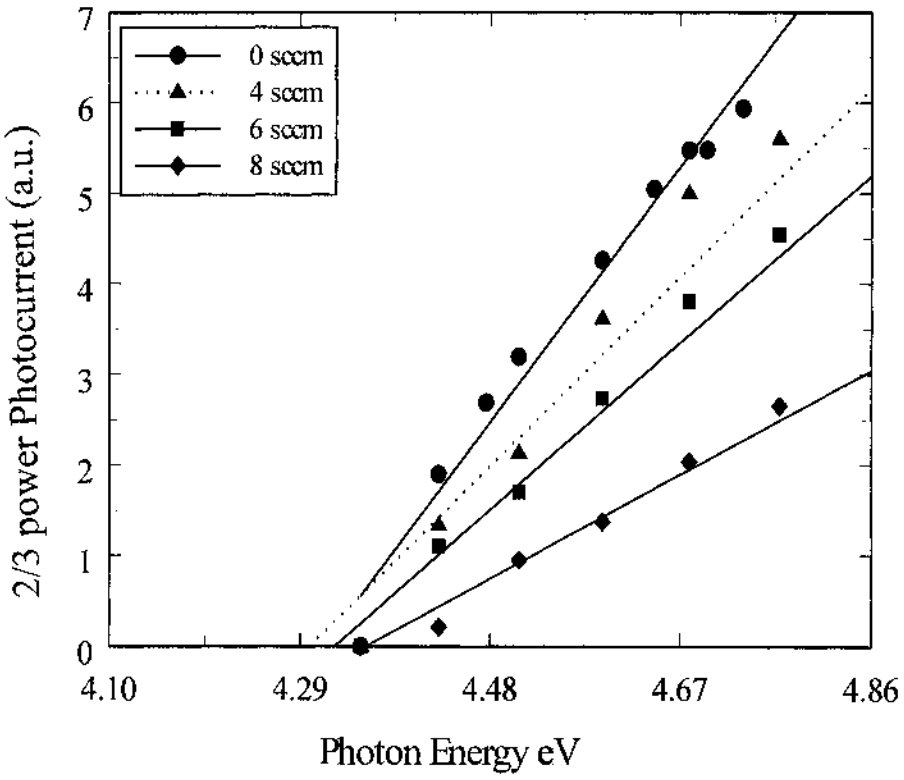

Figure 5.20. Photoelectric response near threshold for chemical vapor deposition polycrystalline diamond films grown using 0, 4, 6, 8, and 10 sccm of boron. The curves are fitted to the function of the form $A(E-E_T)^{3/2}$.

fitting the data to curves of the form $A(E-E_T)^{3/2}$, where A is a constant containing the light intensity and the absorption efficiencies, E is the incident photon energy and E_T is the photoelectric threshold. The photoelectric current results show that E_T is essentially independent of the boron doping for the CVD diamond films investigated. The values of E_T obtained from these data is about 4.35 eV, as shown in figure 5.20. This result, is in agreement with those obtained from UPS measurements.

5.8 Discussion

Figure 5.21 shows a schematic representation of electronic energy levels of the polycrystalline diamond films derived from the analysis of the UPS measurement. The energy level is reference to the vacuum level. According to figure 5.21, the threshold energy for electron emission is located at about 4.38 eV below the vacuum level, independent of boron concentrations. Insensitivity of boron concentration on emission barrier have been reported on field emission studies [15]. It was found that emission barrier does not change irrespective the boron concentration used during growth, in agreement with present results. Comparison of the threshold energy of the boron doped films to that of single-crystal diamond show a significant difference of about 1.1 eV (fig. 5.21). This difference is consistent with the low field electron emission observed in CVD diamond films. It is also seen in figure 5.21, that the number of occupied states contributing to electron emission increases as the excitation energy is increased.

Both undoped [16] and boron doped [17] CVD diamond films have been shown to exhibit a NEA surface. For a NEA surface, the photoelectric threshold occurs at a

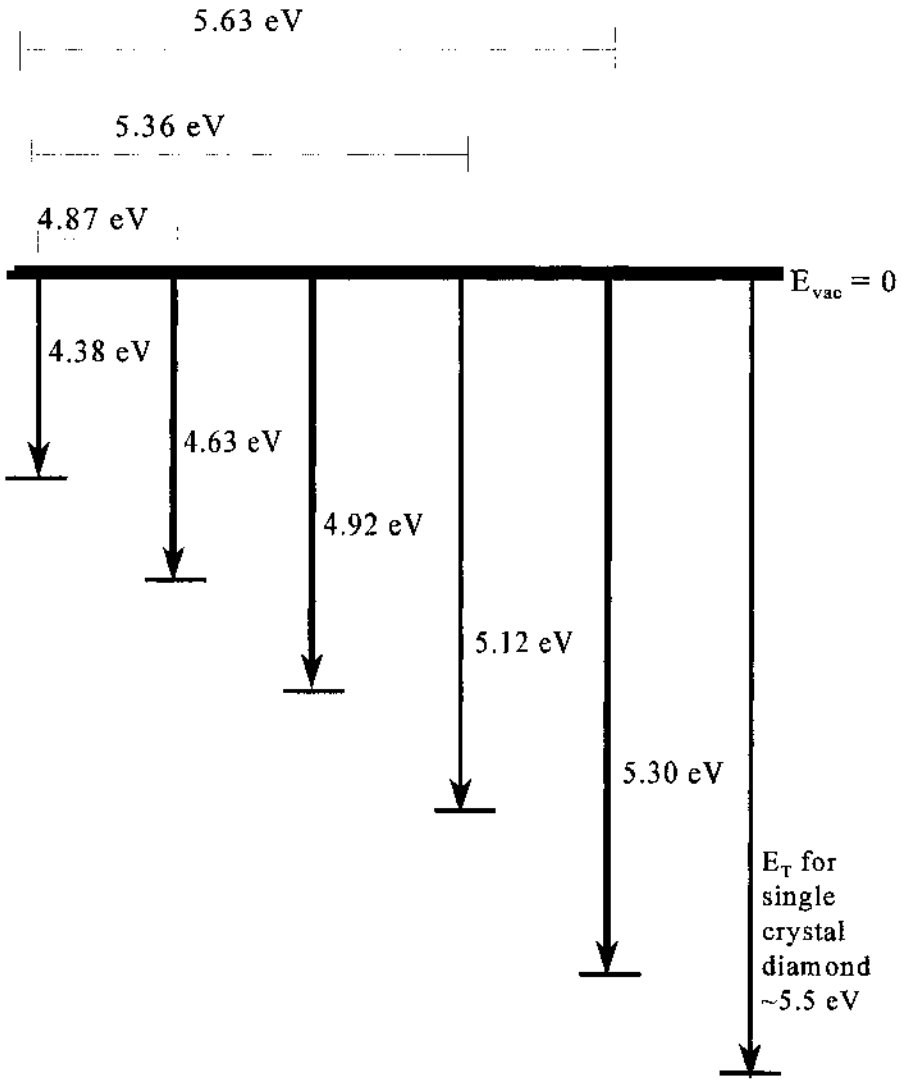

Figure 5.21. Schematic of electronic energy levels of polycrystalline boron doped diamond films derived from the analysis of the UPS measurements.

photon energy equal to the band-gap energy [18]. The diamond films consist of diamond crystallites separated by grain boundaries that consist of sp^3 and sp^2 bonded carbon. The values of $sp^3/(sp^3+ sp^2)$ carbon fraction of the films as determined from XPS and Raman analysis show no appreciable change (Table 4.1), as boron concentrations was varied from 0 to 10 sccm. Recent theoretical calculations predicts that the band-gap of sp^3-sp^2 carbon networks varies as the $sp^3/(sp^3+ sp^2)$ carbon fraction change [19]. In previous chapter, we observed that the a decrease in the value of the $sp^3/(sp^3+ sp^2)$ carbon fraction results in a corresponding decrease in threshold energy, which was attributed to increasing concentration of sp^2 carbon (π states). The calculated value of $sp^3/(sp^3+ sp^2)$ carbon fraction at the surface of the boron doped films was approximately 78% resulting in a threshold energy of about 4.38 eV. This value is consistent with the value that would be expected by considering the trend in Table 4.1 (chapter 4). Since the value of $sp^3/(sp^3+ sp^2)$ carbon fraction and the threshold energy did not change appreciably for different boron doping, therefore we conclude that band-gap of the sp^3-sp^2 networks at the grain boundaries of the polycrystalline boron doped diamond films did not change.

Using band theory of semiconductor, the insensitivity of boron concentrations on energy threshold can be explained. The theory predict that [20]; (1) heavy boron doping (p-type doping) will induce band bending as a result of the presence of surface levels with energies in the forbidden zone (pinned Fermi level). Such behavior will be reflected in lowering of the energy threshold, resulting in an increased emission intensity. (2) In the absence of surface or localized states, the threshold energy is independent of doping (flat

band model or unpinned Fermi level), even though the Fermi level, thus the work function may change. Since boron doping affect the occupation of states through the Fermi distribution function [21], the position of the Fermi level is expected to move towards the valence band with increasing boron doping of the films.

Clearly, our experimental results do not satisfy condition (1) above. The absence of band bending is reflected by the following observations; First, the threshold energy do not change with boron concentrations. Secondly, observed variation in emission intensities is not consistent with band bending effect, since no correlation between an increase in emission intensities with a corresponding increase in boron concentrations can be established. Therefore, the variations in emission intensities observed in these films, can only be attributed to the differences in surface morphology. In fact, our results conform fairly well to the flat band model/unpinning of the Fermi level. This is clearly evident by the very limited influence of boron doping on the threshold energy. Another indication of lack of surface level comes from the functional form of the photoelectric data. The 3/2 power is a characteristic of valence band emission, in agreement with field emission studies of diamond by Bandis et al [21].

By applying Spicer's three steps model of photoelectron emission [22], absorption of light, transportation of electrons to the surface and escape of electron from the surface into vacuum, the differences in emission characteristic of the boron doped films can be explained in terms of surface modification by boron doping, assuming that the probability of electron scattering is small within the energy range studied (4.87 to

5.63 eV). We noted from the SEM results that the films grown with 0, 6, and 10 sccm of boron are characterized by small diamond crystals, consistent with the appearance of microcrystalline peak in their Raman spectra. On the other hand, films grown with 4 and 8 sccm of boron display large diamond crystals. The correlation between electron emission intensities with the surface structure of the films show that the films with smaller diamond crystals and homogenous surface structure have a higher emission intensities than those with larger crystals and rough surface. This result can not be explained by differences in emission barrier (surface potential) as already discussed above.

However, optical absorption loss and electron scattering processes due to the differences in surface structure are more likely responsible for the observed emission behavior. This is consistent with the results of optical studies by Bi et al [23]. They showed that large diamond crystals introduce significant optical scattering loss in comparison to small crystals. They also reported that surface roughness causes significant optical loss for wavelengths on the order of the scale of the surface roughness. This later result could explain observed variations of relative emission intensities at different excitation energies (wavelengths) of the films. Moreover, recent optical studies of semiconductor nanocrystals reveal massive changes in optical properties as a function of crystal size [24, 25]. Specifically, it was found that the absorption band shift to higher energy with decreasing crystallite size [26, 27]. This means that electron emission is expected to increase in intensity at a higher photon energy for microcrystallin films.

However, it is difficult to pinpoint this effect in the present experimental results since the intensity of the light sources is different at different excitation energies used.

In addition to optical loss, a rough surface can effect emission probability of escaping electron depending on the nature of the surface. We noted that the films that contain large diamond crystals (4 and 8 sccm of boron) exhibit rougher surface than the microcrystallin films (0, 6, and 10 sccm of boron). This may in part account for the low emission intensities observed in these films, since electrons can be scattered by rough surface during the escape step.

5.9 Conclusion

If surface states are formed due to boron doping, band bending could be induced that would in turn lower the threshold energy. If no surface states are formed, the threshold energy will be independent of boron doping. The present results are characteristic of valence band emission ($E^{3/2}$ power dependence) and indicate valence band emission at 4.38, 4.63, 4.92, 5.12 and 5.30 eV. The SEM results indicate small diamond crystals for films grown with 0, 6 and 10 sccm of boron. This is consistent with the microcrystallin peak observed in the Raman data and also indicated by the XPS results where another diamond peak is needed the analysis. The 4 and 8 sccm boron samples show large diamond crystals in SEM and no indication of a microcrystallin peak in the Raman data.

The electron emission data shows that films with smaller diamond crystals and more uniform surfaces have higher emission intensities than surfaces with larger crystals

and rougher surfaces. These results conclude that the $sp^3/(sp^3+ sp^2)$ carbon fraction and emission threshold are independent of boron concentrations. However, the emission intensity is sensitive to surface morphology.

References

1. C. Wang, A. Garcia, D.C. Ingram, M. Lake, and M.E. Korderch, *Electron Lett.* **27**, 1459 (1991).

2. N.S. Xu, Y. Tzena, and R.V. Latham, *J. Phys. D* **26**, 1776 (1993).

3. D. Hong and M. Aslam, *J. Vac. Sci. Technol. B* **13**, 427 (1993).

4. F.J. Himpsel, J.A. Knapp, J.A. VanVechten, and D.E. Eastman, *Phys. Rev. B* **20**, 624 (1979).

5. G. Gidenblat, S.A. Grot, C.W. Hatfield, C.R. Wronski, A.R. Badzian, T. Badzian, and R. Messier, *Mater. Res. Bull.* **25**, 129 (1990).

6. C. Tsai, W. Gerberich, Z.P. Lu, J. Herberlein and E. Pfender, *J. Mater. Res.* Vol. **6**, No 10, 2127 (1991).

7. A.W. Phelp, R. Koba, *Pro. 1st Intern. Symp. on Diamond and Diamond-Like Films,* Vol. 89-12 (Electrochem. soc.1989) pp. 38.

8. R.J. Nenamich, J.T. Glass, G. Lucovski, and R.E. Shroder, *J. Vac. Sci Technol.* A**6**, 1783 (1988).

9. K. Miyata, K. Kumagai, K. Nishimura, and K. Kobashi, *J. Mater. Res.*, Vol. **8**, No 11, 2845 (1993).

10. K. Nishimura, K. Das, J.T. Glass, and R.J. Nemanich, Proc. of NATO Advanced

Research Workshop on the Physics and Chemistry of Carbdes Nitrides and Borides, Manchester, U.K. Oct.(1989).

11. J.H. Won, A. Hatta, H. Yagyu, N. Jiang, Y. Mori, T. Ito, T. Sasaka, and A. Hiraki, *Appl. Phys. Lett.* **68**, 2822 (1996).

12. C.N. Berglund and W.E. Spicer, *Phys. Rev.* **136**, 1030 (1964).

13. C.N. Berglund and W.E. Spicer, *Phys. Rev.* **136**, 1044 (1964).

14. E.O. Kane, *Phys. Rev.* **127**, 131 (1962).

15. M. Nagao, T. Kondo, Y. Gotoh, H. Tsuji, J. Ishikawa, K. Miyata, and K. Kobashi, *Appl. Phys. Lett.* **71**, 2806 (1997)

16. I.L. Krainsky, V.M. Asnin, G.T. Mearini, and J.A. Dayton, *Phys. Rev.* **B 53**, R7650 (1996).

17. C. Bandis and B.B. Pate, *Surface Science* **350**, 315 (1996).

18. C. Bandis and B.B. Pate, *Phys. Rev.* **B 52**, 12056 (1995).

19. R. Sen, R. Sumathy, and C.N.R. Rao, *J. Mater. Res.* **11**, 2961 (1996).

20. R. Dalven, *Introduction to Applied Solid State Physics,* Plenum Press, New York, (1981) pp. 139-160.

21. C. Bandis and B.B. Pate, Appl. *Phys. Lett.* **69**, 367 (1996).

22. W.E. Spicer, *Phys. Rev.* **112**, 114 (1958).

23. X.X. Bi, P.C. Eklund, J.G. Zhang, A.M. Rao, T.A. Perry and C.P. Beetz, Jr., *J. Mater. Res.* **Vol. 5**, No. 4, 811 (1990).

24. R. Rossetti, S. Nakahara, L.E. Brus, *J. Chem. Phys.* **79**, 1086 (1983).

25. A. P. Alivsatos, *J. Phys. Chem.* **100,** 13226 (1996).

26. Y. Wang and N. Herron, *J. Phys. Chem.* **95,** 525 (1991).

27. D.M. Mittleman, W.R. Schoenlein, J.J. Shiang, V.L. Colvinet al. *Phys. Rev. B: Condens. Matter*, **49**, 14435 (1994).

CHAPTER 6

PHOTOELECTRON EMISSION PROPERTIES OF NITROGEN DOPED CHEMICAL VAPOR DEPOSITION GROWN DIAMOND FILMS

6.1 Introduction

Impurities are of major importance in all semiconductor devices. Impurities can alter the structure, electronic and optical properties of a semiconducting material. Electron emission properties of CVD diamond films are sensitive to growth parameters of dopant concentrations, and surface conditions [1]. The study of methane (CH_4) concentration on electron emission properties of CVD polycrystalline diamond films discussed in chapter 4 showed a significant decrease in the photoelectric threshold as the $sp^3/(sp^3 + sp^2)$ carbon fraction in the film decreases. For H- terminated (111) and (100) diamond surfaces, negative electron affinity (NEA) has been observed [2,3]. While the negative electron affinity character of the diamond surface suggests low emission barrier for an electron at the surface, practical emission characteristics depend on the electron source and transport of the electrons through the material. Usually, for semiconductors, emitted electrons can originate from the conduction band, the valence band and/or surface

states. In order to take advantage of the diamond NEA to achieve low threshold energy for emission, it is necessary to populate the conduction band with electrons or subbands with energies near or above the vacuum level. Theoretically, such an effect can be achieved by doping diamond with n-type donors. Currently, lack of an electrically active n-type dopant is a limitation to the development of diamond films for device applications. Although, Brandes et al. [4] and Twitchell et al. [5] have reported weak n-type doping using lithium and phosphorus. Nitrogen is one of the most commonly impurities in certain natural diamond, and it is considered to play an important role in modifying the structure, optical and electrical properties of diamond films.

Many studies have been done on the effects of nitrogen on the morphology and quality of diamond films. Significant improvement of the quality of diamond films with addition of small amount of nitrogen during diamond film growth has been observed experimentally, and was attributed to increase concentration the sp^3 bonding [6-7]. By using electron paramagnetic resonance (EPR) and secondary ion mass spectroscopy, Hoikins at al. concluded that N_2 is incorporated into substitutional sites of the diamond lattice [8], resulting in structural distortion. Structural changes can lead to changes in electronic structure, thus emission properties. Recent reports have indicated enhanced field emission from nitrogen doped diamond at low applied voltages [9]. However, the mechanism responsible for the electron emission is not still clear. It is known that addition of high concentration of nitrogen during diamond growth can lead to deterioraton of the film quality and increase formation of graphitic phases. An

understanding of the correlation between the structure and photoelectron emission properties of nitrogen doped CVD diamond films is essential for CVD diamond applications, and have not been reported.

In this chapter, results of the experimental measurements on the effect of nitrogen partial pressure in CH_4/H_2 gas mixture on the photoelectron emission characteristic of CVD grown polycrystalline diamond films are presented. In particular, the effects of the $sp^3/(sp^3 + sp^2)$ carbon fraction on the photoelectric threshold and electron emission characteristics are discussed.

6.2 Experimental

Nitrogen doped polycrystalline diamond films were grown on p-type single crystal Si substrates using hot filament CVD method under an atmosphere of $CH_4+H_2+N_2$. A detail of the growth procedure is already described in chapter 3. The growth conditions are as follows: the tungsten filament temperature was 2220 ^{0} C, the substrate temperature was 870 ^{0} C, the total gas pressure was maintained at 38 torr, the hydrogen and methane flow rates were maintained at 200 and 0.5 sccm respectively. Different nitrogen concentrations was achieved by varying the partial pressure of nitrogen gas in the growth chamber from 15 millitorr to 25 millitorr.

The surface morphology, structure and electron emission properties of polycrystalline nitrogen doped diamond films were examined using a number of methods. The surface morphology of the films were examined using scanning electron microscope. The characteristic habit of diamond crystals were observed in both films, and the crystals

size is found to decrease with an increase in N_2 gas pressure used during growth. The Raman spectra was used to characterize the different forms of carbon and the relative concentrations of sp^3 to (sp^3 + sp^2) carbon fraction in the film. The XPS was used to obtain a quantitative value of the $sp^3/(sp^3 + sp^2)$ carbon fraction at surface of the film. The electron emission properties was studied using UPS and photocurrent measurements. The electron energy distribution and emission current were measured using the Xenon source and monochromator as discussed in chapter 3.

6.3 Morphology of the Film Surfaces

Figures 6.1 show the scanning electron micrographs of polycrystalline diamond films grown on a Si substrate using 15 and 25 millitorr partial pressure of N_2 gas. As can been seen from the images, the surface morphology and crystallinity are function of the N_2 gas pressure used during growth. The film grown using 15 millitorr of N_2 gas pressure have primarily large diamond crystals with (100) faces, as shown in Fig. 6.1(a). The surface morphology changes significantly as the N_2 gas pressure increased to 25 millitorr. Smaller and denser diamond crystals with (111) faces are observed, as shown in fig. 6.1(b). Similar morphological changes were observed in previous studies for CVD diamond films grown at higher CH_4 and B_2H_6 concentrations, and was attributed to high diamond nucleation density.

It is evidence from the SEM data that low nitrogen concentration results in a high

Figure 6.1. Scanning electron micrographs of chemical vapor deposition grown polycrystalline diamond films grown on Si substrate using 15 millitorr (a) and 25 millitorr (b) of partial pressure of N_2 gas.

crystal quality of diamond film with (100) faces, while higher concentrations of nitrogen lead to microcrystalline diamond films with (111) faces and increased grain boundaries. It has been shown that significantly larger nitrogen concentrations lead to (111) faces as compared to (100) faces [9].

6.4 Raman Spectroscopy Results

Figures 6.2 and 6.3 show the Raman spectra of polycrystalline diamond films grown at 15 and 25 millitor of nitrogen partial pressures, respectively. The Raman spectra are fitted with Gaussian and Lorentzian line shape and the fitting parameters; positions and linewidths of individual line and the areas under each peak as well as the intensity ratio (diamond height peak/graphite height peak) were determined. Both spectra show the 1333 cm^{-1} line characteristic of single-crystal diamond and a broad peak extending from about 1549 to 1600 cm^{-1}. The later peak arises from graphite and amorphous carbon. The diamond film grown using 15 millitorr of N_2 partial gas pressure shows features characteristic of good quality diamond film. This is evidenced by the following observations; prominent diamond line, FWHM of about 8 cm^{-1} and weak scattering from non-diamond carbon phases, consistent with the SEM result. On the other hand, the film grown using 25 millitorr of N_2 gas pressure shows relatively strong scattering from non-diamond phases, FWHM of about 10.4 cm^{-1} and an additional peak at about 1210 cm^{-1}, characteristics of microcrystalline diamond, in agreement with the SEM result.

The percentage of the area under the diamond line at 1333 cm^{-1} to the total area

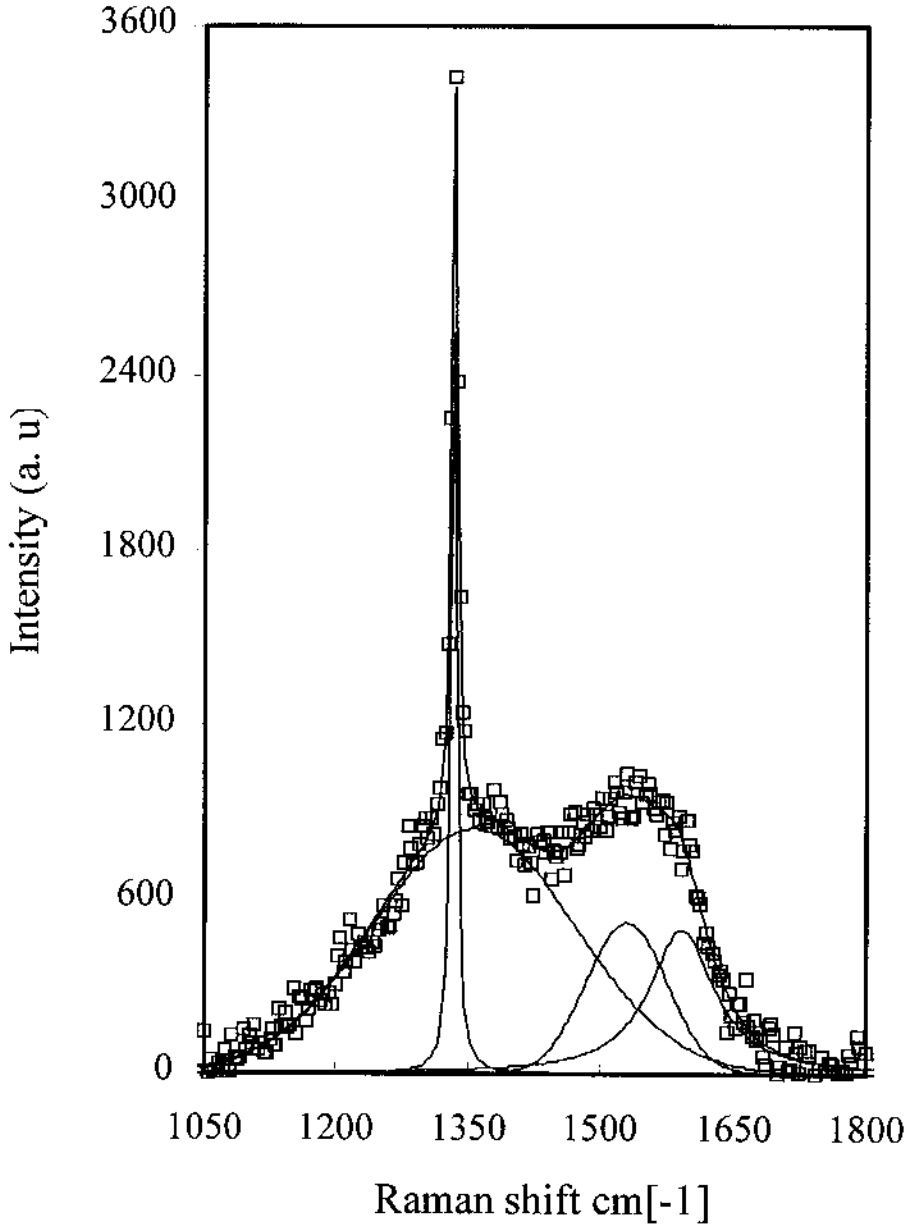

Figure 6.2. Raman spectrum of a chemical vapor deposition polycrystalline diamond film grown using 15 millitorr of partial pressure of N_2 gas.

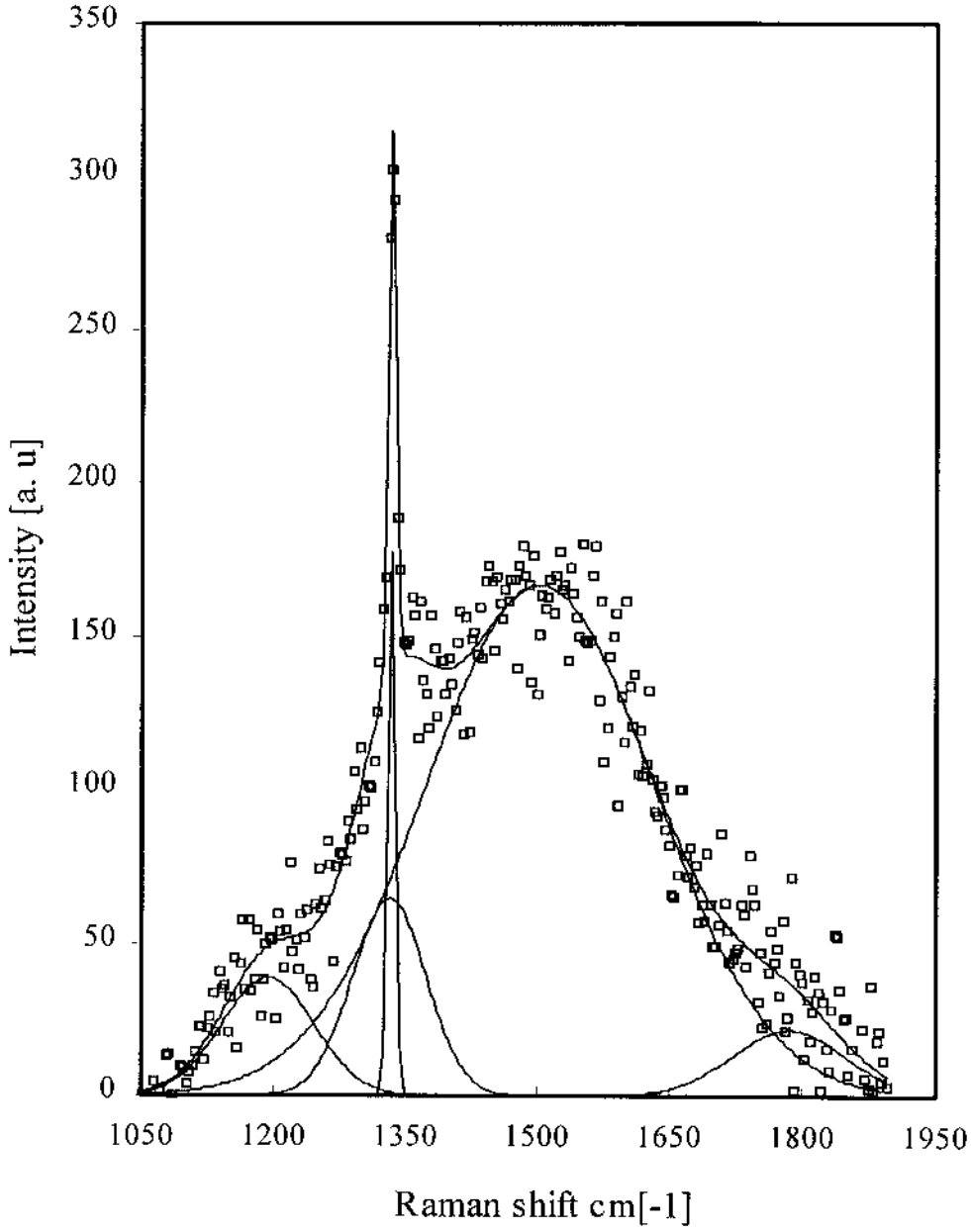

Figure 6.3. Raman spectrum of a chemical vapor deposition polycrystalline diamond film grown using 25 millitorr of partial pressure of N_2 gas.

under all peaks or $sp^3/(sp^3 + sp^2)$ carbon fraction change from 8.1% to 3%, as the N_2 gas partial pressure increases from 15 to 25 millitorr. In addition, the intensity ratio changes from 4.9 to 1.1, as the nitrogen pressure increases from 15 to 25 millitorr. These results show that the $sp^3/(sp^3 + sp^2)$ carbon fraction is a function of the N_2 gas pressure used during growth.

6.5 X-ray Photoelectron Spectroscopy Results

XPS spectra of polycrystalline nitrogen doped diamond films grown using 15 and 25 millitorr of N_2 gas pressures are presented in Figures 6.4 and 6.5, respectively. The data were analyzed by fitting the spectra with three Gaussian lines that are centered at about 283.8, 284.5 and 284.6 eV respectively. The peak at 283.8 eV is attributed to sp^2 carbon, and the two later peaks, separated by about 0.1 eV is believed to be due to sp^3 carbon with large diamond and a microcrystalline diamond peak respectively. This data was used to obtain the quantitative percentage diamond content or the value of $sp^3/(sp^3 + sp^2)$ carbon fraction on the surface of the film. The area calculation showed a significant decrease in diamond content from 76% to 50%, as the nitrogen gas pressure increases from 15 to 25 millitorr, in agreement with the Raman results.

A comparison of the XPS spectra of the investigated films shown in figures 6.4 and 6.5. show that the main peaks is shifted by about 0.15 eV. This shift is attributed to incorporation of nitrogen into the diamond lattice which alters the chemical environment of the core levels, thus the binding energy.

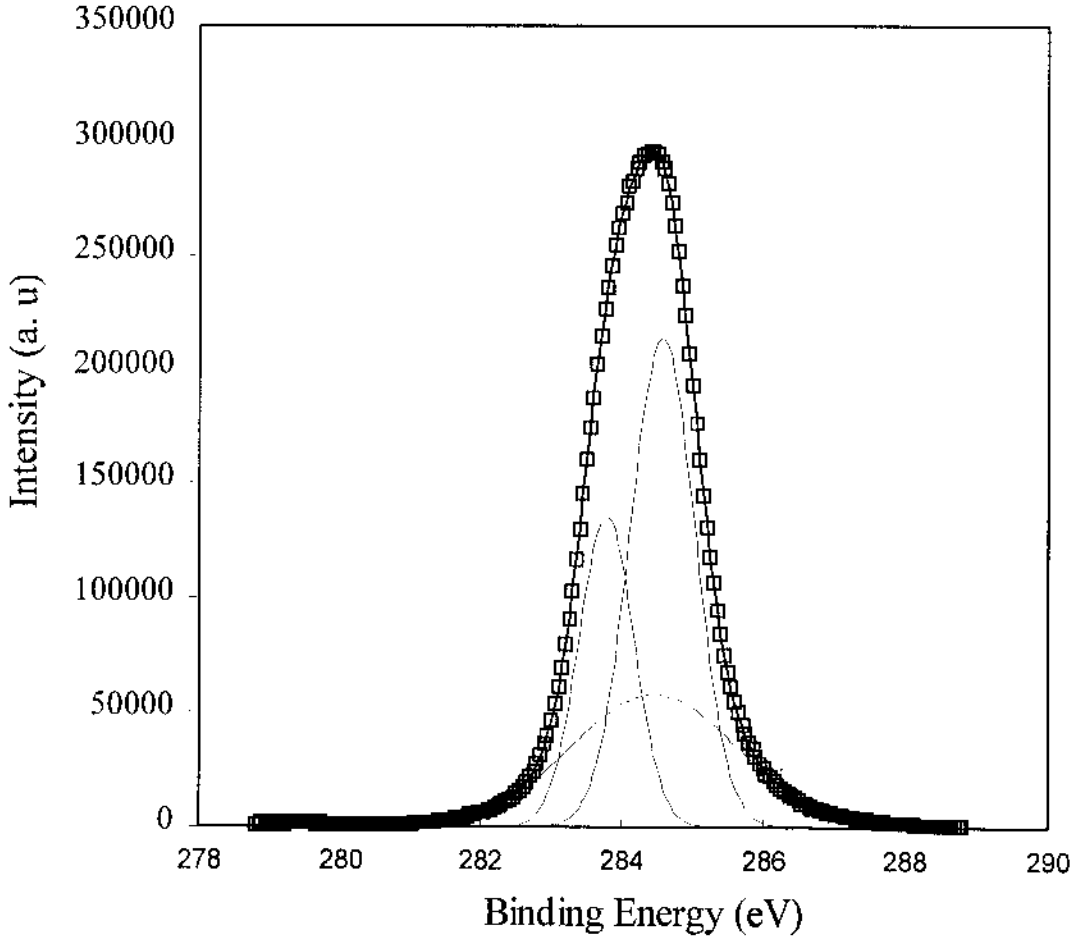

Figure 6.4. X-ray photoelectron spectrum of the C 1s line of a chemical vapor deposition grown polycrystalline diamond film grown using 15 millitorr of partial pressure of N_2 gas.

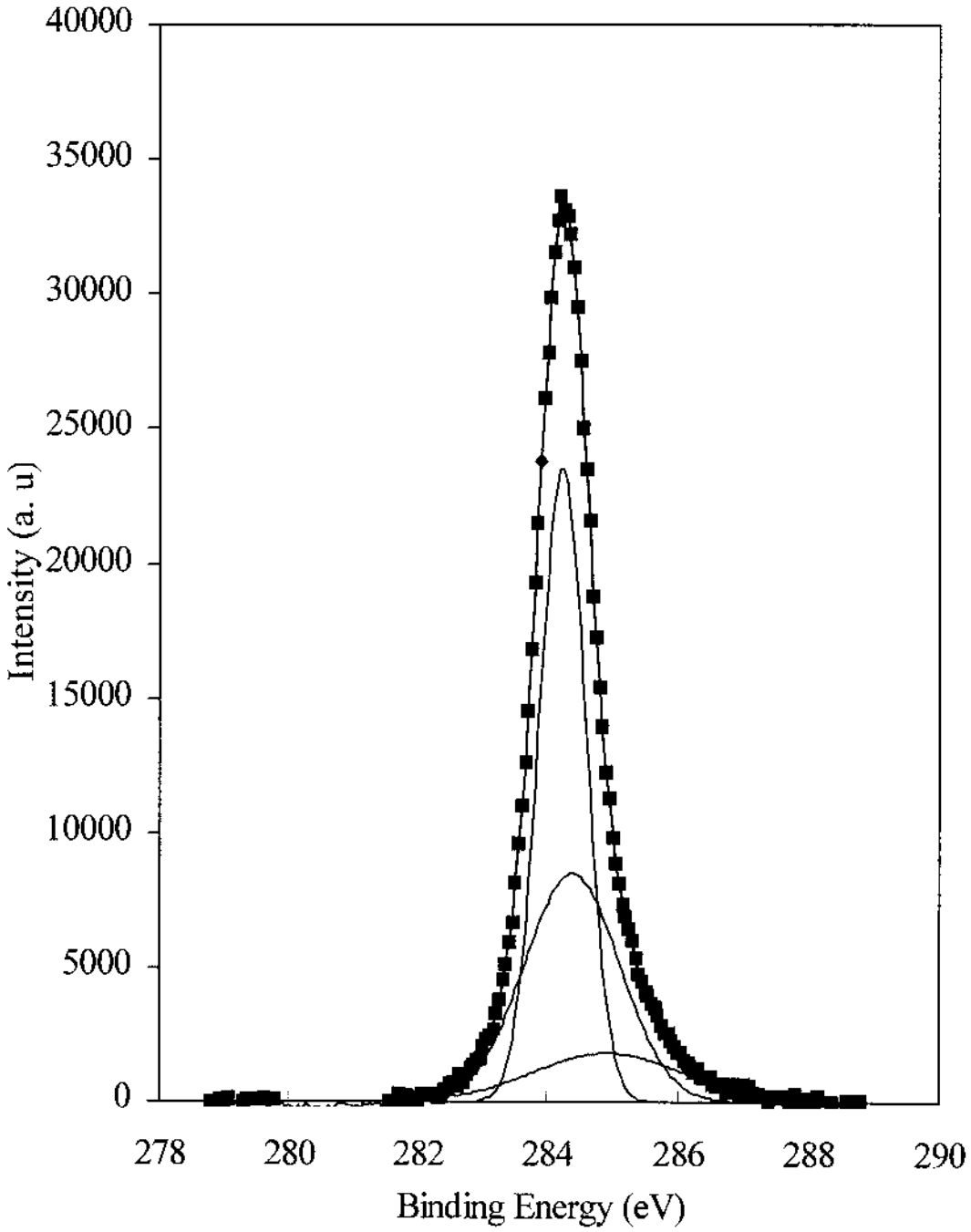

Figure 6.5. X-ray photoelectron spectrum of the C 1s line of a chemical vapor deposition grown polycrystalline diamond film grown using 25 millitorr of partial pressure of N_2 gas.

6.6 Ultraviolet Photoelectron Spectroscopy

Figures 6.6 and 6.7 show the photoemission energy distributions as a function of binding energy, for CVD diamond films grown using 15 and 25 millitorr partial pressure of N_2 gas, respectively. The excitation energies are 4.87 eV and 5.38 eV, as shown in the figures. In general, the UPS spectra depend on the excitation energy similar to those observed in boron doped diamond films. The broadening of the curves, the shift of the main peak positions to higher binding energy, and an increase in emission intensity with increasing photon energy are observed.

A peak fit analysis was used to identify the electronic energy bands contributing to electron emission. These results are displayed in Figs. 6.8- Fig. 6.11 for polycrystalline diamond films grown using 15 and 25 millitorr partial pressure of N_2, at excitation energies of 4.87 eV and 5.38 eV, respectively. At a photon energy of 4.87 eV, the UPS emission is due to peaks at 4.27, 4.51 and 4.83 eV for the film grown using 15 millitorr of N_2 gas, while emission at the same excitation energy from the film grown with 25 millitorr is due to peaks at 4.09, 4.52 and 4.82 eV. At photon energies of 5.36 eV, an additional peak at 5.18 eV also contribute in both films. The lowest energy peak was found at 4.09 eV for the film grown using 25 militorr of N_2 gas pressure, which differs significantly by about 0.18 eV from that of the film grown using 15 millitorr of N_2 gas pressure. Since the values of the lowest peaks correspond to the minium photon energy (threshold energy) necessary to remove an electron from the highest occupied energy levels to the vacuum. Therefore, these results show that the threshold energy of CVD

diamond films is significantly dependent on the N_2 gas pressure used during growth and suggest that the film grown at higher nitrogen concentration (low $sp^3/(sp^3 + sp^2)$ carbon fraction) have better electron emission properties than the film grown at a lower nitrogen concentration (high $sp^3/(sp^3 + sp^2)$ carbon fraction).

For comparison, figures 6.12-6.13 show compilation of both films at a photon energy of 4.87 eV and 5.38 eV, respectively. In general, fig. 6.12-fig. 6.13 show that the film grown using 25 millitorr of N_2 gas pressure exhibit a higher emission intensity than that of the film grown using 15 millitorr of N_2 gas pressure. This is consistent with lower emission threshold energy observed in the film grown at higher N_2 gas pressure. Furthermore, by increasing the photon energy from 4.87 eV to 5.36 eV, emission intensity is observed to increase by a factor of about 3, for the diamond film grown at 25 millitorr of N_2 gas pressure. This increase in emission intensity is attributed to the differences between the surface morphology of the films.

6.7 Photoelectric Measurements

To verify UPS measurements, emission current was measured as a function of photon energy in the threshold region from the nitrogen doped polycrystalline diamond films. Figures 6.14 and 6.15 show a plot of the photoelectric current as a function of photon energy near threshold. The results were analyzed using the functional form expected for figures 6.14 and 6.15 show a plot of the photoelectric current as a function of photon energy near threshold. The results were analyzed using the functional form expected for direct opitical transitions from the valence band, as shown in figure 6.14

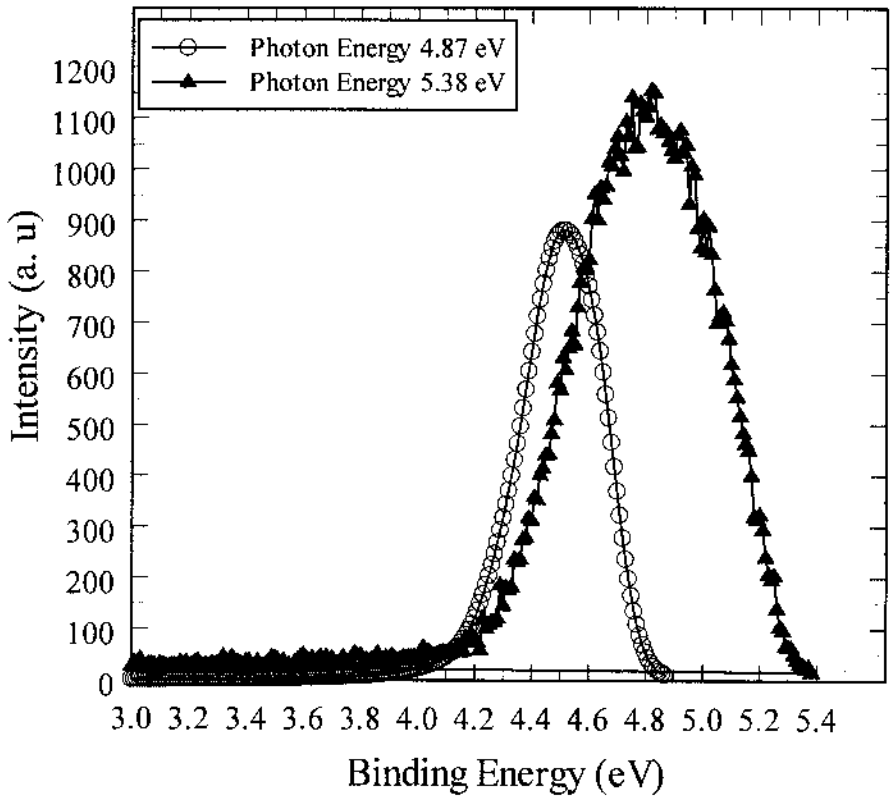

Figure 6.6. Energy distributions of photoemitted electrons from a chemical vapor deposition polycrystalline diamond film grown using 15 millitorr of partial pressure of N_2 gas. The energies of the exciting photons is shown in the figure.

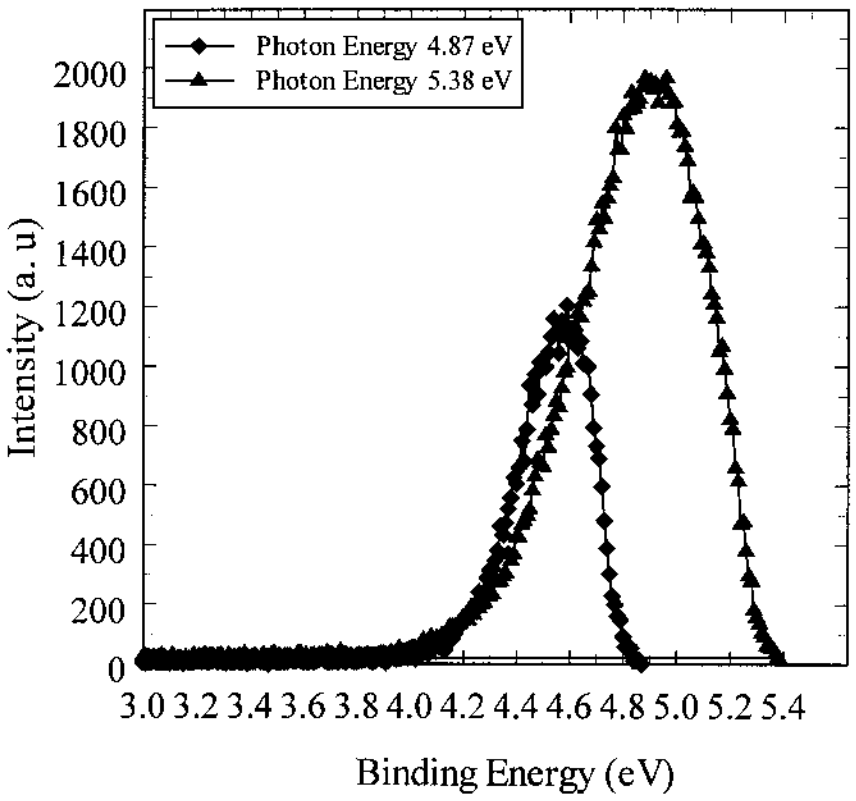

Figure 6.7. Energy distributions of photoemitted electrons from a chemical vapor deposition polycrystalline diamond film grown using 25 millitorr of partial pressure of N_2 gas. The energies of the exciting photons is shown in the figure.

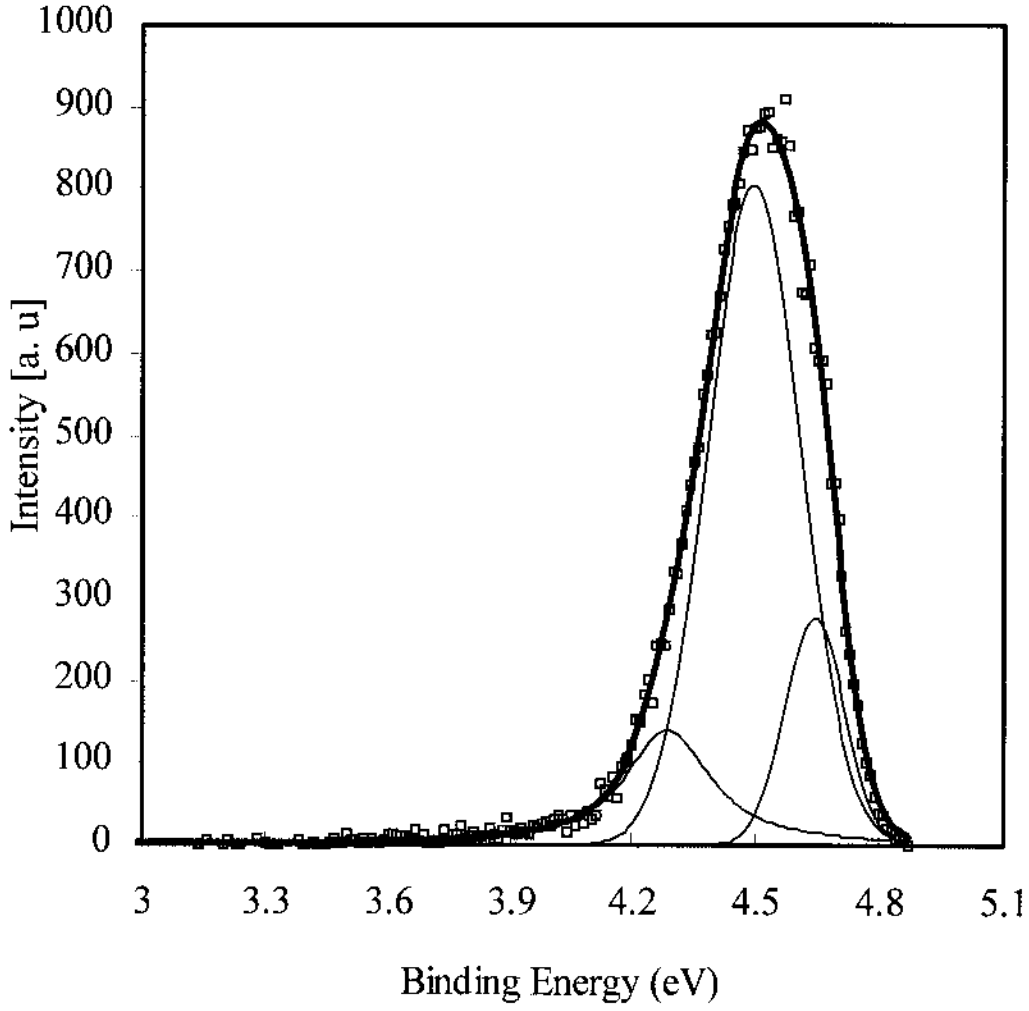

Figure 6.8. Energy distribution of photoemitted electrons from a chemical vapor deposition polycrystalline diamond film grown using 15 millitorr of partial pressure of N_2 gas. The energy of the exciting photons is 4.87 eV. The fit indicate emission bands at 4.27, 4.50 and 4.75 eV.

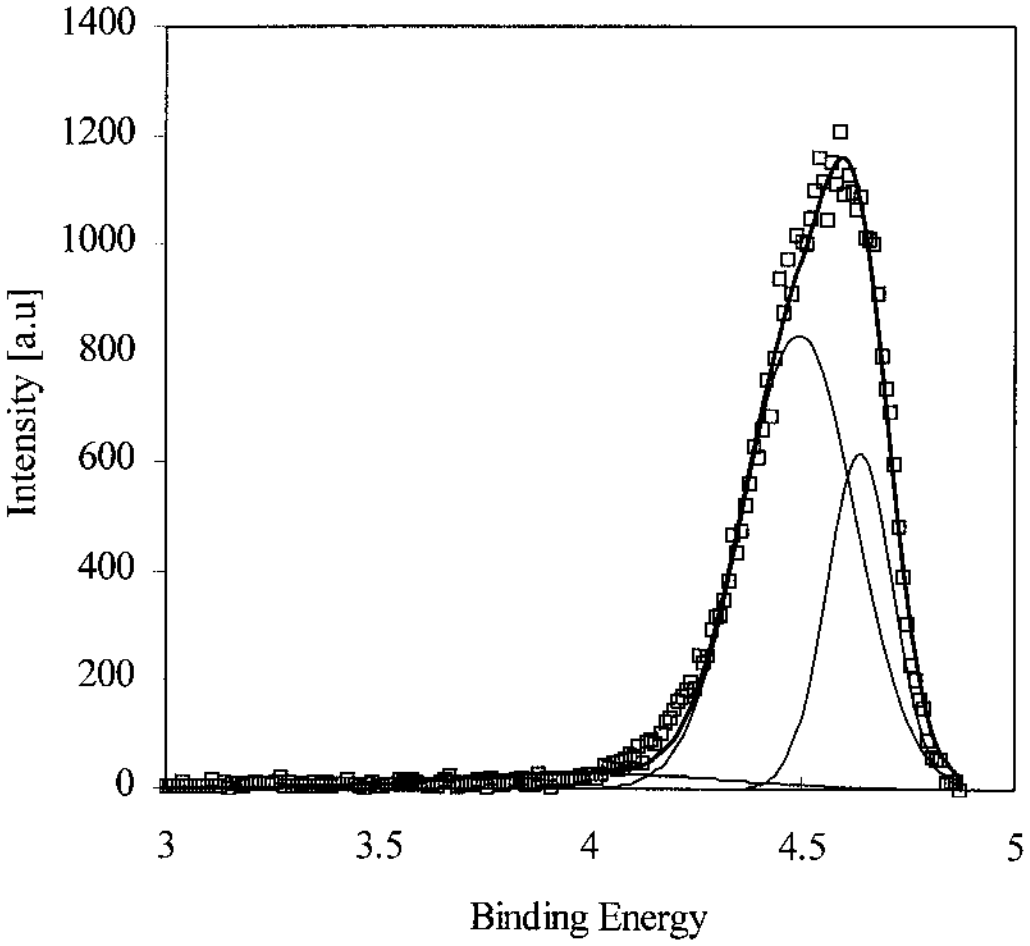

Figure 6.9. Energy distribution of photoemitted electrons from a chemical vapor deposition polycrystalline diamond film grown using 25 millitorr of partial pressure of N_2 gas. The energy of the exciting photons is 4.87 eV. The fit indicate emission bands at 4.10, 4.50 and 4.75 eV.

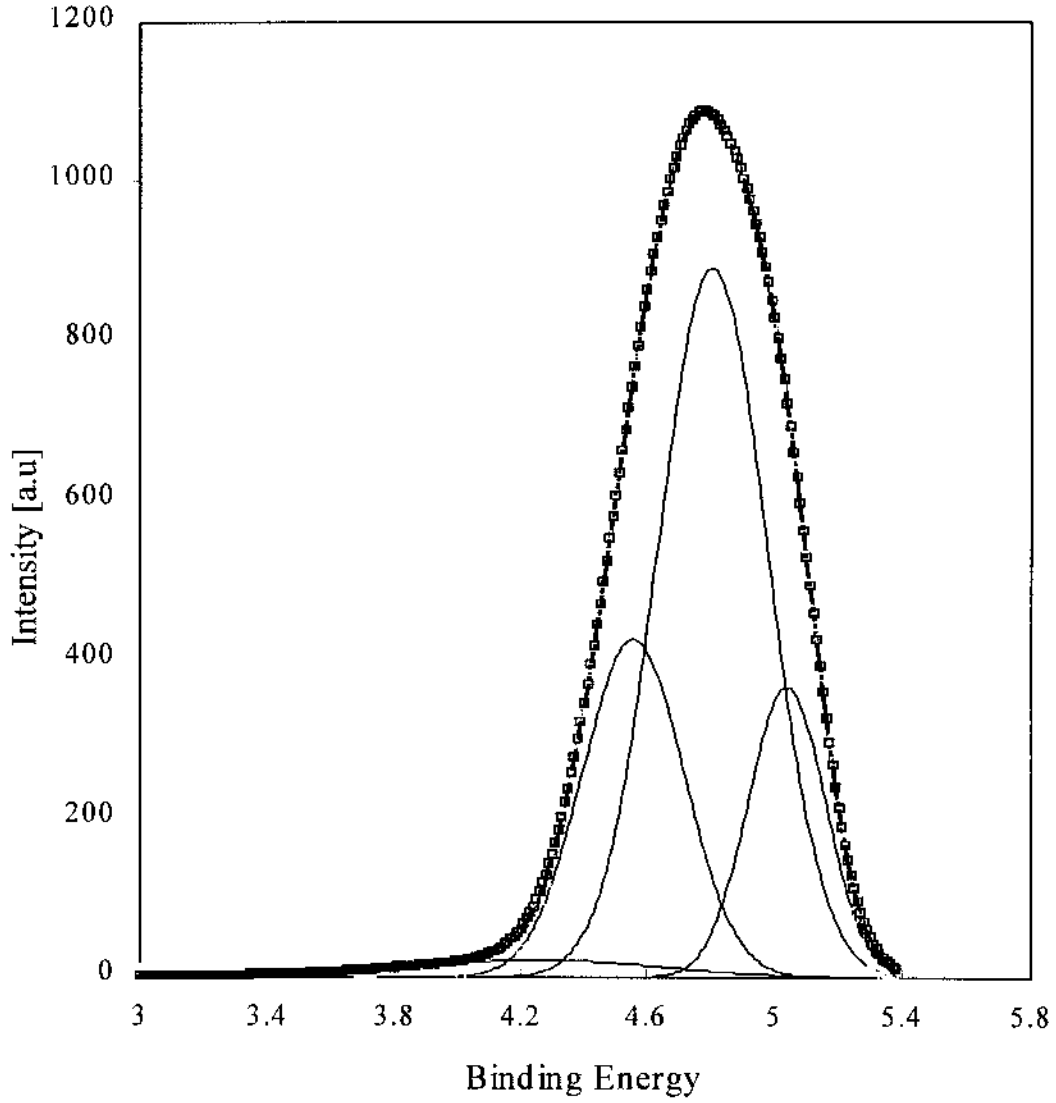

Figure 6.10. Energy distribution of photoemitted electrons from chemical vapor deposition polycrystalline diamond film grown using 15 millitorr of partial pressure of N_2 gas. The energy of the exciting photons is 5.36 eV. The fit indicate emission bands at about 4.26, 4.50, 4.75 and 5.18 eV.

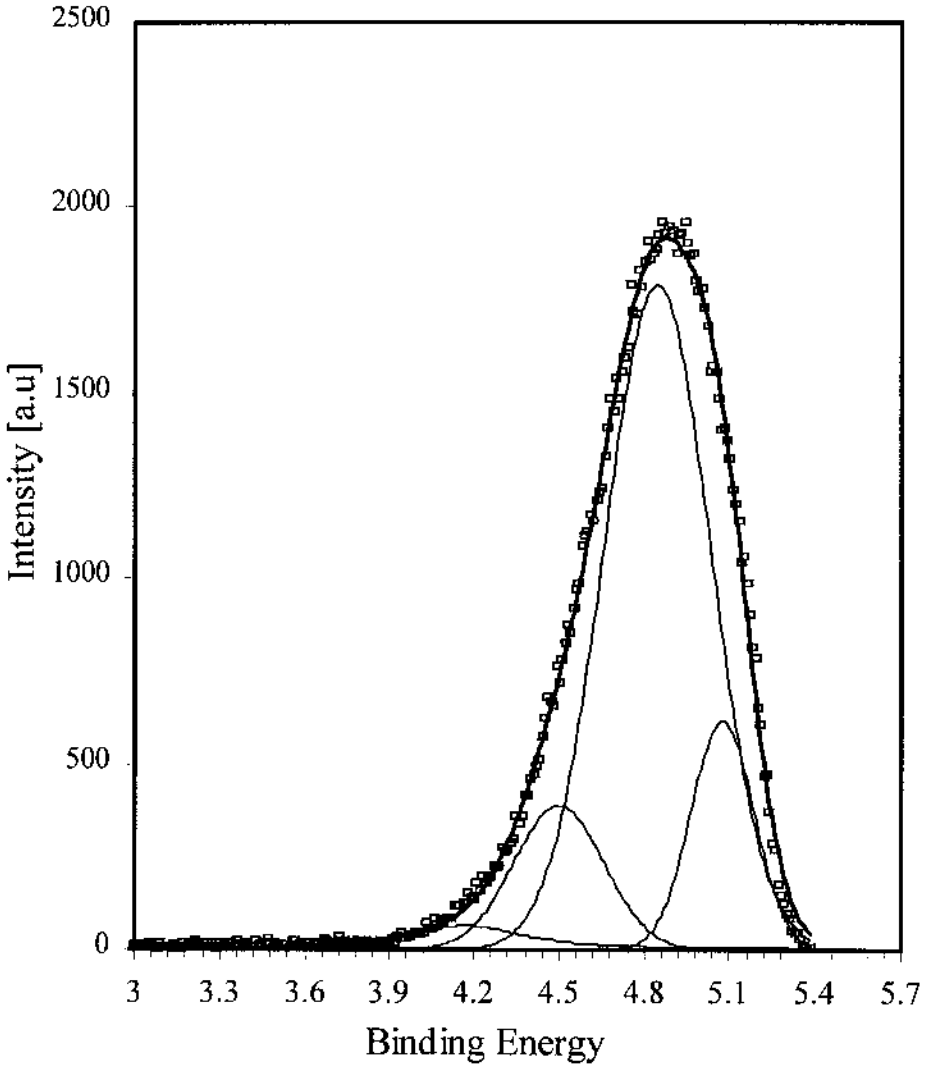

Figure 6.11. Energy distribution of photoemitted electrons from chemical vapor deposition polycrystalline diamond film grown using 25 millitorr of partial pressure of N_2 gas. The energy of the exciting photons is 5.36 eV. The fit indicate emission bands at about 4.10, 4.50, 4.75 and 5.18 eV.

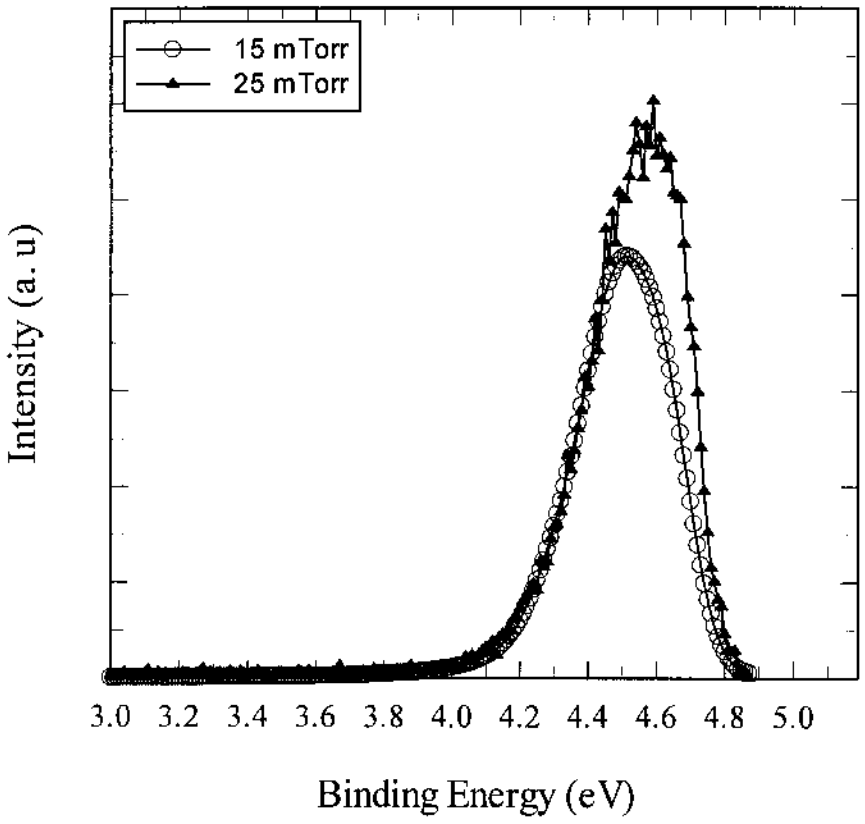

Figure 6.12. Energy distributions of photoemitted electrons from chemical vapor deposition polycrystalline diamond films grown using 15 and 25 millitorr of partial pressure of N_2 gas. The energy of the exciting photons is 4.87 eV. The film grown using 25 millitorr of N_2 gas pressure shows a significant increase in emission intensity.

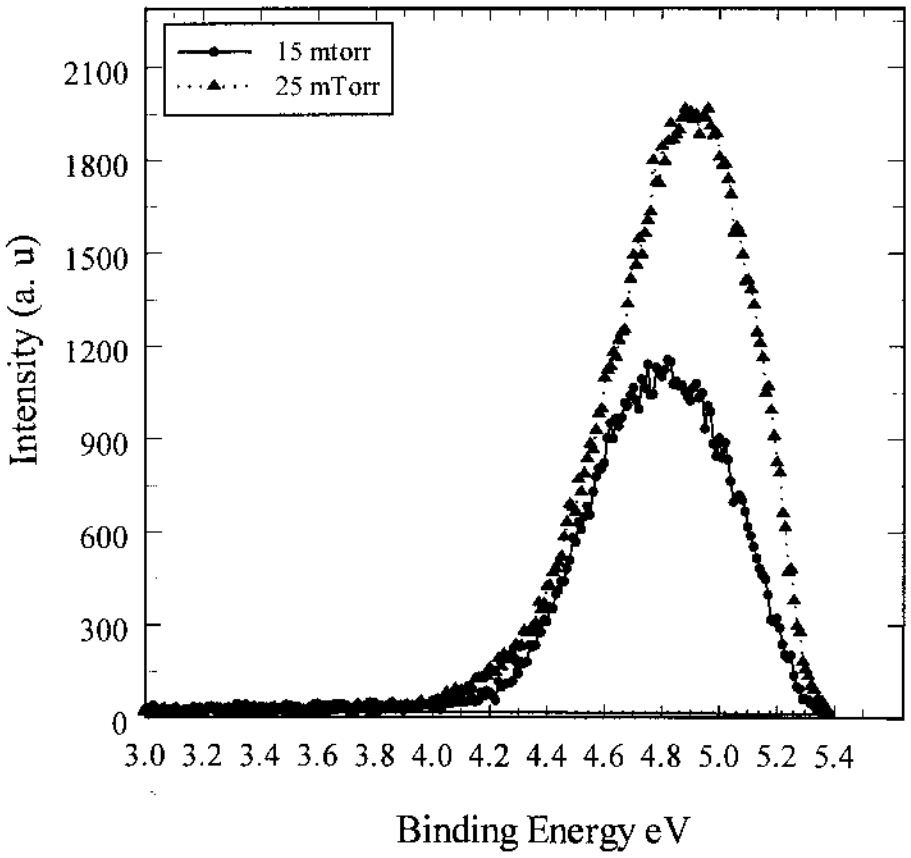

Figure 6.13. Energy distributions of photoemitted electrons from chemical vapor deposition polycrystalline diamond films grown using 15 and 25 millitorr of partial pressure of N_2 gas. The energy of the exciting photons is 5.36 eV. The film grown using 25 millitorr of N_2 gas pressure shows a significant increase in emission intensity.

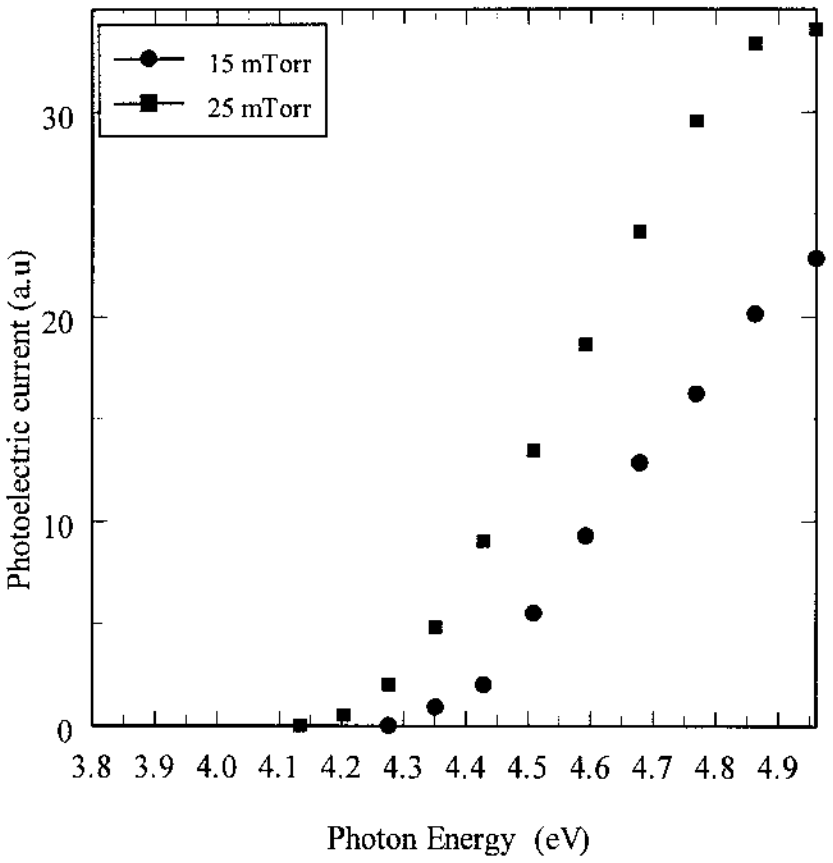

Figure 6.14. Photoelectric response near threshold for chemical vapor deposition polycrystalline diamond film grown using 15 and 25 millitorr of partial pressure of N_2 gas.

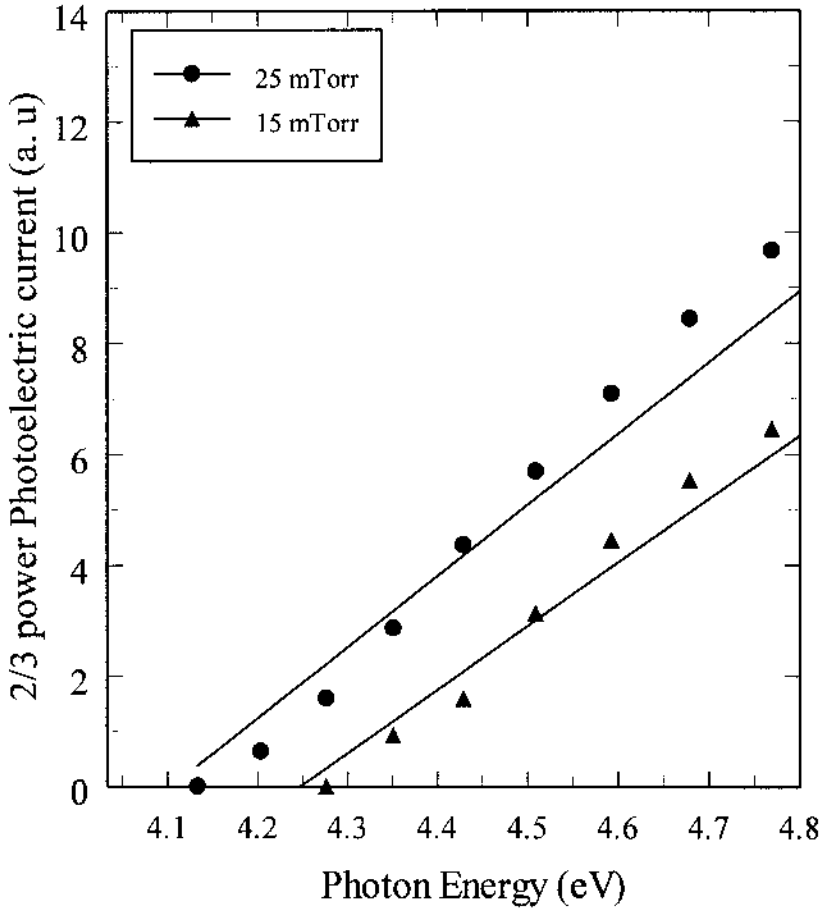

Figure 6.15. Photoelectric response near threshold for chemical vapor deposition polycrystalline diamond film grown using 15 and 25 millitorr of partial pressure of N_2 gas. The curves are fitted to $A(E-E_t)^{3/2}$.

[10].

$$A(E - E_T)^{3/2}$$

The emission current results show that the photoelectric threshold is a function of the N_2 gas partial pressure used during growth. The threshold energy is found to decrease from about 4.28 eV to 4.13 eV, as the N_2 gas pressure increases from 15 millitorr to 25 millitorr, in agreement with the UPS results.

6.8 Discussion

It is well known that CVD diamond films and other carbon based materials contain sp^3 and sp^2 carbon, whose relative concentrations depend on the growth parameters. Changes in the relative concentrations of sp^3 and sp^2 bonded carbon affect the electronic properties of the CVD diamond films. We found in previous chapters that an increase in sp^2 carbon results in a decrease in photoelectric threshold energy, a result that is consistent with field emission results [10]. Therefore, the observed decrease in photoelectric threshold from 4.27 eV to 4.10 eV as the $sp^3/(sp^3 + sp^2)$ carbon fraction at surface decreases from 76% to 50% is consistent with an increase in sp^2 concentration of the films. Since both films were grown under very similar conditions. The change in $sp^3/(sp^3 + sp^2)$ carbon fraction at surface of the film, and the corresponding change in the threshold energy is therefore related to the bonded nitrogen concentration. As the film with higher nitrogen concentration have larger percentage of sp^2 carbon, this could lead to an increase in the sp^2 content. Furthermore, the film grown at higher N_2 gas pressure, characteristic of microcrystalline diamond film exhibits a higher emission intensity than

the film grown at a lower N_2 gas pressure. The significant difference in emission intensity observed at higher photon energy (figs. 6.12-6.13) for the film grown at 25 millitorr of N_2 gas pressure is believed to be due to microcrystallinity of the films. Similar behavior was observed for boron doped polycrystalline diamond films discussed in chapter 5.

6.9 Conclusion

The effects of N_2 gas partial pressure on photoelectron emission properties of CVD grown polycrystalline diamond films was studied. It was found that incorporation of nitrogen significantly affect the $sp^3/(sp^3 + sp^2)$ carbon fraction, threshold energies and electron emission characteristic of polycrystalline diamond films. The $sp^3/(sp^3 + sp^2)$ carbon fraction on the surface is observed to decrease from 76% to 50% as the nitrogen partial pressure increases from 15 to 25 millitorr. The origin of electron emission is due to valence band emission at 4.09, 4.52, 4.82, and 5.18 eV for the film grown using 25 millitorr of N_2 gas pressure. Whereas, the film grown at 15 millitorr of nitrogen gas pressure exhibits emission bands at 4.27, 4.50, 4.83 and 5.18 eV. Emission current measurements give values of the threshold energies at 4.13 and 4.28 eV, for the films grown at 15 and 25 millitorr of nitrogen, respectively. These values are in good agreement with UPS measurements. The decrease in threshold energy is attributed to an increase in concentration of sp^2 carbon.

The morphology examined by SEM revealed large diamond crystals at low nitrogen pressure. As the nitrogen gas pressure is increased, the diamond crystals become microcrystalline. This is supported by an observation of microcrystalline peak in the

Raman data, and also by XPS data where another diamond peak is needed for analysis. These results find that the emission threshold and the emission intensity is dependent on the nitrogen partial pressure used during growth. Better electron emission properties were observed in the film characterized by smaller value of $sp^3/(sp^3 + sp^2)$ carbon fraction and smaller diamond crystals size.

References

1.M. Nagao, T. Kondo, H. Hsuji, J. Miyata and K. Kobashi, *Appl. Phys.* Lett. **71**, 2806 (1997).

2. F.J. Himpsel, J.A. Knapp, J.A. Van Vechten and D.E. Eastman *Phys. Rev.* B **20,** 624 (1979).

3. J. van der Weide and R.J. Nemamich, *J. Vac. Sci. Technol.* B **12**, 2475 (1994).

4. V.S. Vavilar, E.A. Konorova, E.B. Stepanova, and E.M. Trukhan, *Sov. Phys. Senicond.* **13**, 635 (1979).

5. K.Okano, H. Kiyota, T. Iwasaki, Y. Nakamura, Y. Akiba, T. Kurosu, M. Iida and T. Nakamura, *Appl. Phys.* A **51**, 334 (1990).

6. R. Locher, C. Wild, N. Herres, D. Behr, and P. Koidl, *Appl. Phys. Lett.* **65**, 34 (1994).

7. S. Jin and T.D. Moustakas, *Appl. Phys. Lett.* **65**, 403 (1994).

8. M. Hoikins, E.R Weber, M.I. Laundertrass, M.A. Plano, S. Han, and D. Kania, *Appl. Phys. Lett.* **59**, 1871 (1991).

9. Y. Yokota, H. Kawarada, and Hiraki, *Mater. Soc. Symp.* Proc. **162**, 231 (1990)

10. K.Okano, S. Koizumi, S.R.P. Silva, and G.A.J. Amaratunga, *Nature* (London) **381**, 140 (1996).

CHAPTER 7

SUMMARY AND CONCLUSION

The $sp^3/ (sp^3+ sp^2)$ carbon fraction of polycrystalline diamond films has been correlated to the photoelectric threshold energy. Different $sp^3/ (sp^3+ sp^2)$ carbon fractions were obtained by varying the CH_4, H_2 B_6 and N_2 concentrations used during growth. Raman spectroscopy and x-ray photoelectron spectroscopy were used to characterize the fraction of sp^3 carbon in the films. We observed for the first time, a continuous and significant decrease in the photoelectric threshold as the $sp^3/ (sp^3+ sp^2)$ carbon fraction at the surface of CVD grown polycrystalline diamond film decreases. Analysis of the photocurrent measurements show that the electron emission is due to valence band emission.

By varying the CH_4 concentration from 0.10% to 0.70%, we observed a decrease in photoelectric threshold from 4.8 eV to 3.9 eV as the percent of sp^3 carbon at the surface decreases from 91% to 55%, indicating that emission properties of CVD polycrystalline diamond films can be enhanced by increasing graphitic content of the films. According to the Fowler-Nordhiem model [1], field emission (FE) depends exponentially on the

photoelectric threshold. Therefore, this decrease in threshold energy (0.9 eV) would result in an increase in the FE current by a factor of approximately 20. This could be important in flat panel displays industry.

We observed that the percent of sp^3 carbon at the surface is independent of the boron concentrations used during growth. Measurements of the photoelectric current and electron energy distributions show that the photoelectric threshold is insensitive to the boron concentration, indicating absence of surface states. Although the boron doping modified the surface morphology and photoemission intensitiy. The photoemission intensity increases with microcrystalline diamond content. The photoelectric threshold is found to be about 4.4 eV. In addition, emission bands were found at 4.38, 4.63, 4.92, 5.12, and 5.30 eV, respectively.

Effects of the nitrogen dopant on the photoelectron emission properties was studied. It was found that by increasing the partial pressure of N_2 gas during growth, from 15 to 25 millitorr, the photoelectric threshold was decreased by about 0.17 eV, as the percent of sp^3 carbon at the surface decreased from 76% to 50%. This change significantly improved the photoemission intensity, indicating that incorporation of N_2 in diamond plays an important role in determining the electron emission properties.

SEM and Raman results show that the CVD diamond films consist of a wide range of crystal size that depended on the growth conditions. A general observation is that diamond films with large crystal size and high content of sp^3 carbon exhibit poor emission properties, while films with smaller crystals and high sp^2 content show superior

emission properties.

The increase in FE from diamond films was attributed to an increase in defects in the diamond crystallites because the FWHM of the Raman peak at 1332 cm^{-1} was observed to increase as the FE increased [2]. Our results show no correlation between the FWHM of the Raman peak at 1332 cm^{-1} and the photoelectric threshold, showing that defects in the diamond crystallites are not responsible for the high field emission in diamond.

On the basis of these observations, we propose that the decrease in photoelectric threshold is due to a decrease in the band gap of the sp^3- sp^2 carbon networks at the grain boundaries in agreement with recent theoretical calculations. This effect can be used to tailor the electronic properties of diamond films for applications such as photocathode and field emission. However, in order to realize these applications, the emphasis of research should be placed on the electronic properties of nanocrystalline diamond.

References

1. N.S. Xu, R.V. Latham, and Y. Tzeng, *Electron Lett.* **29**, 1596 (1993).

2. W. Zhu, G.P. Kochansk, S. Jin, and L. Seibles, *J. Vac. Sci. Technol.* B **14**, 2011 (1996).

BIBLIOGRAPHY

Alivsatos, A. P., *J. Phys. Chem.* **100,** 13226 (1996).

Alivsatos, A.P., *J. Phys. Chem.* **100**, 13226 (1996).

Angus, J.C., *Proc. First Internat. Sympos. on Diamond and Diamond-like Films*, edited by J.P. Dismukes, (The Electrochemical Society, Pennington, 1989), pp. 1-13.

Angus, J.C., Proc. First Internat. Sympos. on Diamond and Diamond-like Films, edited by J.P. Dismukes, The Electrochemical Society, Pennington, N.J., (1989), pp. 1-13.

Anthony, R.T., *Diamond and Diamond-Like Carbon and Coatings*, edited by R.E. Clausing, L.L. Horton, J.C. Angus, and P. Koidl (Plenum Press, New York, 1991).

Bachmann, P.K., Drawl, W., Knight, D., Weimer, R., and Messier, R.F. in Extended Abstracts No. **15**, *Diamond and Diamond-like Material Synthesis*, edited by G.H. Johnson, A.R. Badzian, and M.W. Geis., (Material Research Society, Pittsburgh, PA, 1988), pp. 99-102.

Badzian, A., Badzian, T., Roy, R., Messier, R., and Spear, K., *Mat. Res. Bull.* **23**, 531 (1988).

Badzian, A., Badzian, T., Roy, R., Messier, R., and Spear, K., *Mat. Res. Bull.* **23**, 531 (1988).

Bandis, C., and Pate, B.B., *Surface Science* **350**, 315 (1996).

Bandis, C., and Pate, B.B., Appl. *Phys. Lett.* **69**, 367 (1996).

Bandis, C., and Pate, B.B. ,*Phys. Rev.* B **52,** 12056 (1995).

Bandis, C., and Pate, B.B., *Phys. Rev.* **B 52**, 12056 (1995).

Berglund, C.N., and Spicer, W.E., *Phys. Rev.* **136**, 1030 (1964).

Berglund, C.N., and Spicer, W.E., *Phys. Rev.* **136**, 1044 (1964).

Berglund, C.N., and Spicer, W.E., *Phys. Rev.* **136**, 1030 (1964).

Bi, X. X., Eklund , P.C., Zhang , J.G., Rao, A.M., Perry , T.A., and Beetz, C.P., Jr., *J. Mater. Res.* **Vol. 5**, No. 4, 811 (1990).

Bransden, B.H., and Joachain, C.J., *Physics of Atoms and Molecules,* John Wiley & Sons, Inc., New York, (1990), pp.155-193.

Breskin, A., Chechik, R., Shefer, E., Bacon, D., Avigal, Y., Kalish, R., and Lifshitz,Y., *Appl. Phys. Lett.* **70**, 3446 (1997).

Buruley, J., and Batson, P.E., *Mat. Res. Soc. Symp. Proc. Vol.* **162**, 255 (1990).

Chen, Q., Yang, J., and Lin, Z., *Appl. Phys. Lett.* **67**, 1853 (1995).

Christensen, N.E., and Feuerbacher, B., *Phys. Rev.* **B 10**, 2349 (1974).

Cusers, J.F.H., *Physica* **18**, 489 (1952).

Dalven, R., *Introduction to Applied Solid State Physics*, Plenum Press, New York, (1980), pp. 145.

Dalven, R., *Introduction to Applied Solid State Physics,* Plenum Press, New York, (1981), pp. 139-160.

Das Gupta, D., Demichelis, F., Pirri, C.F., Spagnolo, R., and Tagliaferro, A., *Diamond and Diamond-Like Films and Coating*, Edited by R.E. Clausing, Plenum Press, New York, (1991), pp. 427.

Devreese, J.T., Kunz, A.B., and Collins, T.C., *Elementary Excitations in Solids, Molecules, and Atoms* (Plenum Press, London 1974).

Einstein, A., Ann *Physik* **17**, 132 (1905)

Feidelman, P.J., and Eastman, D.E., *Phys. Rev.* **B 10**, 4932 (1974).

Feuerbacher, B., and Christensen, N.E., *Phys. Rev.* **B 10**, 2373 (1974).

Fowler, R.H. , *Phys. Rev.* **38**, 45 (1931).

Frenklach, M., *Diamond and Diamond-Like Films and Coatings*, Edited by R.E. Clausing et al., Plenum Press, New York, (1991). pp. 499-523.

Furjimori, N., Ikegaya, A., Imai, T., Fukushima, K., and Ohta, N., *Proc. First International. Sympos.on Diamond and Diamond-like Films*, edited by J.P. Dismukes, (The Electrochemical Society, Pennington, N.J. 1989) pp. 93-105.

Geis, M.W., Twichell, J.C., Macaulay, J., and Okano, K., *Appl. Phys. Lett.* **67**, 1328 (1995).

Gidenblat, G.Sh., Grot, S.A., Hatfield, C.W., Wronski, C.R., Badzian, A.R., Badzian, T., and Messier, R., *Mater. Res. Bull.* **25**, 129 (1990).

Gobeli, G.W., and Allen, F.G., *Phys. Rev.* **127** 141 (1962).

Hanssen, L.M., Carrington, W.A., Butler, J.E., and Snail, K.A., *Mater. Lett.* **7**, 289 (1988).

Haq, S., Tunnicliffe, D.L., Sails, S., and Savage, J.A., *Appl. Phys. Lett.* **68**, 469 (1996).

Himpsel, F.J., Van der Veen, J.F., and Eastman, D.E., *Phys. Rev.* **22**, 1967 (1980).

Himpsel, F.J., Knapp, J.A., VanVechten, J.A., and Eastman, D.E., *Phys. Rev.* B **20,** 624 (1979).

Himpsel, F.J., Knapp, J.A., VanVechten, J.A., and Eastman, D.E., *Phys. Rev.* **B 20**, 624 (1979).

Himpsel, F.J., Knapp, J.A., VanVechten, J.A., and Eastman, D.E., *Phys. Rev.* **B 20**, 624 (1979).

Hoikins, M., Weber, E.R., Laundertrass, M.J., Plano, M.A., Han, S., and Kania, D., *Appl. Phys. Lett.* **59**, 1871 (1991).

Hong, D., and Aslam, M., *J. Vac. Sci. Technol. B* **13**, 427 (1993).

Humphreys, V.L., and Khachan, J., *Electron. Lett.* **31**, 1018 (1995).

Hyer, R.C., Green, M., Mishra, K.K. , *and* Sharma, S.C. , *J. Mater. Sci Lett.*, Vol. **10**, 515 (1990).

Jackson, J.D., *Classical Electrodynamics*, Second Edition, John Wiley and Sons Inc, New York, (1975), pp. 75-78.

Jansen, F., Mochankin, M.A., and Kuhman, D.E., *J. Vac. Sci. Technol. A***8** 3785 (1990).

Jin, S., and Moustakas,T.D., *Appl. Phys. Lett.* **65**, 403 (1994).

Jin S., and Moustakas, T.D., *Appl. Phys. Lett.* **65,** 403 (1994).

Kaiser, W., and Bond, W.L., *Phys. Rev.* **115**, 857 (1959).

Kamo, M., Sato, Y., Matsumoto, S., and Setaka, N., *J. Cryst. Growth* **62**, 642 (1983).

Kane, E.O., *Phys. Rev.* **127**, 131 (1962).

Kane, E.O., *Phys. Rev.* **127**, 131 (1962).

Kane, E.O., *Phys. Rev.* **127**, 131 (1962).

Kane, E.O., *Phys. Rev.* **127**, 131 (1962).

Kaplan, S., Jansen, F., and Machonkin, M., *Appl. Phys. Lett.* **47**, 750 (1985).

Kawato, T., and Kondo, K., *Jpn. J. Appl. Phys.* **26**, 1429 (1987).

Kittle, C., *Introduction to Solid State Physics*, John Wiley & Son, Inc. New York, (1986), pp. 306.

Knight, D.S., and White, W.B., *J. Mater. Res.* **4**, 385 (1989).

Krainsky, I.L., Asnin,V.M., Mearini, G.T., and Dayton, J.A., *Phys. Rev. B* **53**, R7650 (1996).

Langmuir, I., *J. Am. Chem. Soc.* **37**, 417, (1915).

Le Grice, Y. H., Nemanich, R. J., Glass, J. T., Lee, Y. H., Rudder, R.A., and Markunas, R. J., in Diamond, Silicon carbide and Related Wide Bandgap Semiconductors, edited by J. T. Glass, R. Messier, and N. Fujimori, *Mater. Res. Soc. Symp. Proc.* **162**. Pittsburgh, PA, 1990, p. 219.

Locher, R., Wild, C., Herres, N., Behr, D., and Koidl, P., *Appl. Phys. Lett.* **65**, 34 (1994).

Long, D., *Energy Bands in Semiconductor*, John Wiley & Son, Inc. New York , (1968), pp. 197.

Malta, D.P., Posthill, J.B., and Humphreys, T.P., *Appl. Phys. Lett.* **64**, 1929 (1994).

Matsumoto, S., Sato, Y., Kamo, M., and Setaka, N., *Jpn. J. Appl. Phys.* **21**, L183 (1982).

McGinnis, S., Kelly, M., and Hagstrom, S., Appl. Phys. Lett. **66**, 3117 (1995).

McGinnis, S., Kelly, M., and Hagstrom, S., and Alvis,R., *J. Appl. Phys.* **79**, 170 (1996).

Mcnamara, K.M., Gleason, K.K., and Geis, M.W., *Mat. Res. Soc. Symp. Proc. Vol.* **162**, pp.207-212 (1990).

Mcnamara, K.M., Gleason, K.K., and Geis, M.W., *Mat. Res. Soc. Symp. Proc. Vol.* **162**, pp.207-212 (1990).

Mearini, G.T., Krainsky, I.L., Dayton, J.A., Wang, Y., Zorman, C.A., Angus, J.C., and Anderson, D.F., *Appl. Phys. Lett.* **66**, 242 (1995).

Meyerson, B., and Smith, F., *J. Non-Cryst. Solids* **35/36**, 435 (1980).

Miskovsky, N.M., Cutlter, P.H. and Huang, Z. H., *J. Vac. Sci. Technol.* **14**, 2037 (1996).

Miskovsky, N.M., Cutlter, P.H. and Huang, Z. H., *J. Vac. Sci. Technol.* **14**, 2037 (1996).

Mittleman, D.M., Schoenlein, W.R., Shiang, J.J., and Colvinetal, V.L., *Phys.Rev. B: Condens. Matter*, **49**,14435 (1994).

Miyata, K., Kumagai, K., Nishimura, K., and Kobashi, K., *J. Mater. Res.*, Vol. **8**, No 11, 2845 (1993).

Molinari, E., Polini, R., Terranova, M.L, Asccrelli, P., and Fontana, S., *J. Mater. Res.* **7**, 1778 (1992).

Moustakas, T.D., *Solid State Ionics* **32/33**, 861 (1989).

Nagao, M., Kondo, T., Hsuji, H., Miyata, J., and Kobashi, K., *Appl. Phys.* Lett. **71**, 2806 (1997).

Nagao, M., Kondo, T., Gotoh, Y., Tsuji , H., Ishikawa, J., Miyata, K., and Kobashi, K., *Appl. Phys. Lett.* **71**, 2806 (1997)

Nagao, M., Kondo, T., Gotoh, Y., Tsuji , H., Ishikawa, J., Miyata, K., and Kobashi, K., *Appl. Phys. Lett.* **71**, 2806 (1997)

Nenamich, R.J., Glass, J. T., Lucovski, G., and Shroder, R.E., *J. Vac. Sci Technol.* A**6**, 1783 (1988).

Nishimura, K., Das, K., Glass, J.T., and Nemanich, R.J., Proc. of NATO Advanced Research Workshop on the Physics and Chemistry of Carbides Nitrides and Borides, Manchester, U.K. Oct.(1989).

Nutzenadel, C., Kuttle,. O.M., Groning,O., and Schlapbach, L., *Appl. Phys. Lett.* **69**, 2662 (1996).

Nutzenadel, C., Kuttle,. O.M., Groning,O., and Schlapbach, L., *Appl. Phys. Lett.* **69**, 2662 (1996).

Okano, K., Kiyota, H., Iwasaki, T., Nakamura, Y., Akiba,Y., Kurosu, T., Iida,M., and Nakamura, T., *Appl. Phys.* A **51**, 334 (1990).

Okano, K., Koizumi,S., Silva, S.R.P., and Amaratunga, G.A. J., *Nature* (London) **381**, 140 (1996).

Pate, B.B., *Surf. Sci.* **165**, 83 (1986).

Peakfit, Jandel, Scientific, San Rafael, CA.

Peakfit, Jandel, Scientific, San Rafael, CA.

Phelp, A.W., and Koba, R., *Pro. 1st Intern. Symp. on Diamond and Diamond-Like Films,* Vol. 89 (Electrochem. soc.1989), pp. 38.

Purcell, E.M., *Phys. Rev.* **54** 818 (1938).

Robertson, J., *Diamond and Diamond-Like Films and Coating*, Edited by R.E. Clausing, Plenum Press, New York, (1991), pp. 331.

Robertson, J. and O'Reilly, E.P., *Phys. Rev.* **B 35**, 2946 (1986).

Robertson,. J., *Adv. in Phys.* **35**, 317 (1989).

Rossetti, R., Nakahara, S., and Brus, L.E., *J. Chem. Phys.* **79**, 1086 (1983).

Saito, Y., Sato, K., Tanaka, H., Fujita, K., and Matsuda, S., *J. Mater. Sci.* **23,** 842 (1988).

Saito, Y., Sato, K., Tanaka, H., Fujita, K., and Matsuda, S., *J. Mater. Sci.* **23,** 842 (1988).

Sato, Y., in *New Diamond* 1988 (JNDF, Tokyo, 1988) pp.30-35.

Sato, Y., Hata, C., and Kamo, M., *First International Conference on the New Diamond Science and Technology Program and Absr.*, 24-26 October 1988 (JNDF, Tokyo, 1988), pp. 50-51.

Sen, R., Sumathy , R., and Rao, C.N.R., *J. Mater. Res.* **11**, 2961 (1996).

Sen, R., Sumathy , R., and Rao, C.N.R., *J. Mater. Res.* **11**, 2961 (1996).

Setaka, N., *J. Mater. Res.* **4**, 664 (1989).

Sharma, S.C., Dark, C.A., Hyer, R.C., Green, M., Black, T.D., Chourasia, A.R., Chopra, R., and Mishra, K.K., *Appl. Phys. Lett.* **56**, 1781 (1990).

Sharma, S.C., Green, M., Hyer, R.C., Dark, C.A., Black, T.D., Chourasia, A.R., Chopra, D.R., and Mishra, K.K., *J. Mater. Res.*, Vol. **5**, 2424 (1990).

Shirley, D.A., ed.: *Electron spectroscopy. Proc. of the Int. Con.*, Asilomar (calif.) Sept. 1997, North Holland, Amsterdam 1972, pp. 487.

Singh, B., Arie, Y., Levine, A.W., Mesker, O.R., *Appl. Phys. Lett.* **52**, 451 (1988)

Smith, N.V., *Phys. Rev.* **B3**, 1862 (1971).

Solin, S.A., and Ramdas, A.K. , *Phys. Rev.* **B1** (1970).

Solin, S.A., and Kobliska, R.J., *Amorphous and Liquid Semiconductors*, ed. By J. Stuke and W. Brenig, (Taylor and Francis, 1974), p.1251.

Spear, K.E., and Dismukes, J.P., *Synthetic Diamond: Emerging CVD Science and Technology*, John Wiley & Son, New York, 1994.

Spicer, W.E., *Phys. Rev.* **112**, 114 (1958).

Spicer, W.E., *Phys. Rev.* **112**, 114 (1958).

Spitsyn, B.V., Bouilov, L.L., and Derjagin, B.V., *J. Crystal Growth* **52**, 219, (1981).

Stoner, B.R., Ma, G.H., Wolter, S.D., and Glass, J.T., Phys. Rev. B**45**, 11067 (1992).

Stoner, B.R., Glass, J.T., Bergman, L., Nemanich, R.J., Zoltan, L.D., and Vandersande, J.W., *J. Electron. Mater.* **21**, 629 (1992).

Stoner, B., and Glass, J., *Appl. Phys. Lett.* **60**, 698 (1992).

Street, R.A., Seearle, T.M., Auatin, I.G., and Sussmann, R.S., *J. Phys.* C **7**, 1582 (1974).

Stuart, S.A., Prawer, S., and Weiser, P.S., *Appl. Phys. Lett.* **62**, 1227 (1993).

Stubhan, F., Ferguson, M., and Fusser, H.J., *Appl. Phys. Lett.* **66**, 1900 (1995).

Suzuki, K., Sawabe, A., and Inuzuka, T., *Jpn. J. Appl. Phys.* **29**, 153 (1990).

Tiedje, T., and Cebulka, J.M., *Phys. Rev.* B **28** 7075 (1983).

Tsai. C.. Gerberich. W.. Lu. Z.P.. Herberlein. J., and Pfender. E., *J. Mater. Res.* Vol. **6**,

No 10, 2127 (1991).

Van der Weide, J., Zhang, Z., Baumann, P.K., Wensell, M.G., Bernholc, J., and Nemanich, R.J., *Phys. Rev.* **B 50**, 5803 (1994).

Van der Weide, J., Zhang, Z., Baumann, P.K., Wensell, M.G., Bernholc J., and Nemanich, R.J., *Phys. Rev.* **B 50**, 5803 (1994).

Van der Weide, J., and Nemamich, R.J., *J. Vac. Sci. Technol.* B **12**, 2475 (1994).

Vavilar, V.S., Konorova, E.A., Stepanova, E.B., and Trukhan, E.M., *Sov. Phys. Senicond.* **13**, 635 (1979).

Waite, M.M., and Shah, S.I., *Appl. Phys. Lett.* **60**, 2344 (1992).

Wang, C., Garcia, A., Ingram, D.C., Lake, M., and Korderch, M.E., *Electron Lett.* **27**, 1459, (1991).

Wang, Y., and Herron, N., *J. Phys. Chem.* **95,** 525 (1991).

Wild, C., Herres, N., Koidl, P., and Anthony, T., Electrochem. Soc. Proc. **89**, 283 (1989).

Wild,C., Koidl, P., MullerSebert, W., Walcher, H., Kohl, R., Herres, N., Locher, R., Samlenski, R., and Brenn, R., *Diamond Relat. Mater.* **2**, 158 (1993).

Won, J.H., Hatta, A., Yagyu, H., Jiang, N., Mori, Y., Ito, T., Sasaka, T., and Hiraki, A., *Appl. Phys. Lett.* **68**, 2822 (1996).

Xu, N.S., Tzena, Y., and Latham, R.V., *J. Phys. D* **26,** 1776 (1993).

Xu, N.S., Latham, R.V., and Tzeng, Y., *Electron. Lett.* **29**, 1596 (1993).

Yarbrough, W.A., and Messier, R., *Science* **247**, 688 (1990).

Yokota,Y., Kawarada, H., and Hiraki, H., *Mater. Soc. Symp.* Proc. **162**, 231 (1990).

Yoshikawa, M., Katagiri, G., Ishida, H., Ishitani, A., Ono, M., and Matsumara, K., *Appl. Phys. Lett.* 55, 2608 (1989).

Zhu, W., Kochanski, G.P., Jin, S., and Seibles, L., *J. Vac. Sci. Technol.* **B14 (3)**, 2011 (1996).

Zhu, W., Kochanski, G.P., Jin, S., and Seibles, L., *J. Vac. Sci. Technol.* **B14 (3)**, 2011 (1996).